



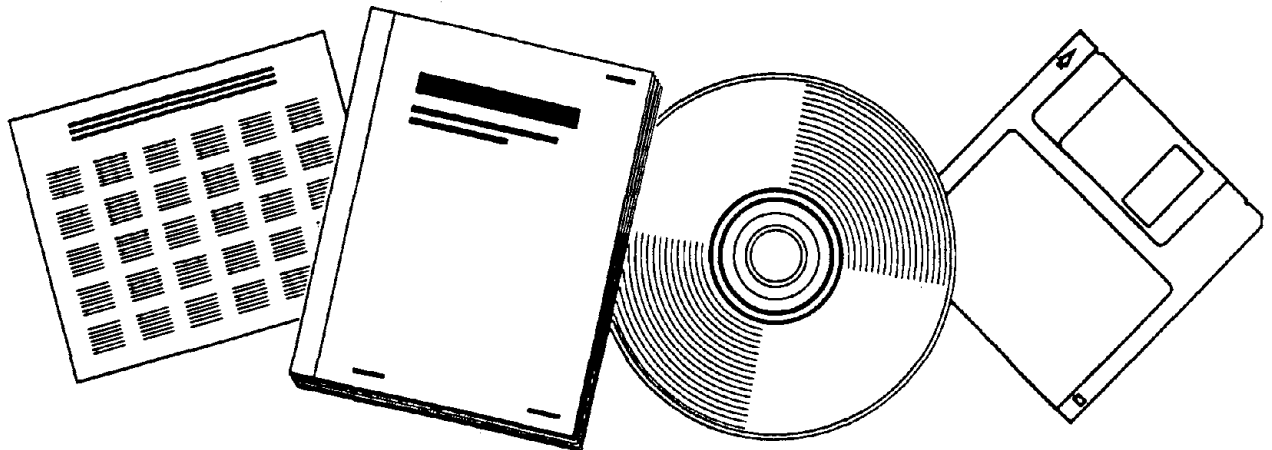
PB97-170427

NTIS[®]
Information is our business.

EXPERIMENTAL AND NUMERICAL SIMULATION OF THE USE OF FIBER REINFORCED COMPOSITE MATERIALS FOR ROAD SIDE SAFETY APPLICATIONS

(U.S.) FEDERAL HIGHWAY ADMINISTRATION, MCLEAN, VA

MAY 97



U.S. DEPARTMENT OF COMMERCE
National Technical Information Service





PB97-170427

Experimental and Numerical Simulation of the Use of Fiber Reinforced Composite Materials for Road Side Safety Applications

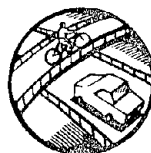
PUBLICATION NO. FHWA-RD-96-026

MAY 1997



U.S. Department of Transportation
Federal Highway Administration

REPRODUCED BY: **NTIS**
U.S. Department of Commerce
National Technical Information Service
Springfield, Virginia 22161



Research and Development
Turner-Fairbank Highway Research Center
6300 Georgetown Pike
McLean, VA 22101-2296

FOREWORD

This report presents the results from an investigation of the feasibility of using pultruded composite materials for road side safety barrier structures. The failure modes and impact rate sensitivity from a series of laboratory drop-weight impact tests are presented here. Reported here also are stress analysis and description of the finite element model of the test fixture of the Federal Outdoor Impact Laboratory. DYNA3D numerical simulation of a series of impact tests of steel guard rails are presented and compared with the laboratory impact tests. The report will be useful for researchers concerned with optimization of the future barrier made of composite material.




A. George Ostensen, Director
Office of Safety and Traffic
Operations Research and Development

NOTICE

This document is disseminated under the sponsorship of the Department of Transportation in the interest of information exchange. The United States Government assumes no liability for its contents or use thereof. This report does not constitute a standard, specification, or regulation.

The United States Government does not endorse products or manufacturers. Trade or manufacturer's names appear in this report only because they are considered essential to the object of this document.

1. Report No. FHWA-RD-96-026		PB97-170427 		3. Recipient's Catalog No.	
4. Title and Subtitle EXPERIMENTAL AND NUMERICAL SIMULATION OF THE USE OF FIBER REINFORCED COMPOSITE MATERIALS FOR ROAD SIDE SAFETY APPLICATIONS		5. Report Date May 1997		6. Performing Organization Code	
7. Author(s) Ala Tabiei		8. Performing Organization Report No.		10. Work Unit No. (TRAIS) 3A5D-0262	
9. Performing Organization Name and Address Turner-Fairbank Highway Research Center 6300 Georgetown Pike McLean, Virginia 22101-2296		11. Contract or Grant No. NHI GRF Project #93-30		13. Type of Report and Period Covered Final Report September 1993-November 1994	
12. Sponsoring Agency Name and Address Office of Safety and Traffic Operations R&D Federal Highway Administration 6300 Georgetown Pike McLean, Virginia 22101-2296		14. Sponsoring Agency Code		15. Supplementary Notes	
16. Abstract The Federal Highway Administration is currently investigating the potential of using fiber reinforced composite materials for applications in highway structures. The feasibility and application of composite materials are analyzed through a series of impact tests on laboratory specimens and numerical simulation. The investigation is conducted in two parts. The objective of the first part is to determine the impact characteristics and failure modes of pultruded box-beams under impact loads. The loading rate sensitivity of pultruded box-beams with different resin systems is investigated. The second study is a numerical simulation of a series of impact tests of steel guard rails. A finite element model of the pendulum fixture of the Federal Outdoor Impact Laboratory is developed with the following objectives: (1) determine the feasibility of simulating a full-scale impact tests of guard rails made of isotropic and anisotropic materials; and (2) identify the critical parameters governing a successful simulation of test fixture pendulum impact. Results of the experimental investigations are presented. A successful simulation is performed, and possibilities for future investigations are recommended.					
17. Key Words Impact, pultruded composite, DYNA3D simulation, roadside safety structures.			18. Distribution Statement No restrictions. This document is available to the public through the National Technical Information Service, Springfield, Virginia 22161.		
19. Security Classif. (of this report) Unclassified		20. Security Classif. (of this page) Unclassified		21. No. of Pages 89	22. Price

SI* (MODERN METRIC) CONVERSION FACTORS

APPROXIMATE CONVERSIONS TO SI UNITS					APPROXIMATE CONVERSIONS FROM SI UNITS				
Symbol	When You Know	Multiply By	To Find	Symbol	Symbol	When You Know	Multiply By	To Find	Symbol
LENGTH					LENGTH				
in	inches	25.4	millimeters	mm	mm	millimeters	0.039	inches	in
ft	feet	0.305	meters	m	m	meters	3.28	feet	ft
yd	yards	0.914	meters	m	m	meters	1.09	yards	yd
mi	miles	1.61	kilometers	km	km	kilometers	0.621	miles	mi
AREA					AREA				
in ²	square inches	645.2	square millimeters	mm ²	mm ²	square millimeters	0.0016	square inches	in ²
ft ²	square feet	0.093	square meters	m ²	m ²	square meters	10.764	square feet	ft ²
yd ²	square yards	0.836	square meters	m ²	m ²	square meters	1.195	square yards	yd ²
ac	acres	0.405	hectares	ha	ha	hectares	2.47	acres	ac
mi ²	square miles	2.59	square kilometers	km ²	km ²	square kilometers	0.386	square miles	mi ²
VOLUME					VOLUME				
fl oz	fluid ounces	29.57	milliliters	mL	mL	milliliters	0.034	fluid ounces	fl oz
gal	gallons	3.785	liters	L	L	liters	0.264	gallons	gal
ft ³	cubic feet	0.028	cubic meters	m ³	m ³	cubic meters	35.71	cubic feet	ft ³
yd ³	cubic yards	0.765	cubic meters	m ³	m ³	cubic meters	1.307	cubic yards	yd ³
NOTE: Volumes greater than 1000 l shall be shown in m ³ .									
MASS					MASS				
oz	ounces	28.35	grams	g	g	grams	0.035	ounces	oz
lb	pounds	0.454	kilograms	kg	kg	kilograms	2.202	pounds	lb
T	short tons (2000 lb)	0.907	megagrams (or "metric ton")	Mg (or "t")	Mg (or "t")	megagrams (or "metric ton")	1.103	short tons (2000 lb)	T
TEMPERATURE (exact)					TEMPERATURE (exact)				
°F	Fahrenheit temperature	5(F-32)/9 or (F-32)/1.8	Celsius temperature	°C	°C	Celsius temperature	1.8C + 32	Fahrenheit temperature	°F
ILLUMINATION					ILLUMINATION				
fc	foot-candles	10.76	lux	lx	lx	lux	0.0929	foot-candles	fc
fl	foot-Lamberts	3.426	candela/m ²	cd/m ²	cd/m ²	candela/m ²	0.2919	foot-Lamberts	fl
FORCE and PRESSURE or STRESS					FORCE and PRESSURE or STRESS				
lbf	poundforce	4.45	newtons	N	N	newtons	0.225	poundforce	lbf
lbf/in ²	poundforce per square inch	6.89	kilopascals	kPa	kPa	kilopascals	0.145	poundforce per square inch	lbf/in ²

* SI is the symbol for the International System of Units. Appropriate rounding should be made to comply with Section 4 of ASTM E380.

(Revised September 1993)

TABLE OF CONTENTS

Part I

EXPERIMENTAL ANALYSIS

Chapter	Page
1. INTRODUCTION	1
Relationship to the Composite Industry	2
2. DESCRIPTION OF THE EXPERIMENT	3
Test Specimens	3
Test Apparatus	3
Test Procedure	3
Data Analysis	5
3. EXPERIMENTAL RESULTS	7
Failure Mechanism	7
Static Test	7
Dynamic Test	7
4. DISCUSSION AND CONCLUSION	21

Part II

NUMERICAL SIMULATION

Chapter	Page
5. INTRODUCTION	23
6. FINITE ELEMENT MODEL	27
Fixture with a Single Rail Section	27
Fixture with Multiple Rail Sections	39
Simplified Model	39
7. TESTS AND NUMERICAL SIMULATION	43
Stress Analysis	43
Tests	44
Simulation	48
8. DISCUSSION AND CONCLUSION	79
9. FINAL REMARKS AND RECOMMENDATION	81
REFERENCES	83

LIST OF FIGURES

Figure	Page
1. Drop weight test machine.	4
2. Static and impact test for polyester specimens.	8
3. Static and impact test for vinylester specimens.	9
4. Impact load versus deflection, drop height $h=0.25$ m.	11
5. Impact load versus deflection, drop height $h=0.5$ m.	12
6. Impact load versus deflection, drop height $h=1.0$ m.	13
7. Impact load versus deflection, drop height $h=1.5$ m.	14
8. Impact load versus deflection, drop height $h=2.0$ m.	15
9. Impact load versus deflection, drop height $h=2.5$ m.	16
10. Impact load versus deflection, drop height $h=3.0$ m.	17
11. Maximum impact load versus drop height.	18
12. A specimen after an impact test.	19
13. Test fixture assembly.	25
14. Box beam with vertical brace and gusset.	29
15. Box beam assembly with cross beam.	30
16. Guard rail post assembly.	31
17. Steel and wooden spacers.	32
18. Spacers and post assembly.	33
19. FOIL pendulum.	34
20. Finite element model of the pendulum.	35
21. Finite element model of the pendulum fixture.	36
22. Finite element model of the pendulum fixture with three rail sections.	40
23. A simplified finite element model of the pendulum fixture.	42
24. Strain gauge rosettes.	45
25. Isoparametric view of a fixture.	46
26. Pendulum displacement versus time.	49
27. Pendulum velocity versus time.	50
28. Pendulum acceleration versus time for full FE model.	52
29. Pendulum acceleration versus time for simplified FE model.	53
30. Pendulum acceleration versus time for multiple rail section FE model.	54
31. Impact simulation single section front view, $t=0$ ms.	55
32. Impact simulation single section front view, $t=40$ ms.	56
33. Impact simulation single section front view, $t=80$ ms.	57

34. Impact simulation single section front view, t=120 ms.	58
35. Impact simulation single section front view, t=160 ms.	59
36. Impact simulation single section front view, t=200 ms.	60
37. Impact simulation single section front view, t=220 ms.	61
38. Impact simulation single section rear view, t=0 ms.	62
39. Impact simulation single section rear view, t=40 ms.	63
40. Impact simulation single section rear view, t=80 ms.	64
41. Impact simulation single section rear view, t=120 ms.	65
42. Impact simulation single section rear view, t=160 ms.	66
43. Impact simulation single section rear view, t=200 ms.	67
44. Impact simulation single section rear view, t=220 ms.	68
45. Average displacement of three tests and simulation prediction. . .	69
46. Average velocity of three tests and simulation prediction.	70
47. Pendulum acceleration of test #1 and simulation prediction.	71
48. Pendulum acceleration of test #2 and simulation prediction.	72
49. Pendulum acceleration of test #3 and simulation prediction.	73
50. Impact simulation multiple sections, t=10 ms.	74
51. Impact simulation multiple sections, t=50 ms.	75
52. Impact simulation multiple sections, t=90 ms.	76
53. Impact simulation multiple sections, t=140 ms.	77
54. Impact simulation multiple sections, t=190 ms.	78

LIST OF TABLES

Table	Page
1. Components of the finite element model.	37
2. Contact surface definitions.	38
3. Mechanical properties of materials considered.	38
4. Principal stresses (N/m ²) at time t=145 (ms).	47

Part I: EXPERIMENTAL ANALYSIS

Chapter 1. INTRODUCTION

Little work can be found in the literature on the impact and load rate sensitivity of composite materials.⁽¹⁾ Specifically, the strain rate sensitivity of pultruded composite materials has not been established. With the increasing demand to use unconventional materials for infrastructure applications, understanding of the behavior of such materials becomes necessary. The Federal Highway Administration (FHWA) is currently investigating the potential of using fiber reinforced composite materials for applications in highway structures. In particular the use of fiber reinforced composites for highway safety structures, such as luminare supports, sign supports, and roadside barriers (rail systems) are being investigated. The feasibility and application of composite materials are analyzed through a series of impact tests on laboratory specimens. Pultruded glass-fiber reinforced composite materials are being considered because of the ease of mass production and they are one of the least expensive composite materials available to date. These tests have been conducted to determine the impact behavior and material characteristics under dynamic load. The tests of these small scale specimens and pultruded sections give an understanding of the different failure modes and aid in the prediction of the behavior of a full-scale structure.

The current geometry of guard rails is a W-shape cross-section made of steel.⁽²⁾ They perform adequately and provide satisfactory behavior for redirecting and containing an errant vehicle. The constant demand, in the past few years, for rebuilding the infrastructure of this country points researchers to investigate innovative materials and structures. Roadside safety structures made of composite materials need to be analyzed to determine their potential as compared to the existing structures. Almost all fibers used in advance composite materials are brittle, in that they are elastic to failure with no significant plasticity. The human capacity to withstand shock loading is strongly dependent on the duration of the impulse. Longitudinal-forward and aft loads of over 45 g being survivable for only about 100 ms.⁽³⁾ Thus, energy absorbing systems need to be carefully designed since larger crushing forces would result in too great a deceleration and smaller crushing forces would require greater crushing distance to absorb the necessary energy. Unlike penetration resistance to impacting projectiles, where total energy absorption is all important, crashworthiness of composite rail systems is concerned with controlled failure processes that maintain a constant load during energy absorption. This can be achieved through progressive failure rather than a sudden fracture.

In this investigation, the building block approach is currently used to design a composite roadside barrier. With this approach, the data from impact tests of different pultruded box-beams are evaluated to determine the design of a structure that would carry the applied load for the duration of the impact without catastrophic failure. The fibers are most important since they carry the majority of the load and fracture energies

are greater when more fibers are broken. The matrix material is important in shear and compression, providing support for the fibers, and, in these cases, failure modes can change if matrix properties are altered. In this study, two types of resin systems, normally used in pultruded composites, are used. These two resin systems are polyester and vinylester. The objectives of the current study are to determine the impact characteristics and failure modes of pultruded box-beams under impact loads. An errant vehicle could strike a rail at different speeds. Therefore, it is important to determine the loading rate sensitivity of pultruded box-beams with different resin systems.

A standard drop weight Material Testing System (MTS) is used for the impact tests. All test specimens are simply supported and impacted at mid span. Impact tests with a practical range of impact velocities as well as static tests are conducted. Testing is conducted at FHWA's Turner-Fairbank Highway Research Center (TFHRC) located in McLean, Virginia.

Relationship to the Composite Industry

Fiber reinforced plastics lack design codes and appropriate specifications for the structural engineer to use these materials as a construction material for the infrastructure and our highway systems. The need for the development of definitive guidance and criteria for the design and performance of fiber reinforced plastics and composite materials is essential for wide spread applications of these materials. This investigation, like many others, is expected to contribute to the better understanding of the behavior of fiber reinforced plastics for use in highway safety structures.

Chapter 2. DESCRIPTION OF THE EXPERIMENT

Test Specimens

The test specimens were cut from standard single cell pultruded sections made by Creative Pultrusion, Inc. The dimensions of the cross-sections are 50.8 by 50.8 mm. The thickness is uniform on all sides. The thickness is 3.18 mm. The specimens were cut to a length of 800 mm with an effective span of 600 mm. The fiber architecture and orientation consist of alternating layers of unidirectional fibers and layers of continuous strand mat. In addition, there was a polymeric surface veil on the top and bottom layers which provided a smooth outer surface. Two types of resin systems were considered, polyester and vinylester. Based on volume fraction tests of similar material of flat specimens, it was found that the fiber volume content was about 30 percent.⁽⁴⁾

Test Apparatus

An MTS vertical drop weight test machine, model 850-02A-01, was used for the impact tests. The drop weight and striker assembly was about 86 kg. An accelerometer mounted on the drop weight provided a complete acceleration versus time history of the impact event. The accelerometer output was collected at a sampling frequency of 37878.78 samples per second by a computer and data acquisition system. That is equivalent to collecting acceleration data every 0.000264 second. The data acquisition system was triggered by a light sensor as the weight fell. A light reflector tape was placed on the drop weight so that light reflect to the light sensor just before impacting the specimen. The specimen was struck by a cylindrical striker head 15.24-cm long by 2.54-cm wide perpendicular to the surface at the center of a 60 cm simply supported span. Figure 1 shows the test apparatus with a specimen placed for impact.

Test Procedure

The specimens were placed on cylindrical support with a radius of 1.9 cm. The effective span was 60 cm with over hang of approximately 10 cm from each sides. The drop weight was raised to the test height and released to impact the specimen at the center. Since one of the objectives of the present study is to determine the rate effect on the impact characteristics, tests were conducted at different heights corresponding to different impact velocities. The velocity of the striker increases at a linear rate during free fall. At the time of impact, the velocity is given as a function of drop height by the following relation:

$$v=(2gh)^{1/2}$$

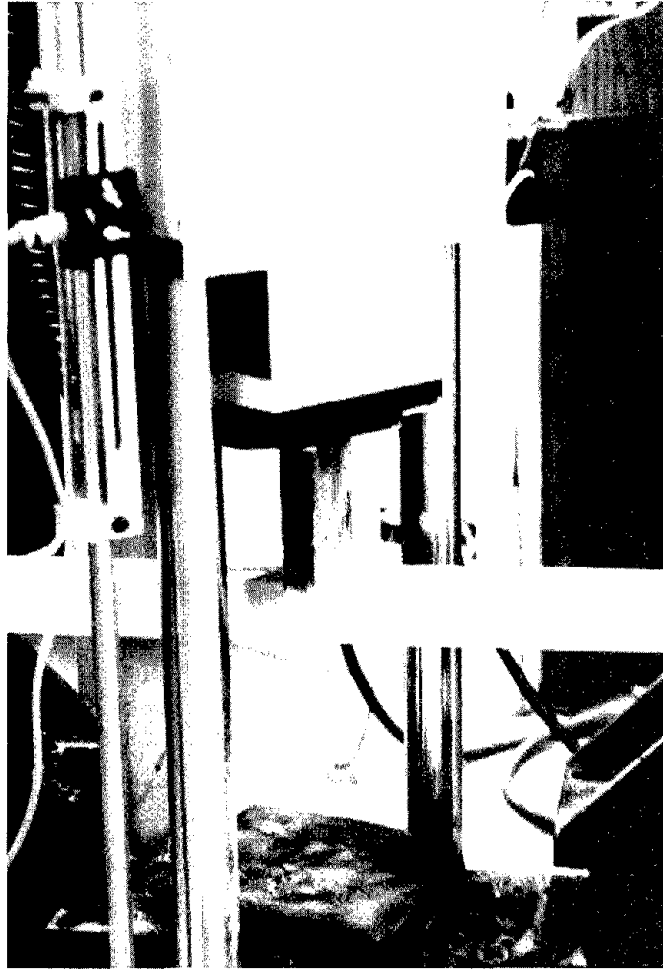


Figure 1. Drop weight test machine.

where h is the drop height and g is the gravitational acceleration constant. The drop height range was 0.25 m to 3.5 m. This gives velocities of impact from 2.21 m/s to 8.29 m/s. The impact energies ranged from 210 J to 2955 J.

Data Analysis

The data from the accelerometer provided a time history of the instantaneous acceleration of the instrumented striker. This data was imported to the software (GLOBAL LAB), and data was filtered at 600 Hz. Then, the data was imported to a LOTUS spreadsheet to calculate the instantaneous velocity and displacement. The instantaneous velocity of the striker becomes nonlinear during the impact event and is reduced due to the stiffness of the specimens. The instantaneous velocity can be calculated by integrating the instantaneous acceleration once. Similarly the displacement of the striker as a function of time can be calculated by integrating the instantaneous acceleration twice.⁽⁵⁾ The spreadsheet calculated the input energies into the system as a function of time and also calculated the average of the three impact tests. The average of all parameters was calculated and is presented here.

Chapter 3. EXPERIMENTAL RESULTS

Failure Mechanism

The failure started with a localized compression failure of the corners of the square box-beam under the loading head. When the load reached its maximum, a shear crack was formed on the top side of the box beam and propagated longitudinally along the top corners of the box beam. After this shear crack had propagated from the midspan, the sides of the box beam began to buckle outward causing the shear crack on the top to propagate further along the box beam in both directions. While the loading head was bearing on the outward moving sides of the box beam, the horizontal top face of the box beam bent further down into the open cross section of the box beam. The compression in these top fibers caused it to buckle downward. As the sides of the box beam flattened out the intersection of these vertical elements, the bottom plate of the box beam cracked; however, an open crack was never formed as observed in the top corners of the box beam. Tensile or compressive fiber failure was not observed. Shear failure of the resin caused the ultimate failure of this section.

Static Test

Quasi-static tests were performed on both polyester and vinylester resin box-beams. One specimen of each type was tested. The setup for the experiment was identical to the impact experiment as far as the span, specimen support, and loading tap are concern. Displacement control was used to load the specimens. Transducers were placed on the top and the bottom surfaces of the specimens at the point of loading to obtain the load deflection behavior. Figures 2 and 3 show the load as a function of top deflection of the loading tub for box beams with polyester and vinylester resin respectively. The failure mechanism in the static tests was observed to be identical to that of the impact tests.

Dynamic Test

Results are presented for polyester single cell box beams impacted at different heights. The striker was raised to a height of $h=0.25, 0.5, 1.0, 1.5, 2.0, 2.5, 3.0,$ and 3.5 m to have different impact velocities. For the case of vinylester single cell box beams, the drop heights were $h=0.25, 1.0, 2.0,$ and 3.0 m. Figures 4, 6, 8, and 10 show the load for vinylester box beams, while figures 4 through 10 show the load for polyester box beams. As expected, the time required to reach the maximum load carrying capacity of these specimens was reduced as the input energy was increased. In all impact tests performed, the specimens fell off the support before any significant fiber failure. The failure was limited to shear failure of the matrix material only.

For the vinylester resin and drop heights greater than 1 m, two distinct peaks in the load versus time curves were observed. While, for polyester resin,

Impact Velocity $v=2.2$ (m/s)

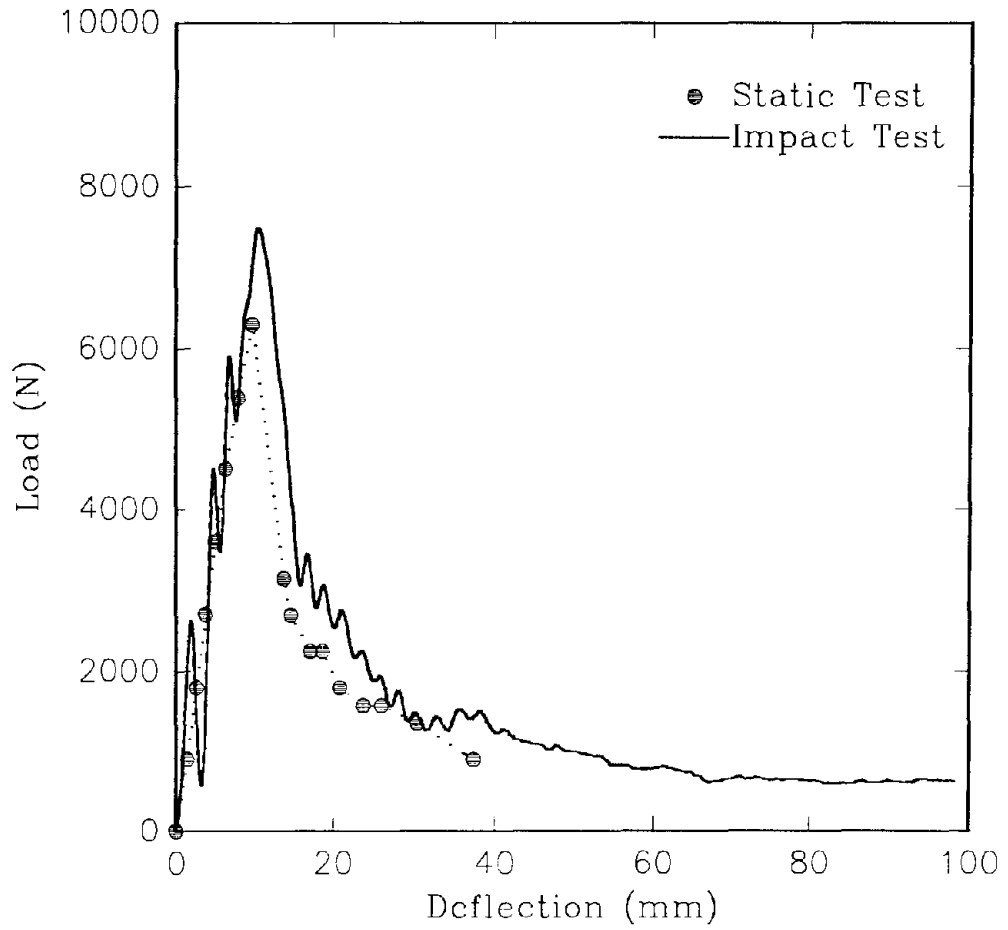


Figure 2. Static and impact test for polyester specimens.

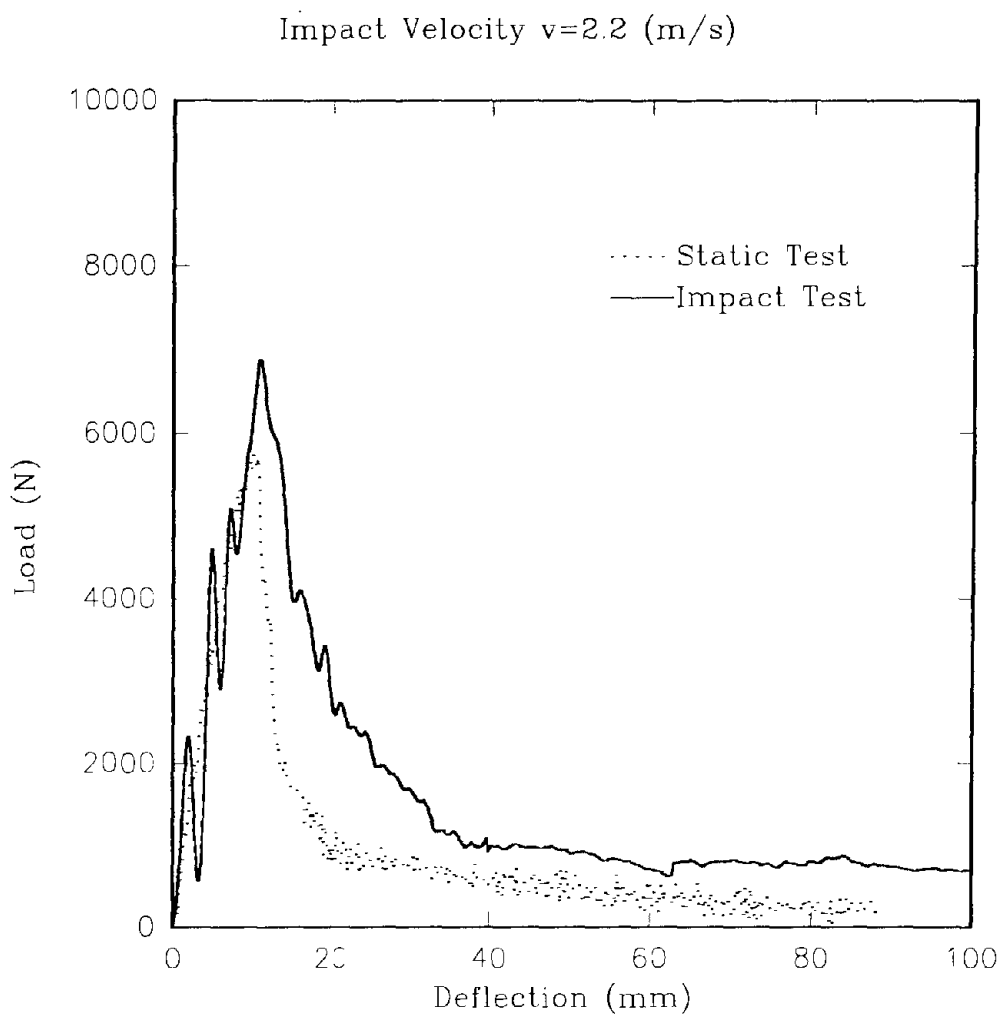


Figure 3. Static and impact test for vinyl ester specimens.

three distinct peaks were observed. From the analysis of the high-speed films of the impact event, it was observed that the first peak corresponded to a localized crushing of the edges of the box beams at the line of impact. The second peak corresponded to the initiation of buckling of the sides of the box beams. The subsequent peaks corresponded to the matrix cracking of the sides as these sides went more in buckling. From figures 4 to 10, it can be observed that the initial peak, for polyester resin, increased as the drop height increased. This was due to a combination of the inertial load (load required to bring the specimen to the same velocity as the striker) and the slight increase in the stiffness of the specimens because of the loading rate. This phenomenon was not observed for the vinylester resin. The first peak for the polyester resin specimens was the ultimate load when the drop heights were greater than 2 m. The maximum loads are plotted as a function of drop heights (including the static tests) for all specimens tested in figure 11. Figure 12 shows a specimen after impact.

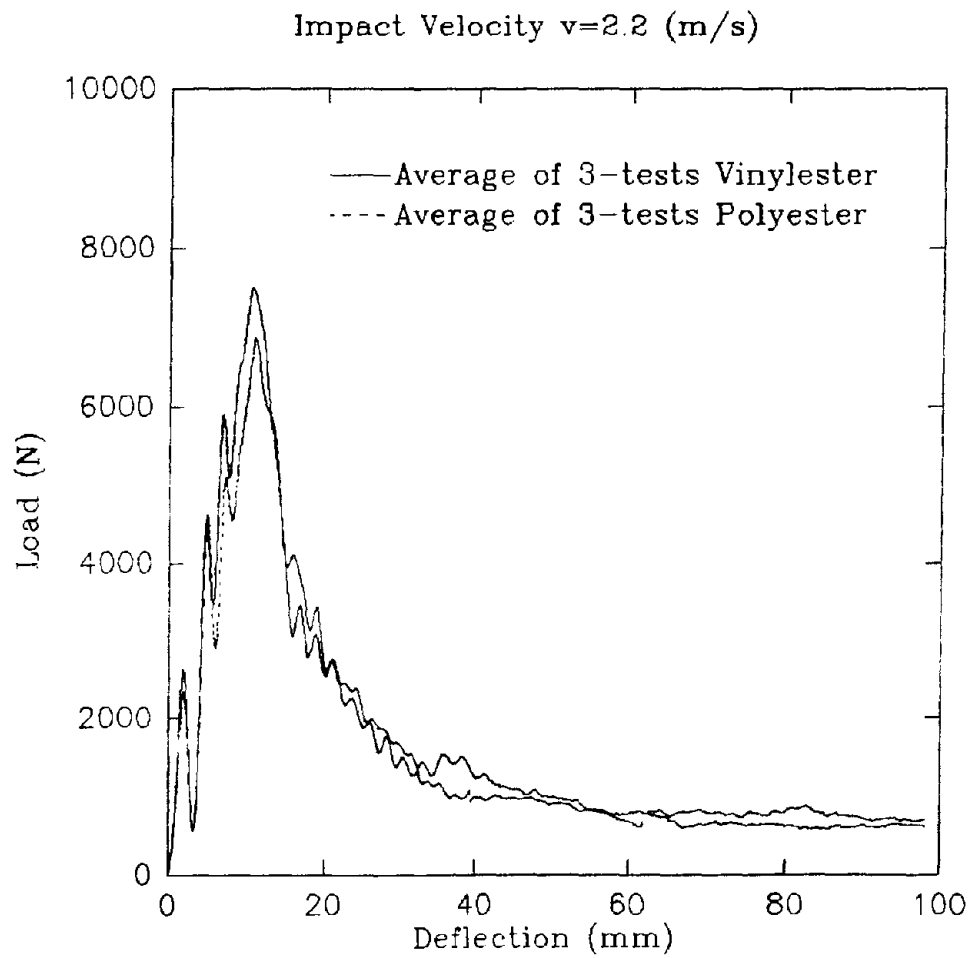


Figure 4. Impact load versus deflection, drop height $h=0.25$ m.

Impact Velocity $v=3.1$ (m/s)

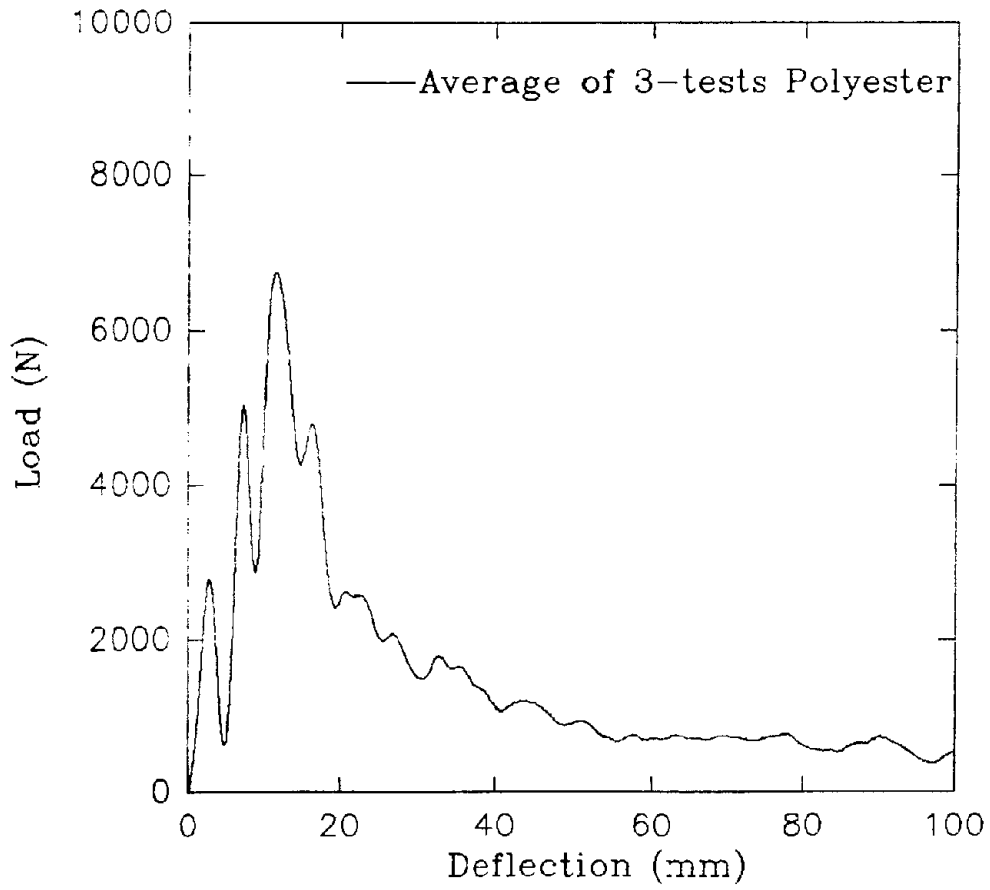


Figure 5. Impact load versus deflection, drop height $h=0.5$ m.

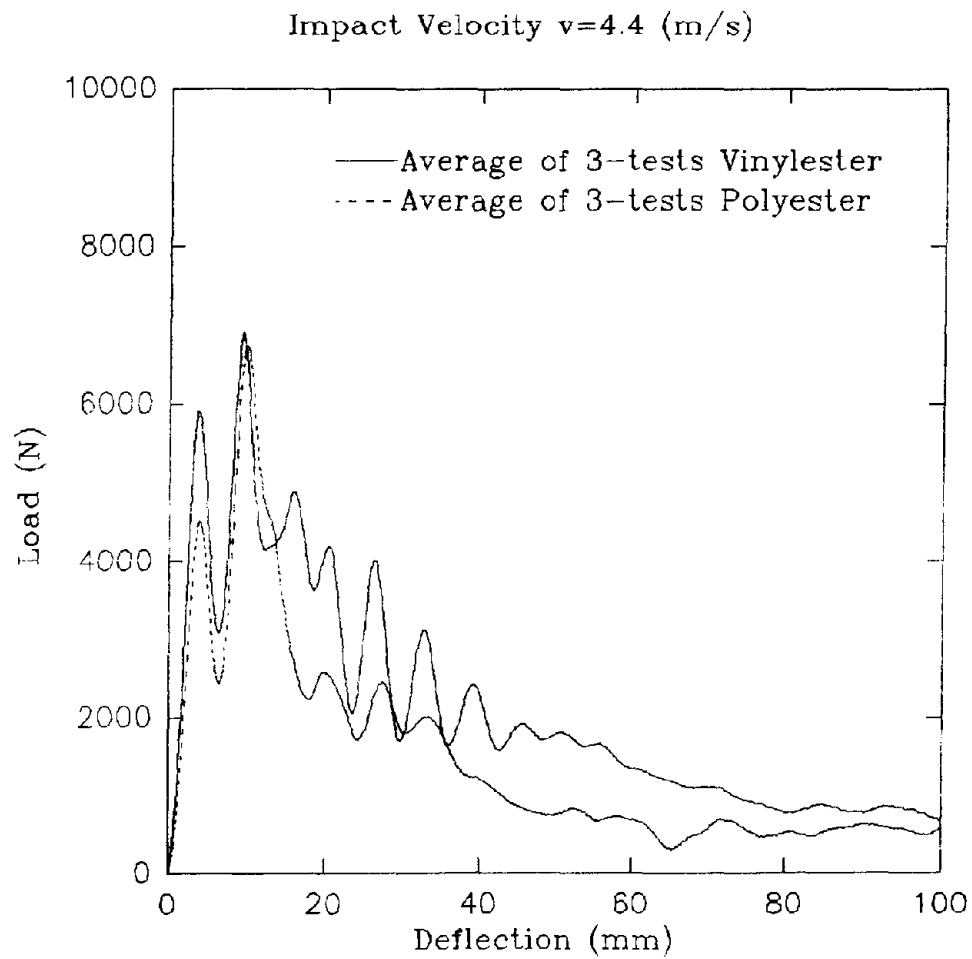


Figure 6. Impact load versus deflection, drop height $h=1.0$ m.

Impact Velocity $v=5.4$ (m/s)

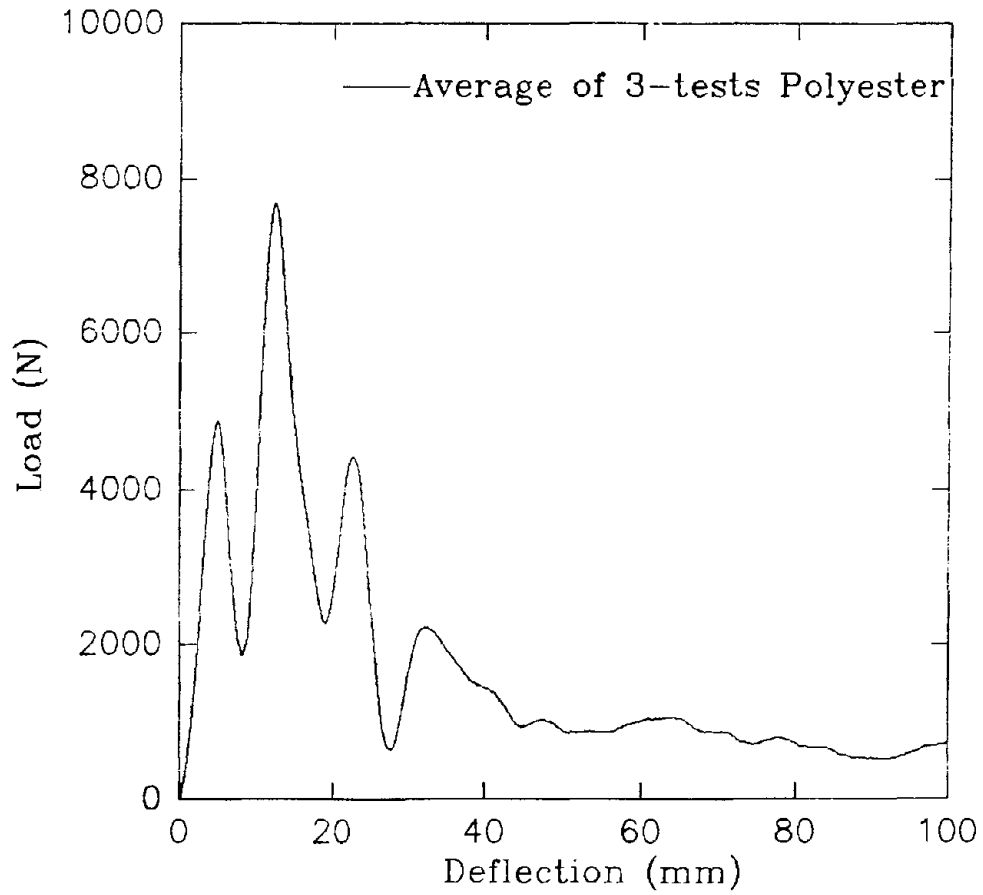


Figure 7. Impact load versus deflection, drop height $h=1.5$ m.

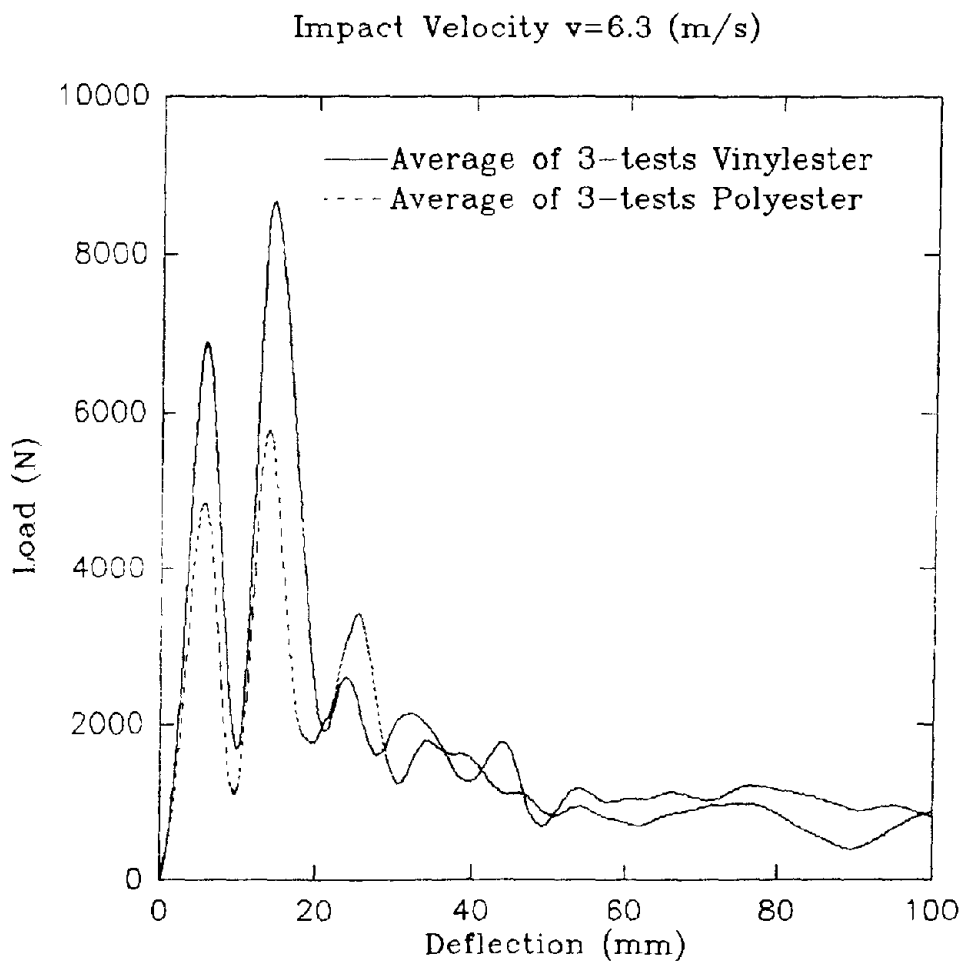


Figure 8. Impact load versus deflection, drop height $h=2.0$ m.

Impact Velocity $v=7.0$ (m/s)

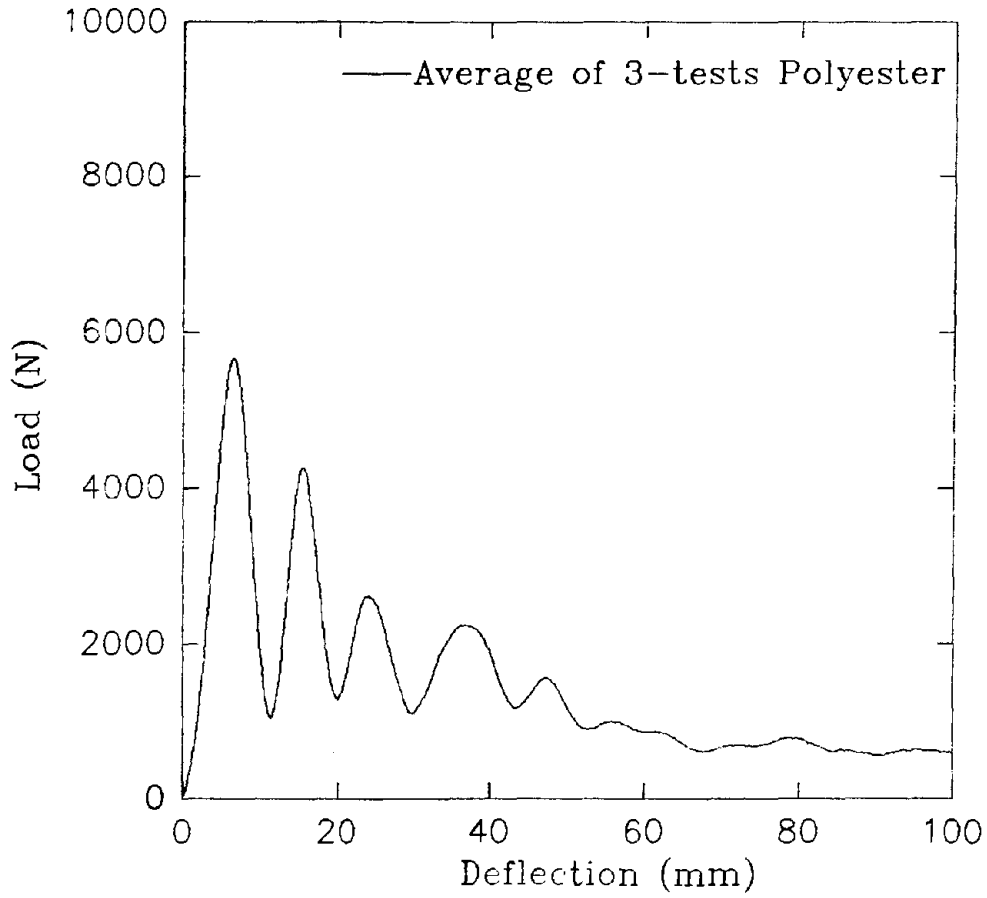


Figure 9. Impact load versus deflection, drop height $h=2.5$ m.

Impact Velocity $v=7.7$ (m/s)

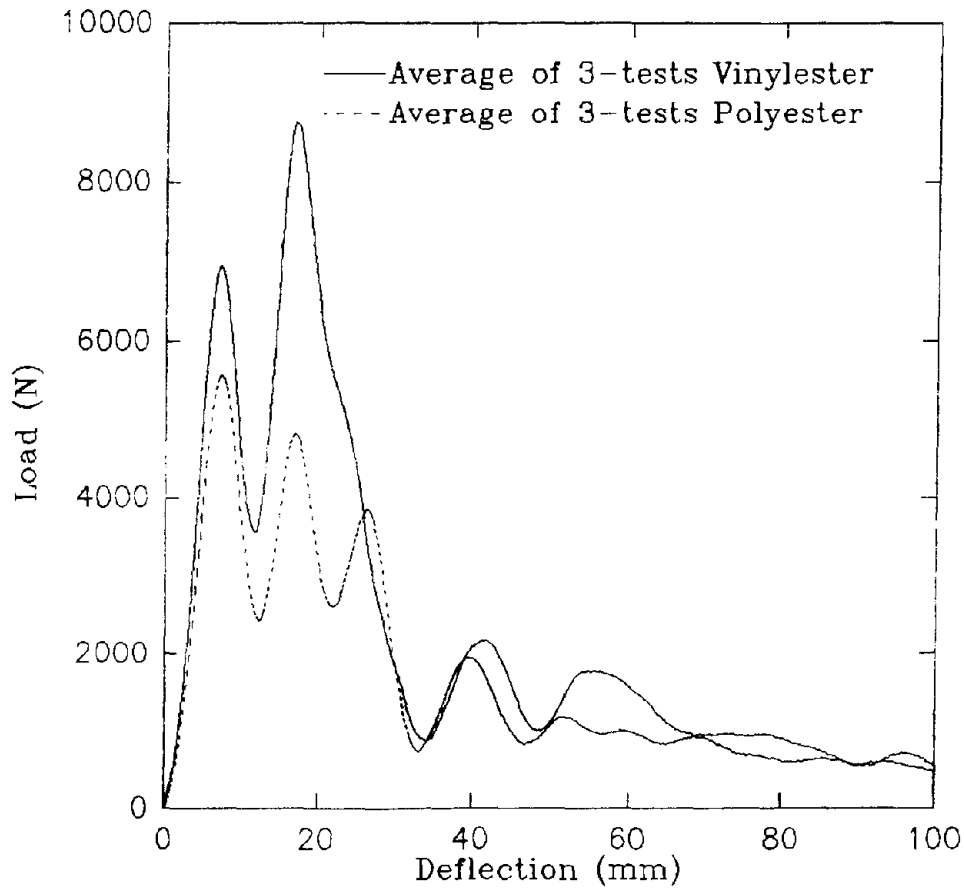


Figure 10. Impact load versus deflection, drop height $h=3.0$ m.

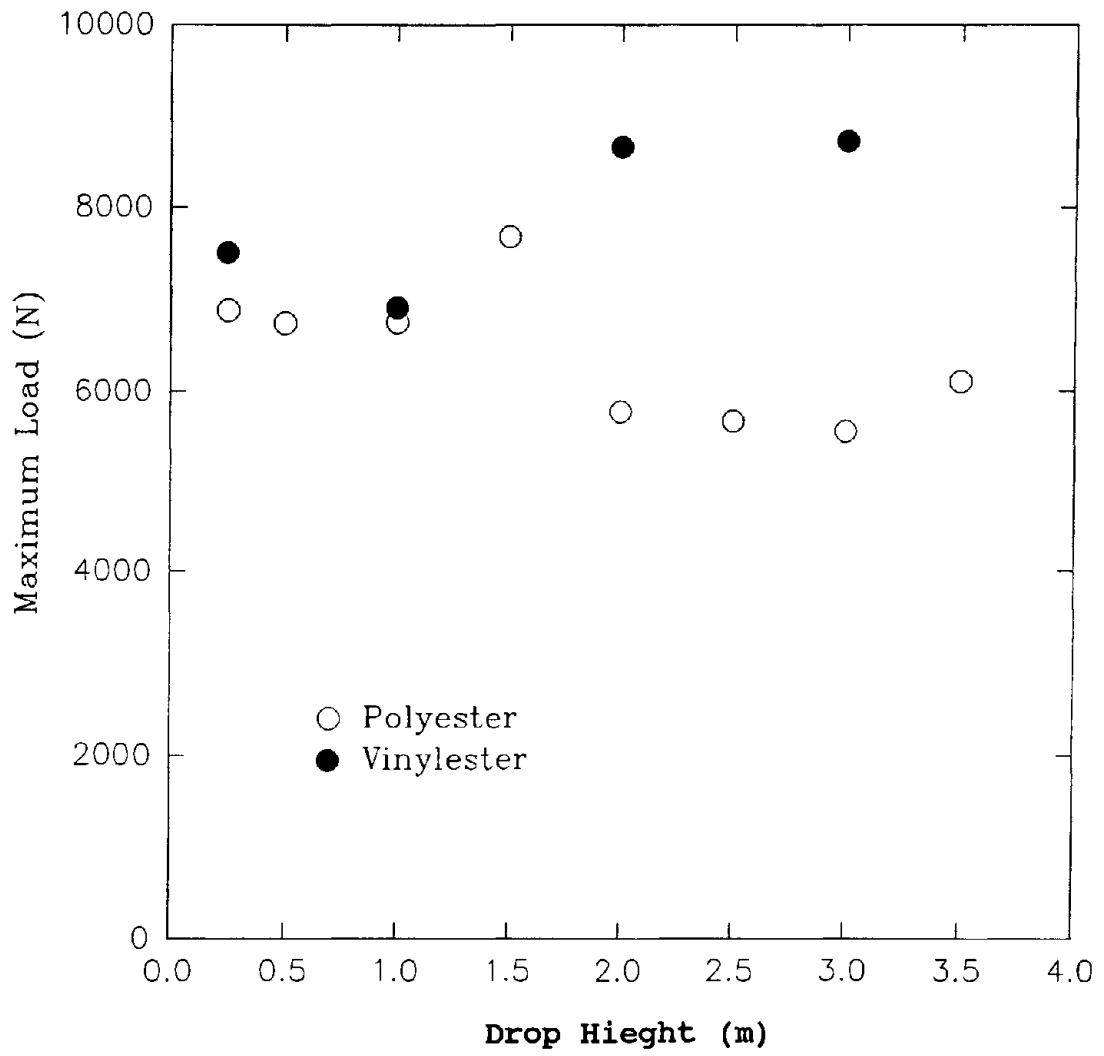


Figure 11. Maximum impact load versus drop height.

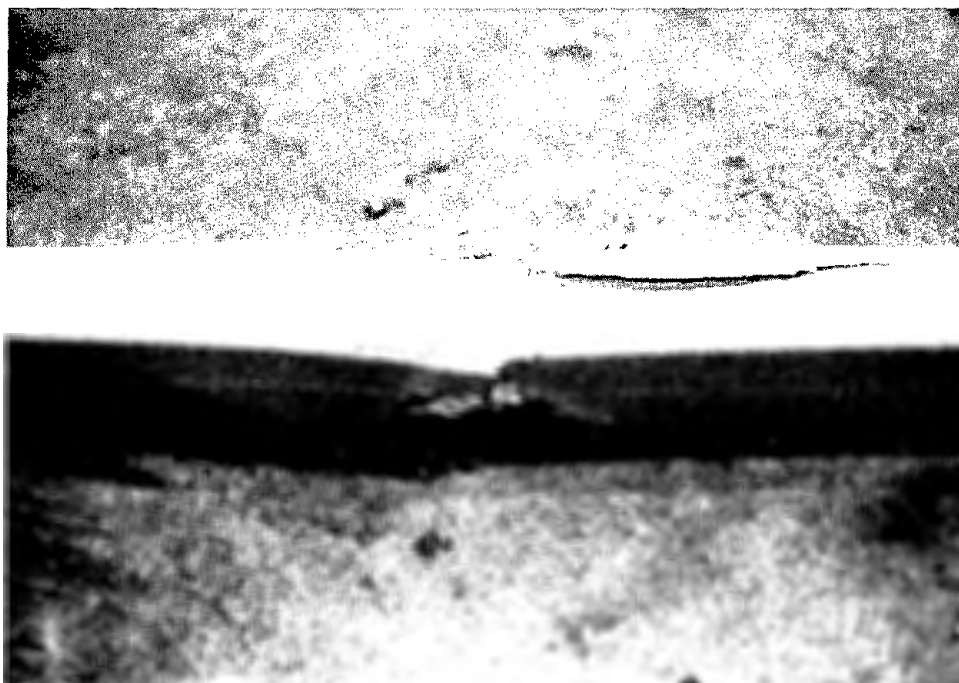


Figure 12. A specimen after an impact test.

Chapter 4. DISCUSSION AND CONCLUSION

One of the objectives of this study was to determine the failure mode of pultruded box beams impacted at the mid span. From the high speed films of the impact event, it was observed that only shear failure occurs. This was due to the test setup. The specimens slipped off the support long before significant fiber breakage occurred. To determine the suitability of these materials for highway safety barriers, a different test setup must be used so that the most important failure mode is obtained. In the modified test setup, the end connection must also be addressed. More fiber failure should be obtained before bearing or shear failure occurs at the end connections. The current study provided useful information about the bending stiffness of such pultruded box beams.

The ultimate load obtained by static tests was comparable to the one obtained by impact tests. Therefore, if a designer is interested in the ultimate load carrying capacity of these pultruded box beams, static test is sufficient. On the other hand, to determine the details for the load deflection or load time curves, an impact test is necessary.

Vinylester resin specimens carried more load in all impact velocities before ultimate failure. Note that the ultimate load, for both polyester and vinylester resin specimens, as a function of drop height did not vary as expected. It was expected that the ultimate load increases as the impact velocity increases. Part of this expectation was because of the fact that the inertial load increases as the impact speed increases. The ultimate load variation as a function of drop height was different for the two resin systems considered. The variation in the ultimate load as a function of impact velocity was more significant for the polyester specimens.

Part II: NUMERICAL SIMULATION

Chapter 5. INTRODUCTION

The Safety Design Division of the FHWA Turner-Fairbank Highway Research Center is actively involved in investigating the potential of fiber reinforced composite materials for use in highway safety structures. Particularly, guard rails are considered. For composite materials to be used in guard rails, an optimum fiber structure and section geometry (shape) need to be investigated. An experimental study of this magnitude where, geometry, stacking sequence, fiber orientation and resin type need to be optimized is costly and time consuming.

In past decades, most of such studies were performed experimentally and through an iterative process of design, build, test, redesign, and retest, until the product met a certain criteria. In the last decade, many computer codes based on finite element methods, for impact problems, have been developed. One of the most comprehensive and successful codes is DYNA3D. This explicit three-dimensional nonlinear finite element software was developed by the Lawrence Livermore National Laboratory. With the recent advancements in computer technology and the availability of cheap and efficient computational power, many of the current engineering problems and designs are tackled numerically. Numerical simulation is becoming one of the most important and powerful tools for today's engineers.

In the current study, DYNA3D is employed to simulate the full scale impact tests of guard rails conducted at the Federal Outdoor Impact Laboratory (FOIL). A test fixture exist at the FOIL for center impact of poles and wooden posts. This fixture is redesigned and modified for impact of guard rails. The design is suitable for regular guard rail posts and also can be used for composite posts that are larger in dimensions. Figure 13 shows the test fixture with the modifications and the additions. The test fixture is fabricated and installed by the Special Projects and Engineering Division at the FHWA.

A finite element model of the test fixture and the pendulum is developed. The model will be used to simulate the impact of 850 kg mass (pendulum) into a guard rail section. A simplified model is proposed to capture most of the behavior and the curtail elements of the impact. The objectives of this part of the study can be summarized by the following:

- Develop a finite element model of the pendulum-fixture of the FOIL.
- Perform stress analysis of the test fixture to predict and identify potential failure.
- Determine the feasibility of simulating a full-scale impact tests of guard rails made of isotropic and anisotropic materials.
- Identify the critical parameters governing a successful simulation of test fixture pendulum impact.

- Propose a simplified model that captures the impact behavior obtained by the full model.
- Test and simulation of the impact of steel rails serves as a baseline for behavior comparison with composite rails. Once a successful simulation is performed and the finite element model captures most of the impact behavior of guard rails, a parametric study can be conducted numerically to optimize the design parameters.

Initially, guard rails made of isotropic material are tested. Later, guard rails made of composite materials are going to be tested. The first test and numerical simulation is conducted for a single guard rail section mounted on the test pendulum-fixture. Next, multiple guard rail sections (three sections) are mounted and tested. This numerical simulation serves as part of the initial effort of developing roadside barriers made of composite materials.

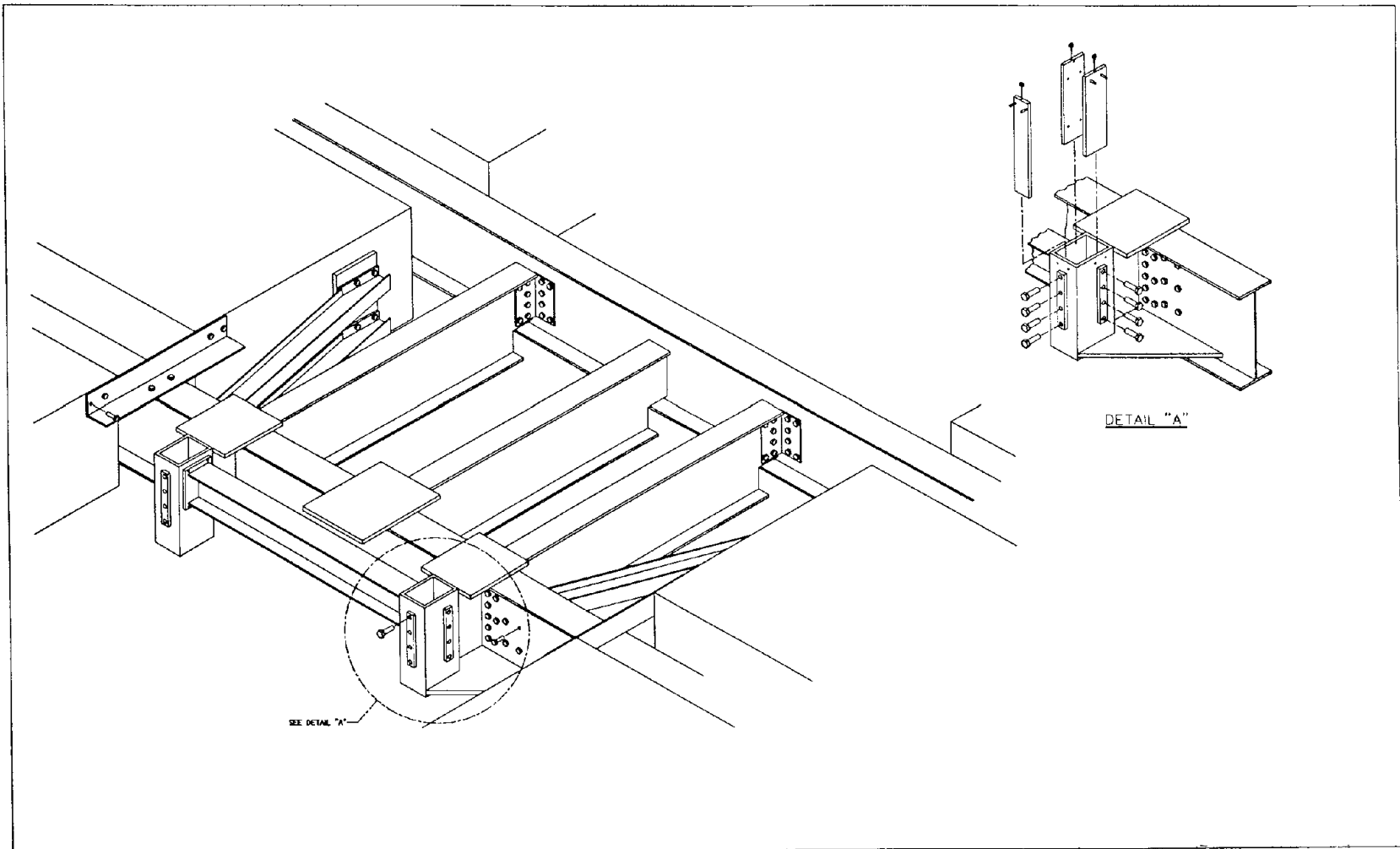


Figure 13. Test fixture assembly.

Chapter 6. FINITE ELEMENT MODEL

Fixture with a Single Rail Section

The finite element model is generated, for DYNA3D, using the preprocessor TruGrid, which is a commercial version of the preprocessor INGRID. The coordinate system is a right-handed system. The axis of impact is taken to be the opposite of the positive direction of the z-axis. The test pendulum-fixture model consists of 6,217 nodes, 200 beam (truss) elements, 3,615 shell elements, and 1,082 solid elements. Table 1 lists the pendulum-fixture model components, element type, and material type used for each part.

The finite element model consists of a single guard rail section mounted on a blockout which in turn connects to a post. The guard rail post assembly is housed in a box beam which is designed to hold steel posts as well as composite posts. Composite posts are larger in dimensions. To hold the steel posts, it is necessary to place spacers around the posts. The function of the spacers is to provide full support to the posts inside the box beam. Figure 14 shows one of the box beams with a vertical brace and bottom gusset. The vertical brace is welded to the back side of the box beam and to the front large I-beam. The bottom gusset is welded to the bottom and to the side of the box beam. Upon impacting the guard rail, the posts tend to bend backward, bend toward each other, and twist. In bending toward each other, the lower portion of the posts would move away in the opposite direction from the bending of the upper parts of the posts. Figure 15 shows the box-beam assembly with a cross beam. The vertical brace, bottom gusset, and cross-beam function are to resist backward bending, twist and outward bending, and inward bending respectively. The ends of the cross beam are merged to plates which in turn are tied to the sides of the box beams through a tied contact surface.

The guard rail post assembly is placed inside the box beam as shown in figure 16. The steel and wooden spacers, figure 17, are placed around the post as shown in figure 18. All spacers are modeled by solid elements. The front large I-beam is connected to the back large I-beam by three longitudinal braces. Four cross beams, two on the left side and the other two on the right side, are connected at an angle to the front large I-beam in one end and to the concrete base by the other end. The purpose of these cross beams is to provide additional support to the assembly. All beams and braces are modeled by shell elements.

The pendulum consists of three components: the nose, body, and cables. The nose of the pendulum is made of hard wood. The body of the pendulum is made of concrete. The pendulum is modeled by solid elements. The cables that hold the pendulum is modeled by beam (truss) elements. The truss elements used can resist tension only. They act as a mechanism with no resistance to axial compression. Gravity

has been applied on the entire structure. Figures 19 and 20 show a photograph of the pendulum and the finite element model respectively.

Two types of slide interface surfaces are used in the finite element model. The two slide interface surfaces are tied contact surface and contact surface with friction respectively. Contacting surfaces are identified by defining sets of nodes on one master and slave surfaces. The position of nodes on the slave surface are checked against the positions of the nodes on the master surface at each time step. If penetration is detected, the position is corrected and the proper forces are applied. A total of 14 contact surfaces are used. The identification of contact surfaces is based on intuition and observation of the simulation. Table 2 lists the contact surface definitions. Several assumptions are made in the development of the finite element model of the pendulum-fixture. Some of the assumptions are as follows:

- Parts are joined by merging adjacent nodes.
- Bolted joints are modeled by merging several nodes of the jointed parts.
- The cables that hold the pendulum are modeled by truss elements.
- Tied contact surfaces are used in merging parts with incompatible meshes.
- Parts connected to the concrete base structure are assumed to be fully constrained.

All material models used are elastic-plastic (type 3) except the guard rail and the cables. The mechanical properties are obtained from published literature. The material model for the guard rail is rate dependent elastic-plastic (type 24). The mechanical properties are obtained by altering some input parameter in a simulation attempt to match a tension test curve obtained by testing four specimens. The material model for the cable is elastic (type 1). The mass of the cables is taken to be small to ignore its inertia. The modulus of elasticity for the cable material is taken to be twice that of steel to prevent any elongation. Table 3 lists the mechanical properties for the material considered. Figure 21 shows the complete finite element model of the pendulum-fixture.

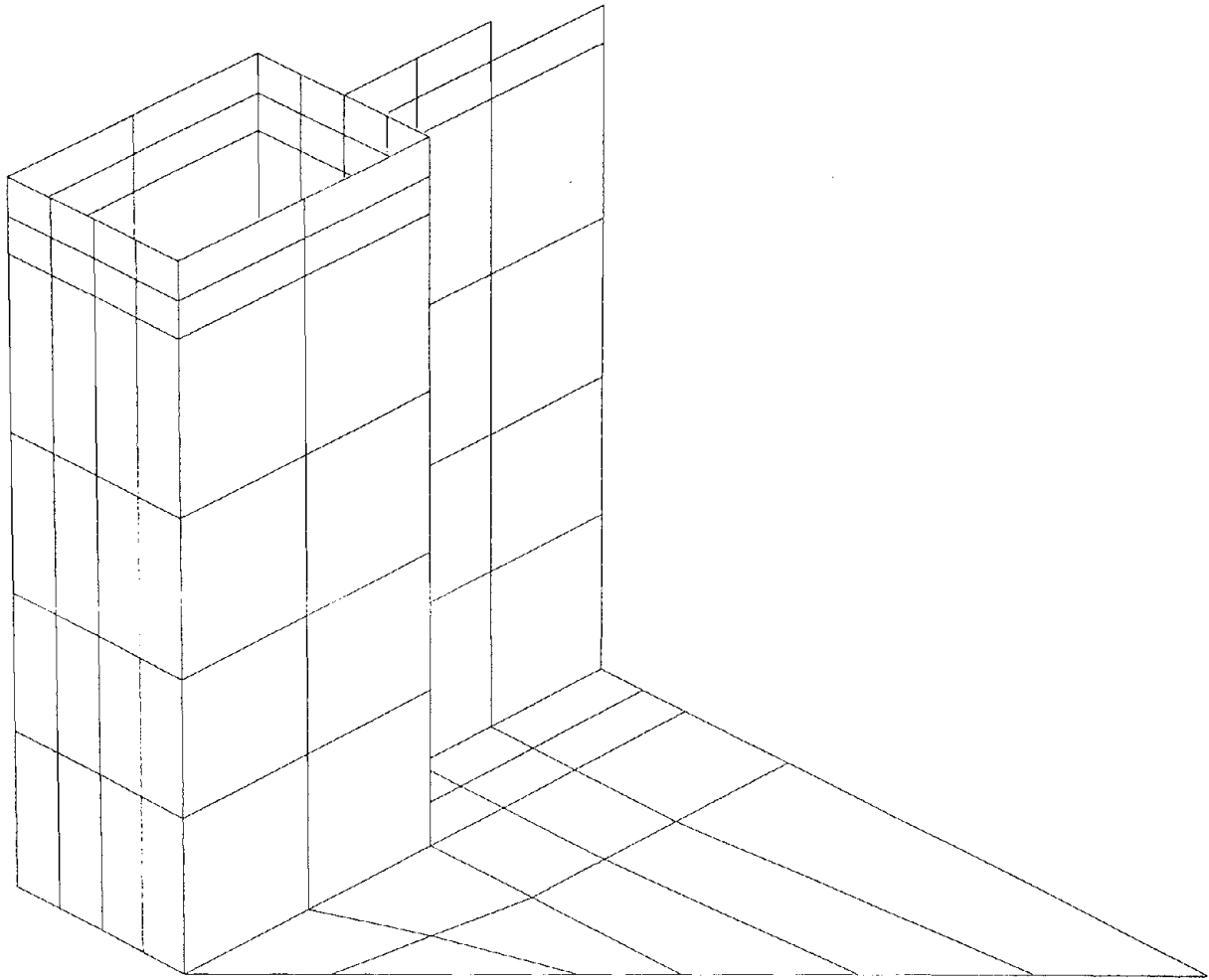
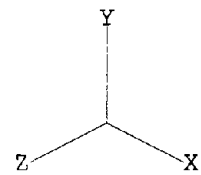


Figure 14. Box beam with vertical brace and gusset.



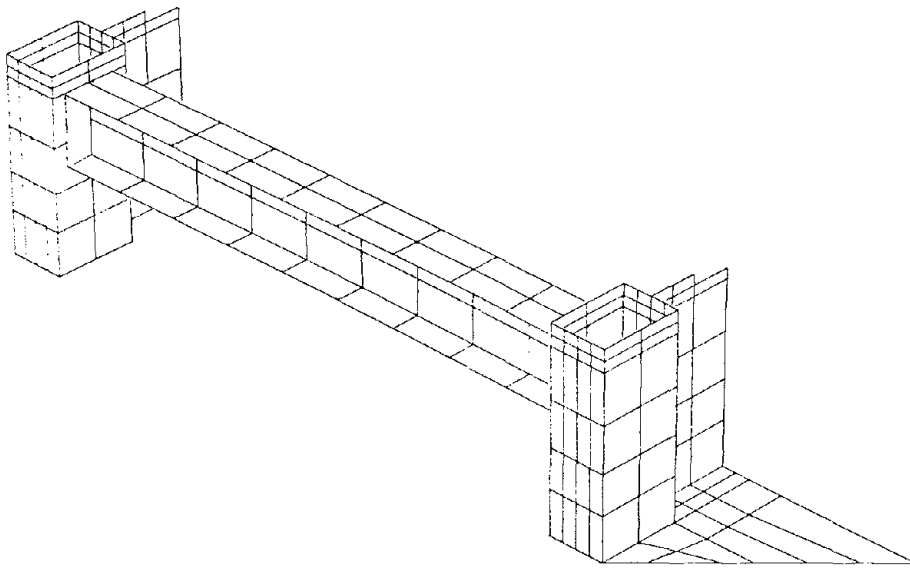
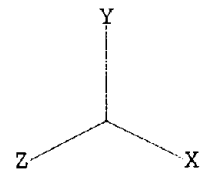


Figure 15. Box beam assembly with cross beam.



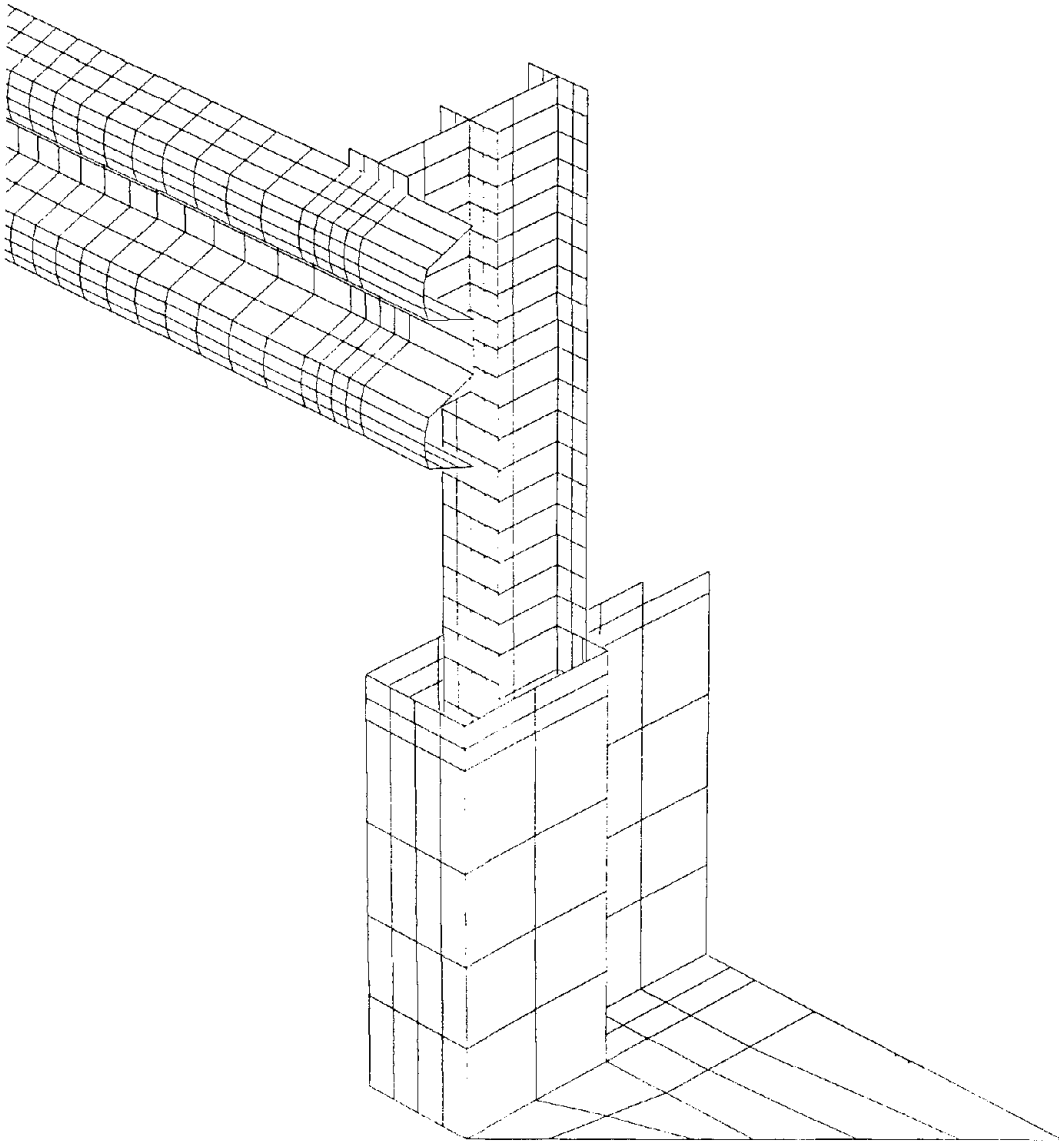
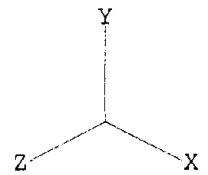


Figure 16. Guard rail post assembly.



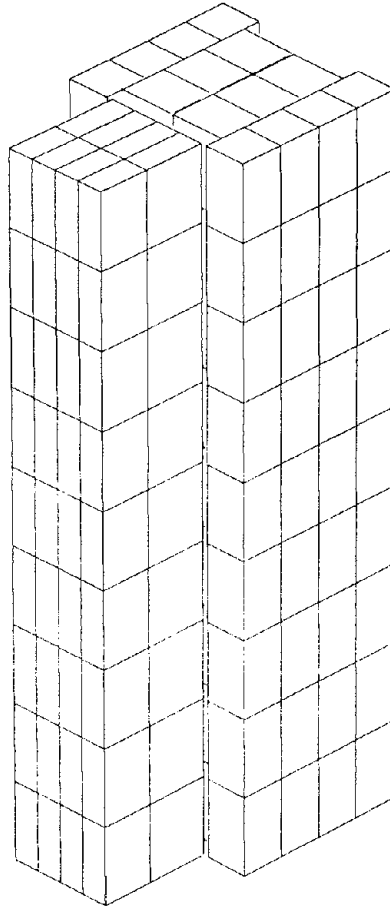


Figure 17. Steel and wooden spacers.

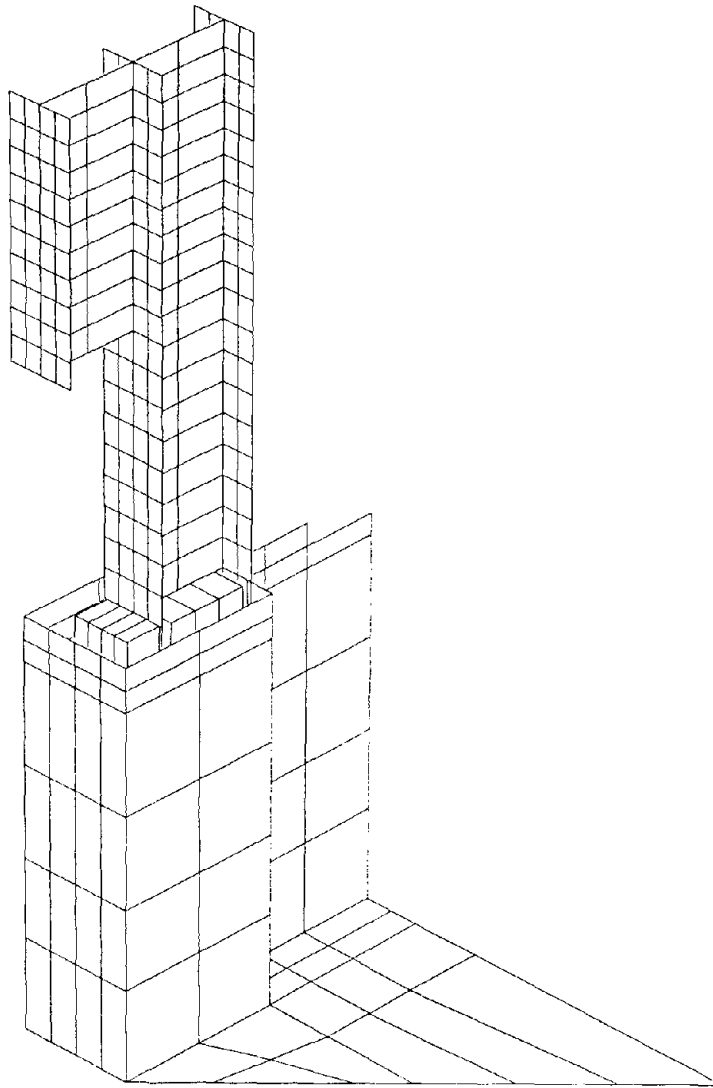
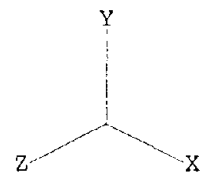


Figure 18. Spacers and post assembly.



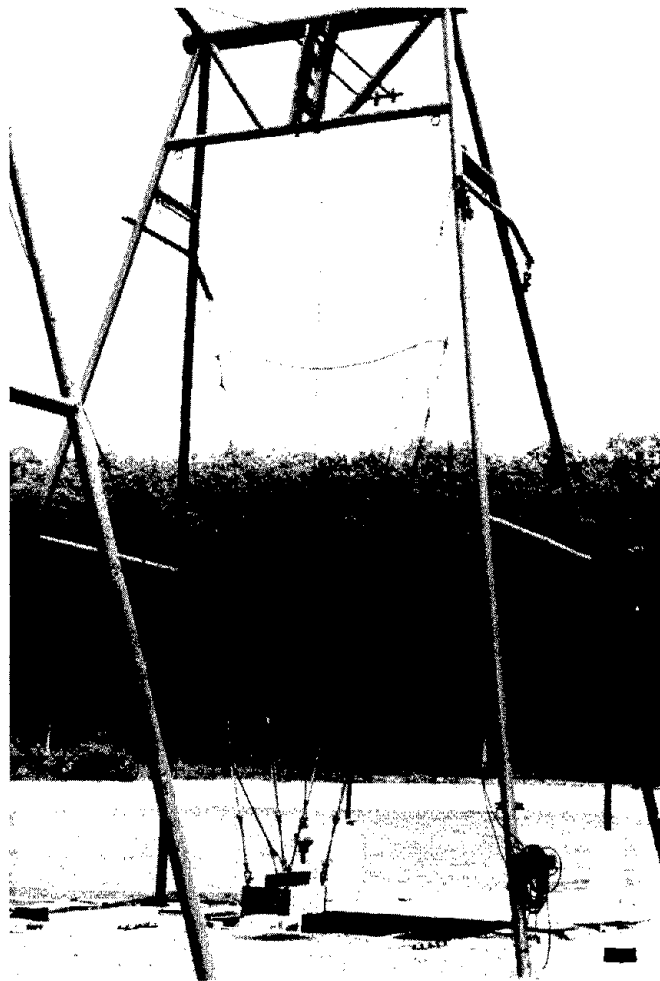


Figure 19. FOIL pendulum.

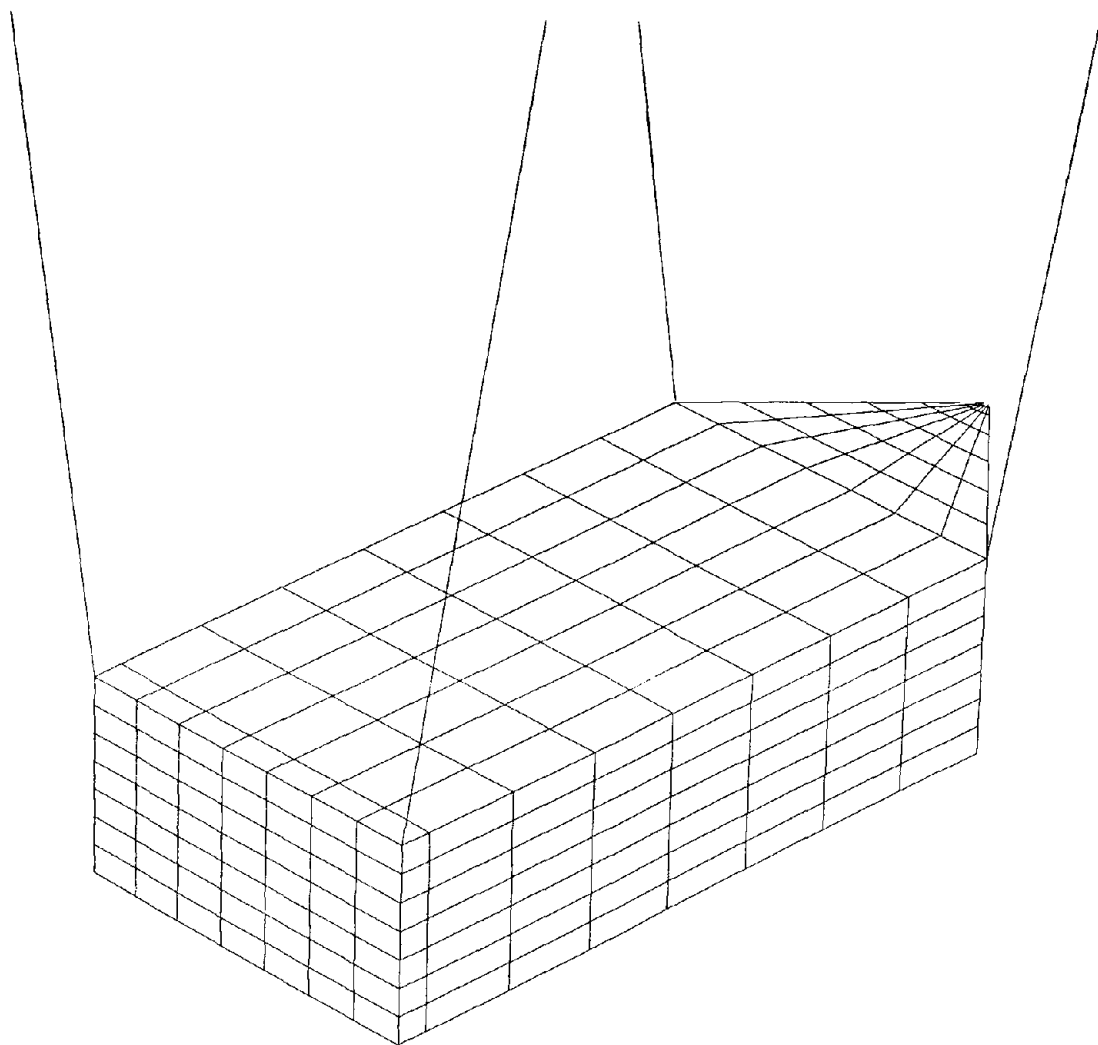
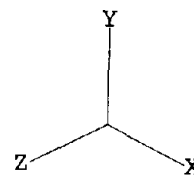


Figure 20. Finite element model of the pendulum.



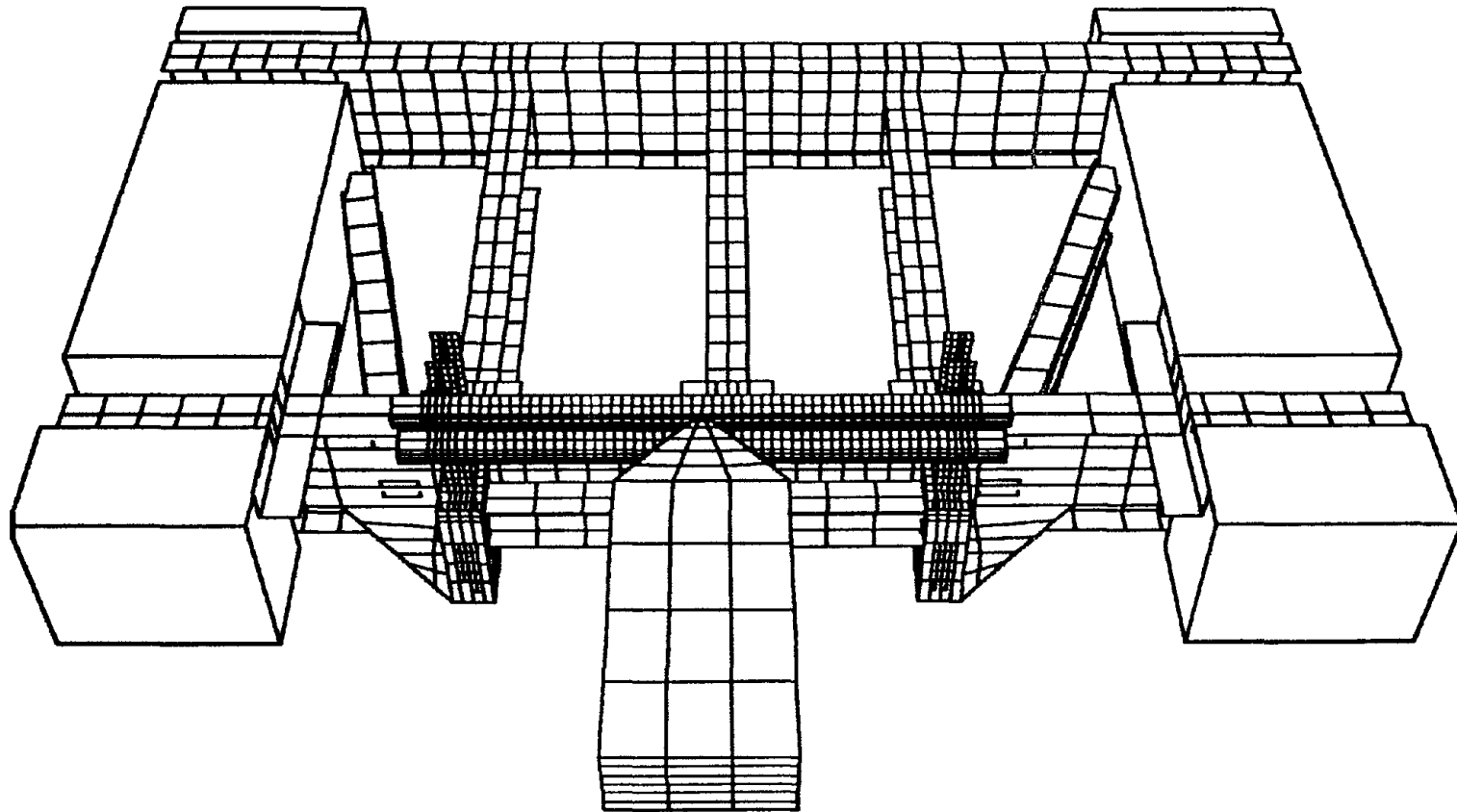


Figure 21. Finite element model of the pendulum fixture.

Table 1. Components of the finite element model.

Component	Element Type	Material Type
Front and Back Large I-Beam	Shell	Elastic-Plastic
Longitudunal Braces	Shell	Elastic-Plastic
Bottom Gussets	Shell	Elastic-Plastic
Vertical Braces	Shell	Elastic-Plastic
Post Holders (Box Beam)	Shell	Elastic-Plastic
Top Plates	Shell	Elastic-Plastic
Cross Beam	Shell	Elastic-Plastic
Left and Right Cross Beams	Shell	Elastic-Plastic
Guard Rail	Shell	Rate Depend. Elastic-Plastic
Posts and Blockouts	Shell	Elastic-Plastic
Wooden Spacers	Solid	Elastic-Plastic
Front Adjusting Plates	Solid	Elastic-Plastic
Side Adjusting Plates	Solid	Elastic-Plastic
Side Fixed Plates	Solid	Elastic-Plastic
Pendulum Head	Solid	Elastic-Plastic
Pdedulum	Solid	Elastic-Plastic
Cabels	Beam	Elastic

Table 2. Contact surface definitions.

Surface	Type	Slave	Master
1	6, dnt	Top Plate	Front I-Beam
2	6, dnt	Longitudunal Brace Head	Front I-Beam
3	6, dnt	Cross Beam Head	Post Holder
4	3, sv	Guard Rail	Blockout
5	3, sv	Guard Rail	Pendulum Head
6	3, sv	Post	Post Holder
7	3, sv	Front Adjusting Plate	Post Holder
8	3, sv	Right Fixed Plate	Post Holder
9	3, sv	Left Fixed Plate	Post Holder
10	3, sv	Wooden Spacer	Front Adjusting Plate
11	3, sv	Wooden Spacer	Post
12	3, sv	Side Wooden Spacer	Post
13	3, sv	Side Wooden Spacer	Side Fixed Plate
14	3, sv	Side Wooden Spacer	Post

Table 3. Mechanical properties of materials considered.

Material	E	v	Et	SIGMAy	EPS	Material Type
Wood	11.5e9	.20	11.5e6	50.e6	-----	3
Concrete	24.e9	.15	24.e6	10.e6	-----	3
Steel, EP	200.e9	.33	200.e6	260.e6	-----	3
Steel, REP	200.e9	.33	-----	(345-415)e6	.0-.66	24

EP = Elastic Plastic

REP = Rate Dependent Elastic Plastic

EPS= Effective Plastic Strain

Fixture with Multiple Rail Sections

Full-scale tests must be very close to the service conditions of the guard rails. Therefore, it is essential that multiple sections be tested and numerically simulated to reduce the unrealistic twist and deformation in the posts. The finite element model of the pendulum-fixture with multiple-rail sections (three sections) is shown in figure 22. The finite element model consists of 7,587 nodes, 200 beam (truss) elements, 4,955 shell elements, and 1,082 solid elements. A fine mesh is assigned to the middle rail section where the impact occurs; while a cross mesh is assigned to the other two sections. As in the single section model, the intermediate posts are mounted on the fixture inside the post holders. The two outer posts are considered to be imbedded in a concrete structure and therefore assumed to be completely fixed. This model is not yet a good representation of the reality where an infinite number of guard rail sections are the bounds of the guard rail section impacted by an object. It is very difficult and may be impossible to have an infinite number of guard rail sections. A better representation would be to connect the middle portions of the two bound guard rails to the outer posts by cables. This technique have been used in end terminals to simulate the infinite boundary condition which in this case, has an infinite number of guard rail sections.

Simplified Model

The technique in generating a finite element model of a structure is sometimes an art rather than an exact science. The question of the number of nodes or elements used to obtain the proper response has always faced engineers since the use of finite element analysis. Is a fewer number of nodes (or elements) and consequently less detailed mesh adequate to capture the behavior of a structure under loading? Or is it more appropriate to have a more detailed mesh in which the computer run time is more and the numerical error propagation is significant? This question is addressed for this particular finite element model. Figure 23 shows the simplified model. The finite element model consists of 4,498 nodes, 200 beam (truss) elements, 2,186 shell elements, and 1,082 solid elements. This model basically has the same mesh for the pendulum, guard rail, posts and blockouts, cross beam, post holders, and spacers. By observing the full model in figure 21, one can see that the post holders are connected to the rest of the model by the vertical braces at the back side and by the bottom triangular gussets. Therefore, in the simplified model, it is assumed that the back sides of the post holders are completely fixed (rigid). Also, it is assumed that the lower edges

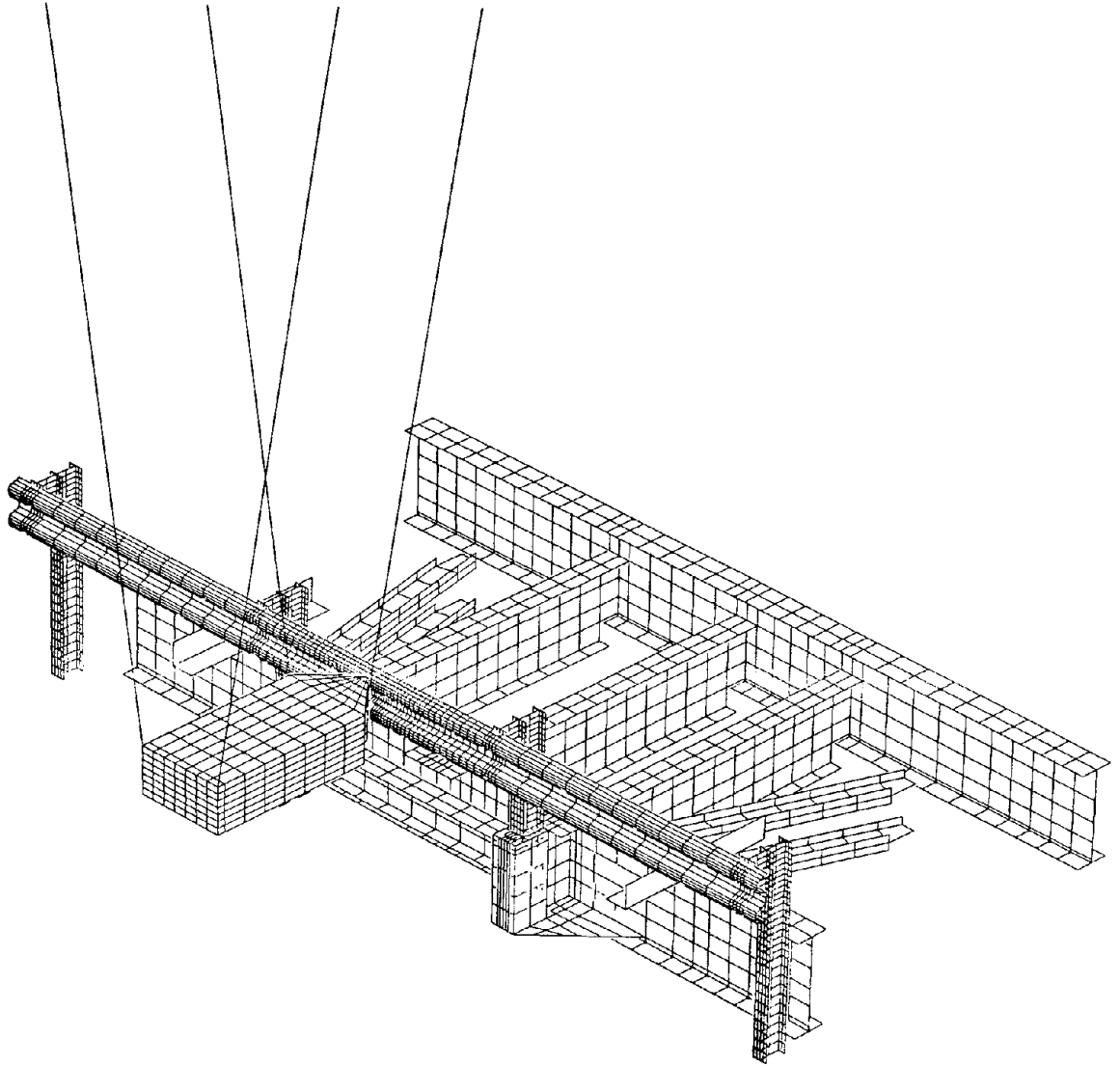
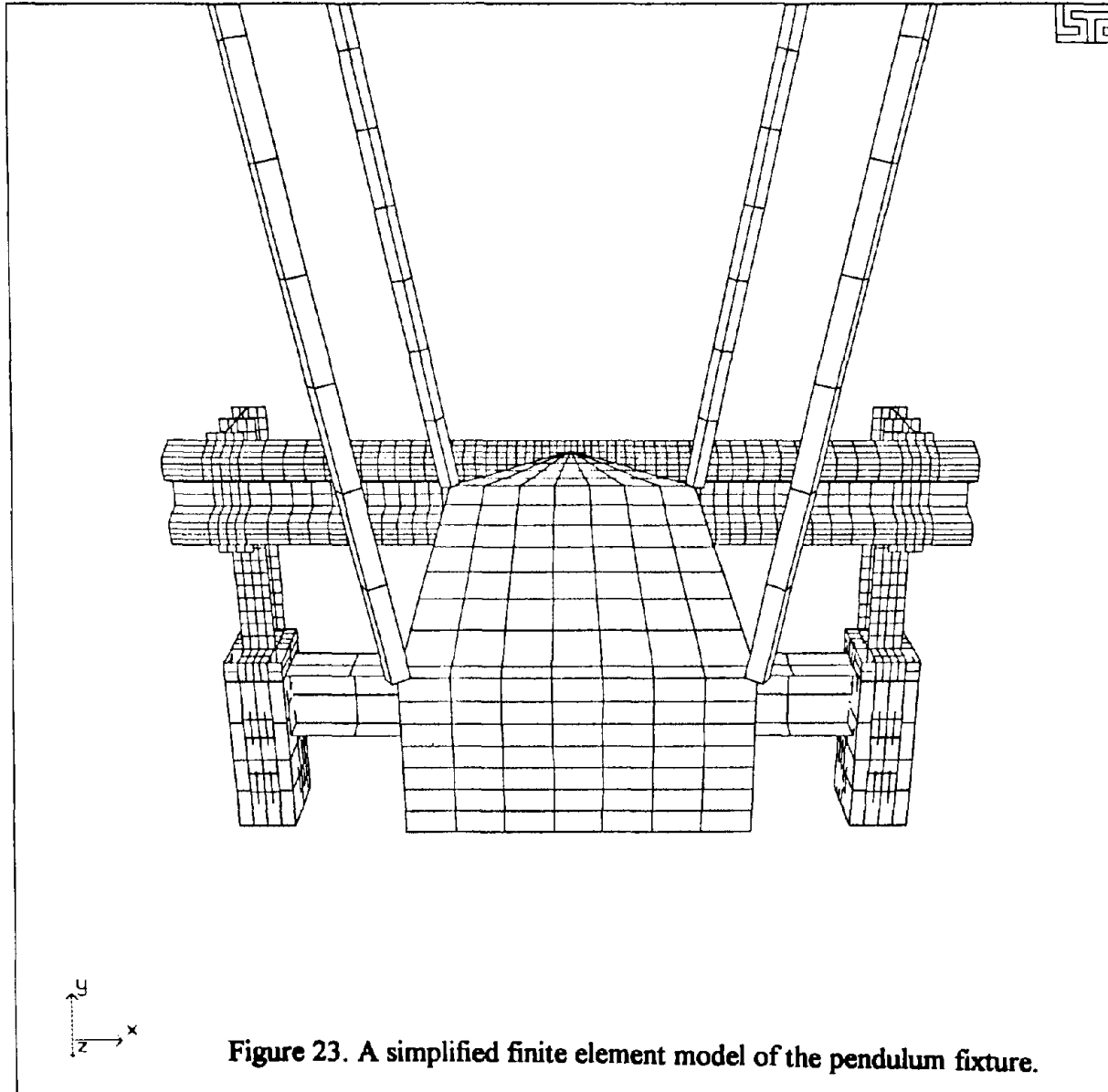


Figure 22. Finite element model of the pendulum fixture with three rail sections.

of the out sides of the post holders are completely fixed. The objective here is to determine if the simplified model would capture most of the behavior of the guard rail and the impact scenario as compared to the full model.



Chapter 7. TESTS AND NUMERICAL SIMULATION

Stress Analysis

The fixture for pendulum impact is designed based on experience and sound judgment. Some stress analysis and design iterations were performed using the finite element code NISA. Parts of the structure that were thought to carry a significant impact force were strengthened. Fortunately, the large-scale finite element modeling takes advantage of modern digital computers to provide numerical solutions of the principal stresses for virtually any design configuration under any loading condition. For this study, the finite element model of the test fixture was considered for stress analysis. The stress analysis is performed to identify the high stress concentration areas. These areas will be strain gauged for verifications of the numerical values obtained by the finite element model. Figure 24 shows the strain gauge rosettes mounted on the fixture. Perhaps the only absolutely positive way of determining whether a material can sustain a particular combination of principal stresses without undergoing plastic deformation or fracture is by experimental verification. Unfortunately, many combinations of stresses are possible, and tests of all of them are impractical. As an alternative, many qualitative models have been developed to predict the onset of permanent deformation and failure. These models are the so-called failure criteria.

Several failure criteria have been used, by engineers, for brittle materials like Rankine and all materials like Tresca. Of all the failure models, the Von Mises failure criteria has the best correlation with the experimental results from tests on ductile materials subjected to combined stresses. On the other hand, the Tresca failure criterion is considered to be conservative. Except for the special cases of uniaxial and hydrostatic stress states, it will usually predict failure at moderately lower values of principal stresses than are found experimentally.

The Tresca criterion, based on maximum shear theory, predicts yielding will occur when the maximum shear stress in any plane reaches the value of the maximum shear stress occurring under simple tension. Yielding will occur when any one of the following three conditions is reached:

$$(S_1 - S_2) = S_y$$

$$(S_1 - S_3) = S_y$$

$$(S_2 - S_3) = S_y$$

The Von Mises yield criterion is based on distortion energy in which it assumes that yielding begins when the distortion energy equals the distortion energy at yield in simple tension. The yield condition is :

$$(S_1-S_3)^2+(S_3-S_2)^2+(S_1-S_2)^2=2S_y^2$$

Figure 25 show an isoparametric view of the fixture with critical points labeled one to nine. Contour plots of stresses, principal stresses, and maximum shear stresses are obtained using the post processor TAURUS (developed by the Lawrence Livermore National Laboratory). The stresses are collected every 20 ms. The range of time considered is 5 to 185 ms. It was found, from the fringe plots, that the highest stresses occur at 145 ms. Table 3 lists the magnitude of the principal stresses at the locations considered on the fixture.

The location of point 3 has the highest stress concentration relative to other locations of the fixture. Due to the unsymmetry in the fixture (the center line of the pendulum is 10 cm with respect to the center line of the fixture), the stress distribution is not symmetric. This location is inside the post holder where the upper portion of the posts contact the inside surface of the post holder. The stresses are higher at this location because of intense interaction and load transfer. Strain gauge rosettes are placed at locations 2 and 8, see figure 25, and strain history is collected. The strains are used to calculate the principal strains and principal stresses. The location of point 3 is chosen to perform failure analysis and to determine the safety factor. Using the three principal stresses at point 3 and the Trasca yield criterion, it is found that the safety factor is about 3.8. On the other hand, the Von Mises yield criterion, which is more accurate for ductile materials, yields a safety factor of about 2.2. The strain history for the impact event was collected using strain rosettes by a data acquisition system. The principal strains were calculated using standard handbook tables. It was observed that maximum principal strains were significantly below the strains for the onset of material yield strains.

Tests

Three tests were conducted on a single rail section at the FOIL in McLean, Virginia. The pendulum is raised to a height that would give an impact velocity of 35 km/h. The pendulum was then released to impact the rail sections at the center. Two accelerometers are positioned at the center back of the pendulum. Accelerometer data is collected a few moments before impact, and data collection continued until the pendulum came to rest. A speed trap instrument is positioned just before impact to capture the speed of the pendulum at the moment of impact for verification.

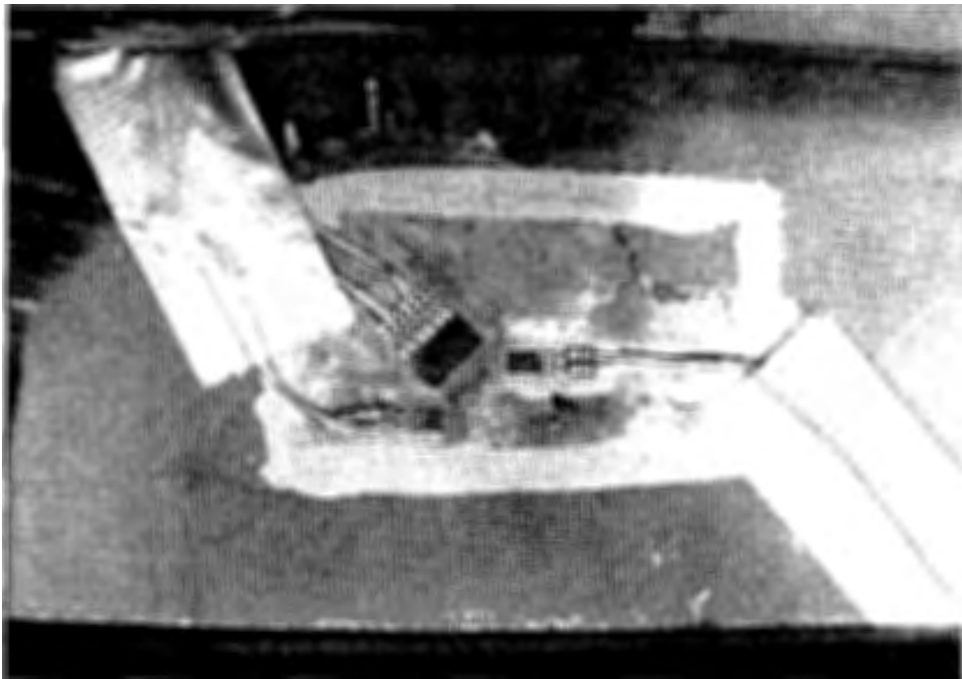


Figure 24. Strain gauge rosettes.

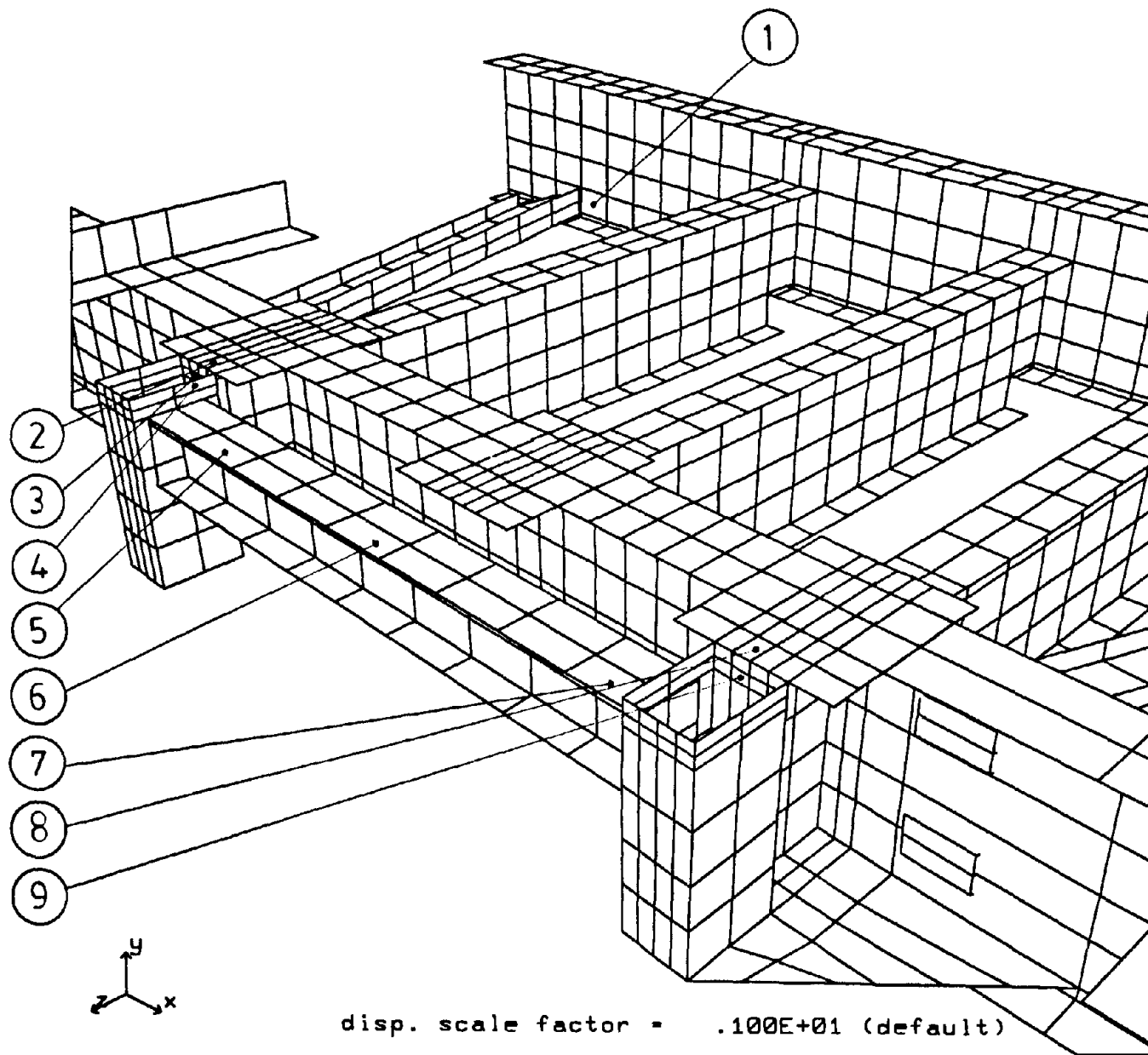


Figure 25. Isoparametric view of a fixture.

Table 4. Principal stresses (N/m²) at time t=145 (ms).

Point	SIGMA-1	SIGMA-2	SIGMA-3
1	-7.86e5_4.29e6	-1.79e6_5.82e5	-3.27e6_3.33e5
2	2.45e7_2.96e7	-1.79e6_-4.14e6	-1.41e7_-1.76e7
3	3.98e7	9.86e6	-2.79e7
4	1.95e7_2.45e7	2.96e6_3.29e6	-1.04e7_-1.41e7
5	-7.86e5_4.29e6	-1.79e6_5.82e5	-1.41e7_1.76e7
6	-7.86e5_4.29e6	-1.79e6_5.82e5	-1.04e7_-1.41e7
7	-7.86e5_4.29e6	-1.79e6_5.82e5	-3.27e6_-8.87e6
8	9.36e6_1.44e7	-4.17e6_-6.54e6	-1.76e7_-2.12e7
9	2.96e7_3.37e7	3.39e6_7.71e6	-8.87e6_-1.04e7

The pendulum motion is a long and circular arc. The center of the arc is some place between the four point of constrains of the cables to the tower. As the pendulum impacted the rail section and moved forward, it raised up because of the constrains of the cables. At 140 ms, the lower edge of the front surface of the pendulum raised to the center line of the rail section. At approximately 200 ms, the pendulum climbed the rail section and was no longer in contact with the pendulum. In all tests, the upper edge of the rail sections teared. The bolts that mount the rail section to the blockout did not fail. Because of the upward motion of the pendulum, the loading was no longer symmetric on the rail. Only 140 ms of the event, was considered to be appropriate as a base line. This base line will be used to compare with the behavior of the composite guard rail. The accelerometer output is filtered at 300 Hz. The filtered data is then imported to a LOUITS spreadsheet. A numerical integration is performed to obtain the corresponding velocity and displacements. Figures 26 and 27 show the displacement and the velocity, as a function of time, of the three rail sections respectively.

Simulation

The DYNA3D finite element models run on an IBM work station. Four nodes where used to collect kinematic variables (displacement, velocity, and acceleration). The postprocessor TAURUS is used to obtain these variables. The time interval for output of these variables was the same as that of the actual impact tests. The location of these nodes in the finite element model where taken to be very close to the position of the accelerometers at the back of the pendulum. The kinematic variables for the four nodes are averaged. These kinematic results are filtered, at 300 Hz, using the same filter used for the raw data from the impact tests.

Figures 28, 29, and 30 show the acceleration in meters per second squared for single section rail, simplified model, and multiple rails respectively. The entire simulated event of 200 ms are presented in these figures. Figures 31 to 37 and 38 to 44 show the progressive impact event obtained from the postprocessor for single section rail. The deformed shape of the rail in the finite element model simulation was identical to that of the impact tests. The finite element model indicated failure of some elements at the center upper edge of the rail. The failure location in the model was the same as observed in the tests. The average displacement of the three impact tests is compared to the DYNA3D simulation in figure 45. The average velocity and the velocity obtained from the simulation is shown in figure 46. In general, velocities and displacements obtained from simulation are very close to impact tests as in this case. A good

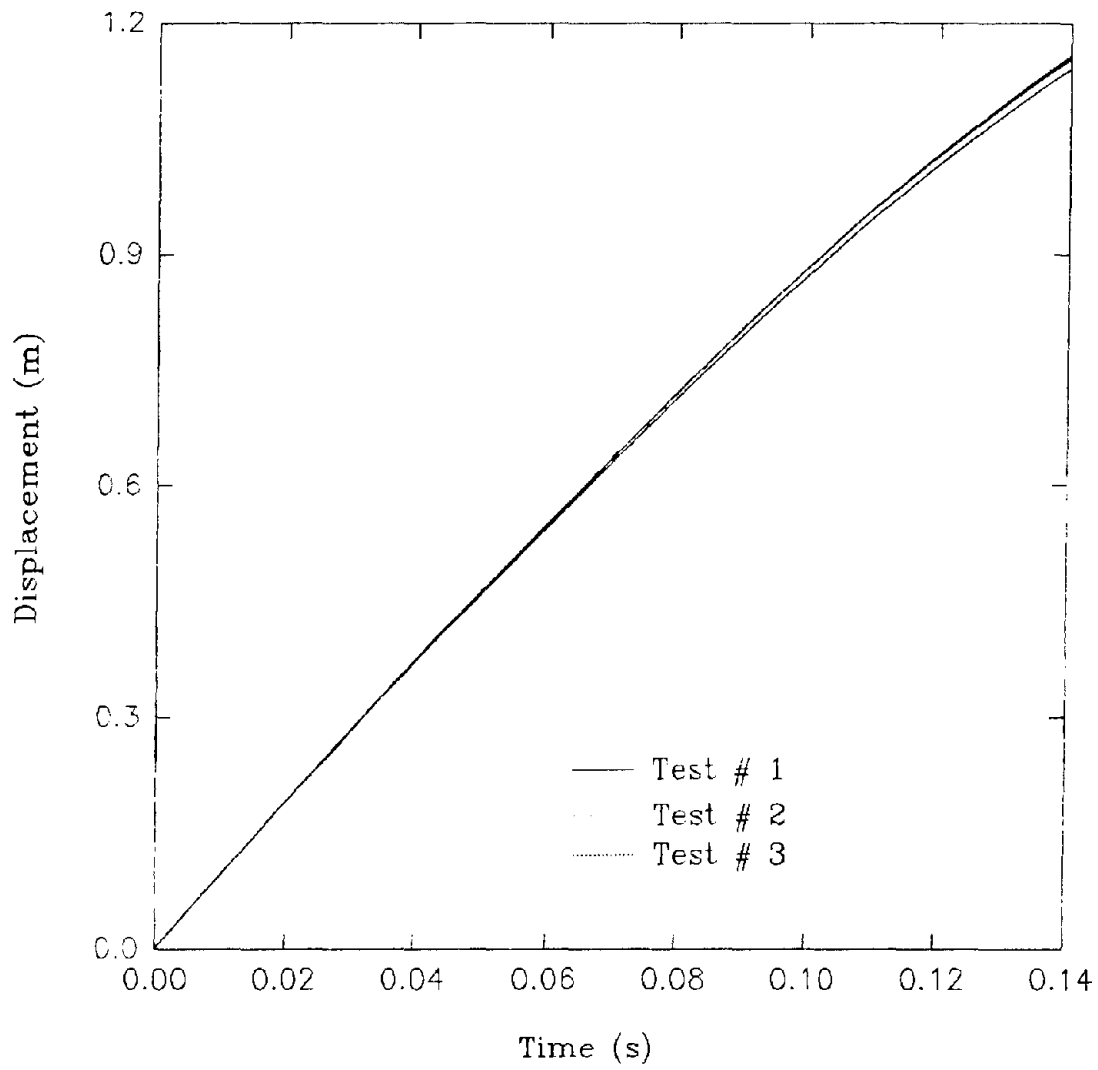


Figure 26. Pendulum displacement versus time.

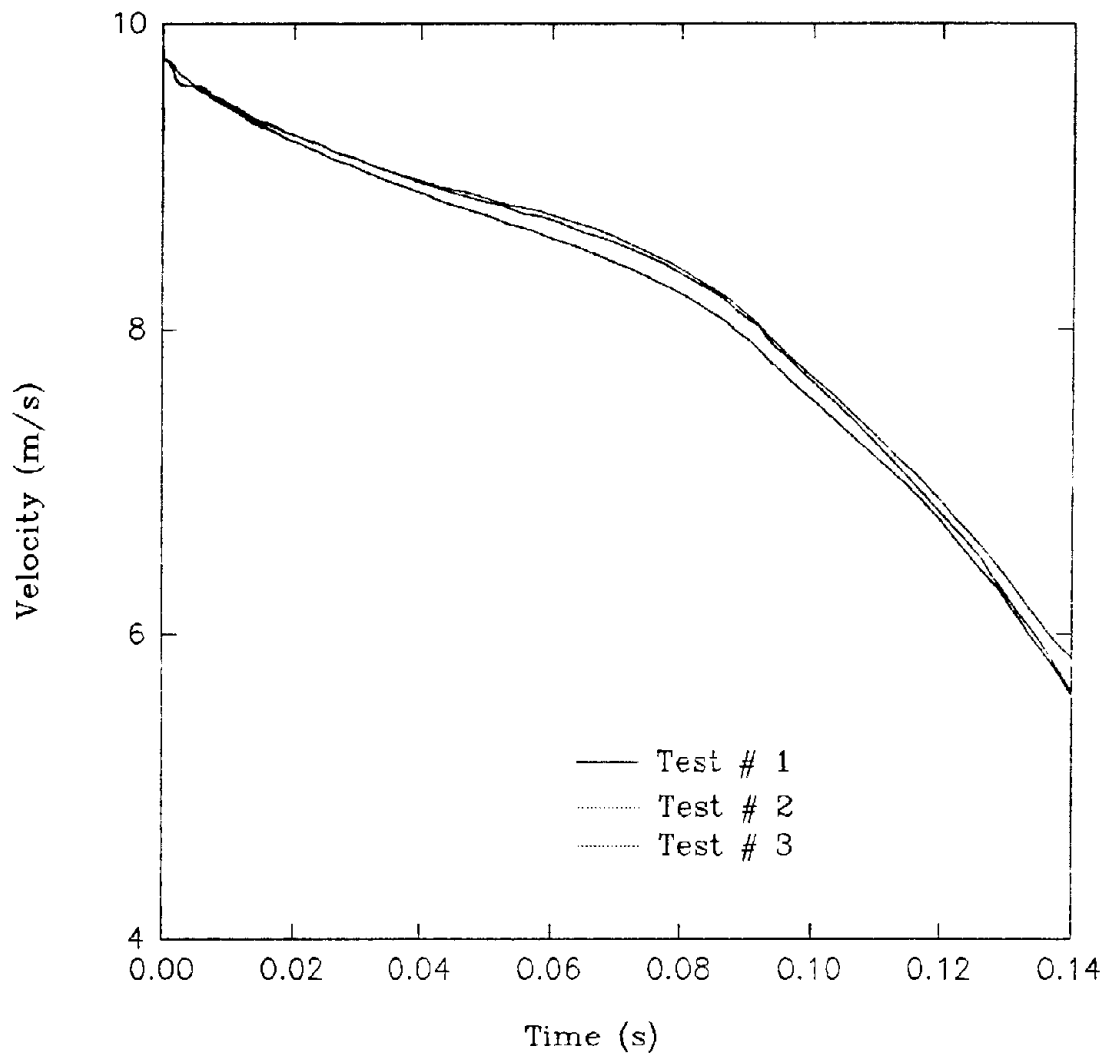


Figure 27. Pendulum velocity versus time.

indication of a successful simulation is the acceleration curves. Figures 47, 48, and 49 show the acceleration obtained from the tests and simulation for test one, two, and three, respectively. Figures 50 to 54 show the progressive impact event for the multiple rail sections.

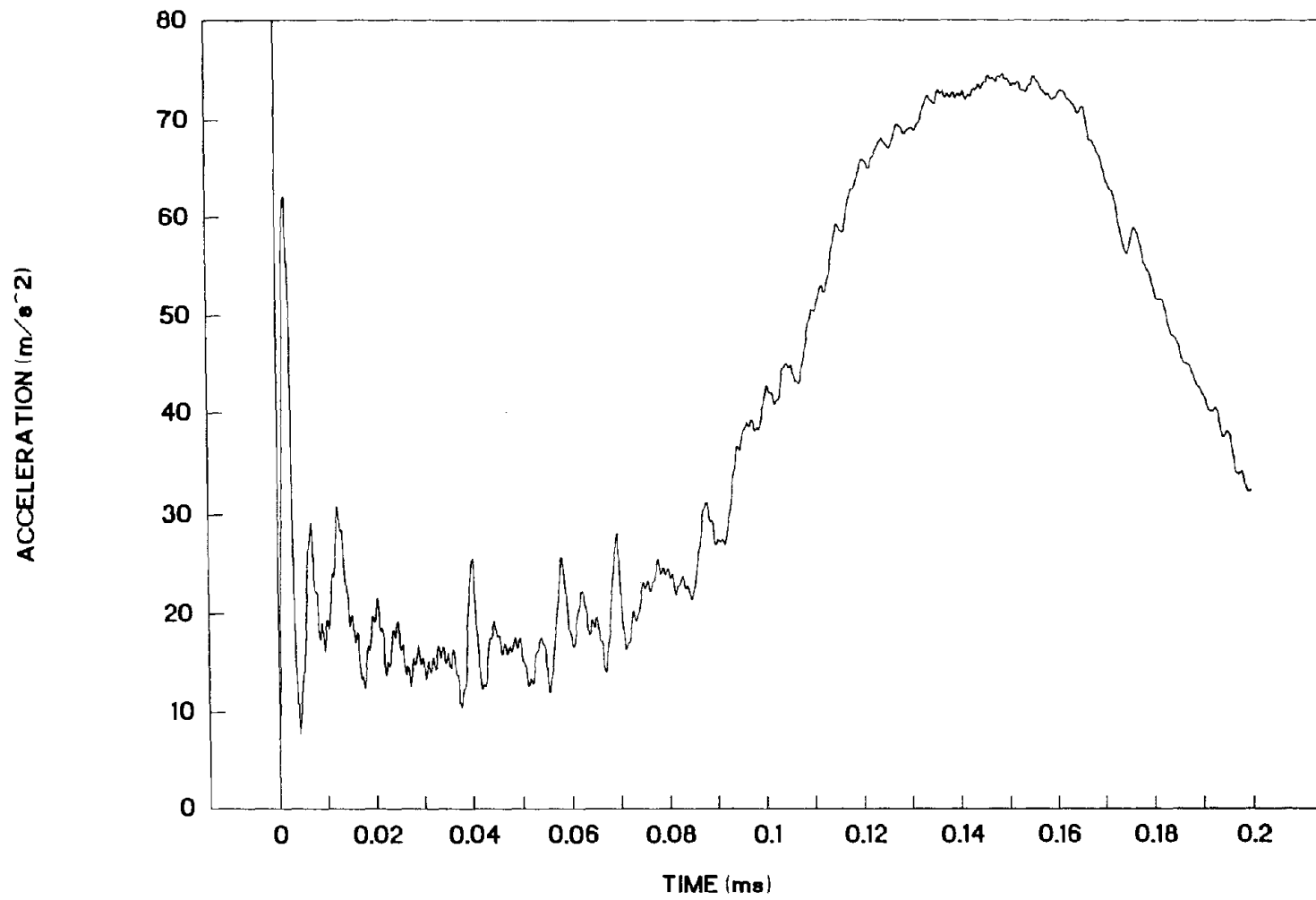


Figure 28. Pendulum acceleration versus time for full FE model.

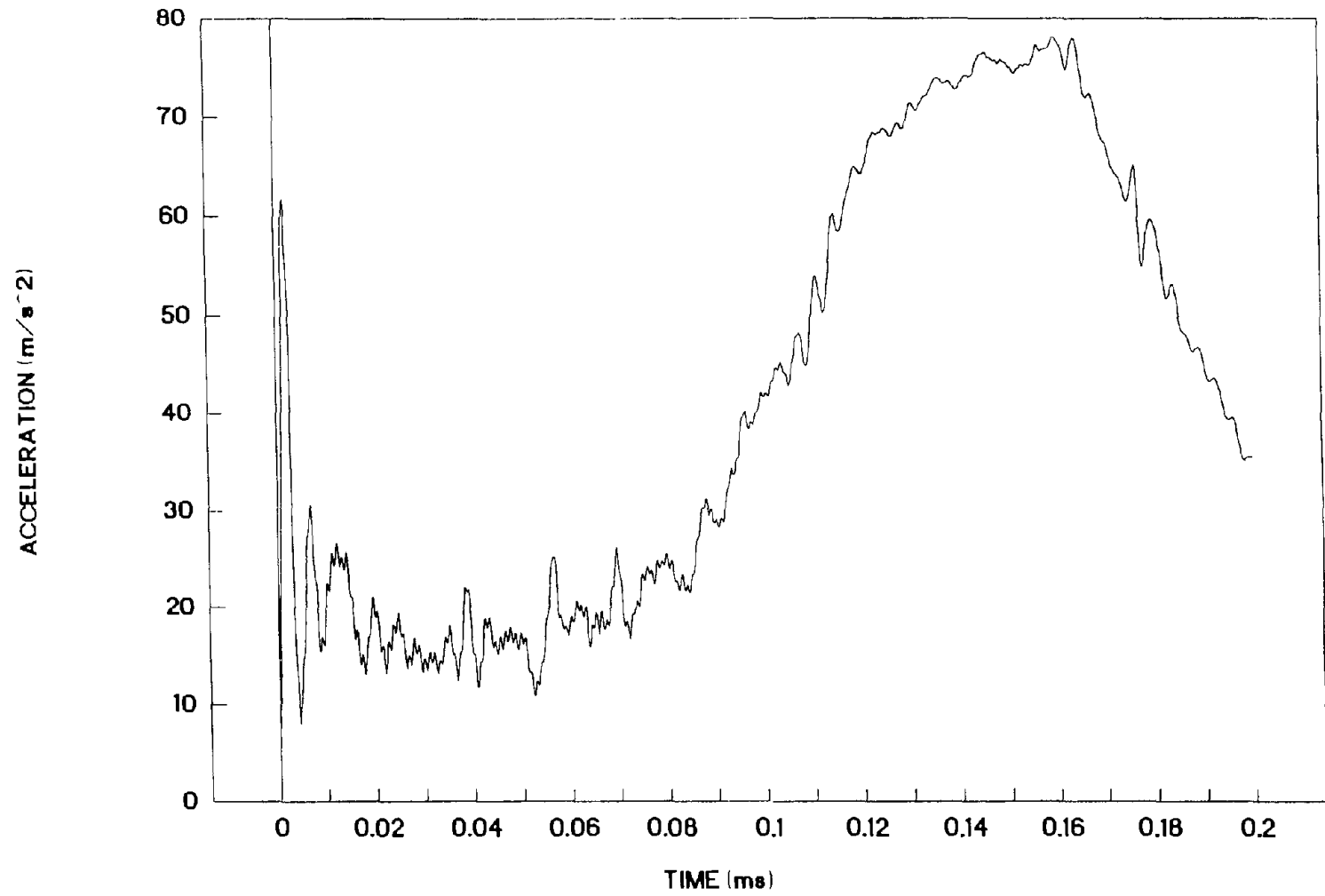


Figure 29. Pendulum acceleration versus time for simplified FE model.

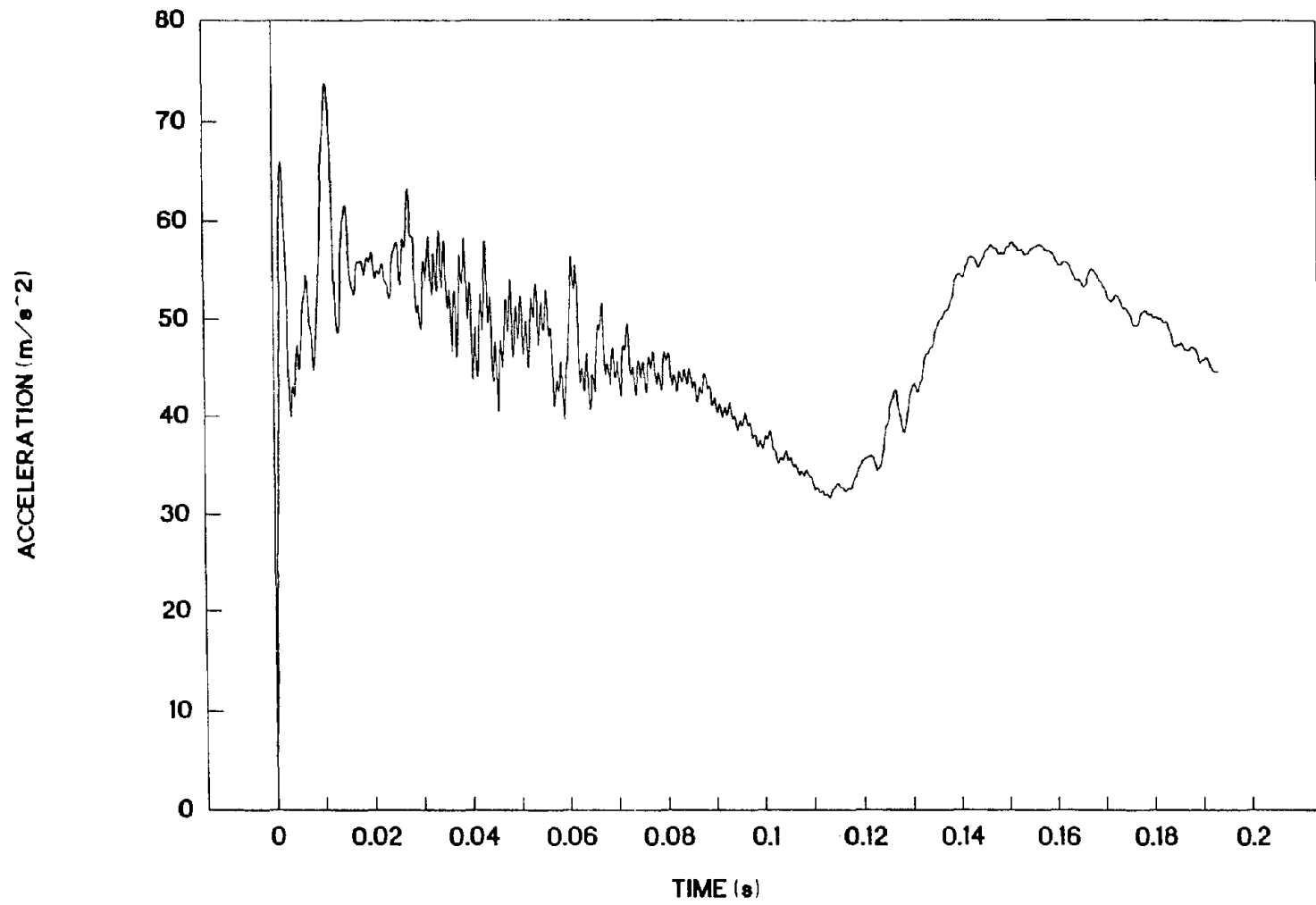
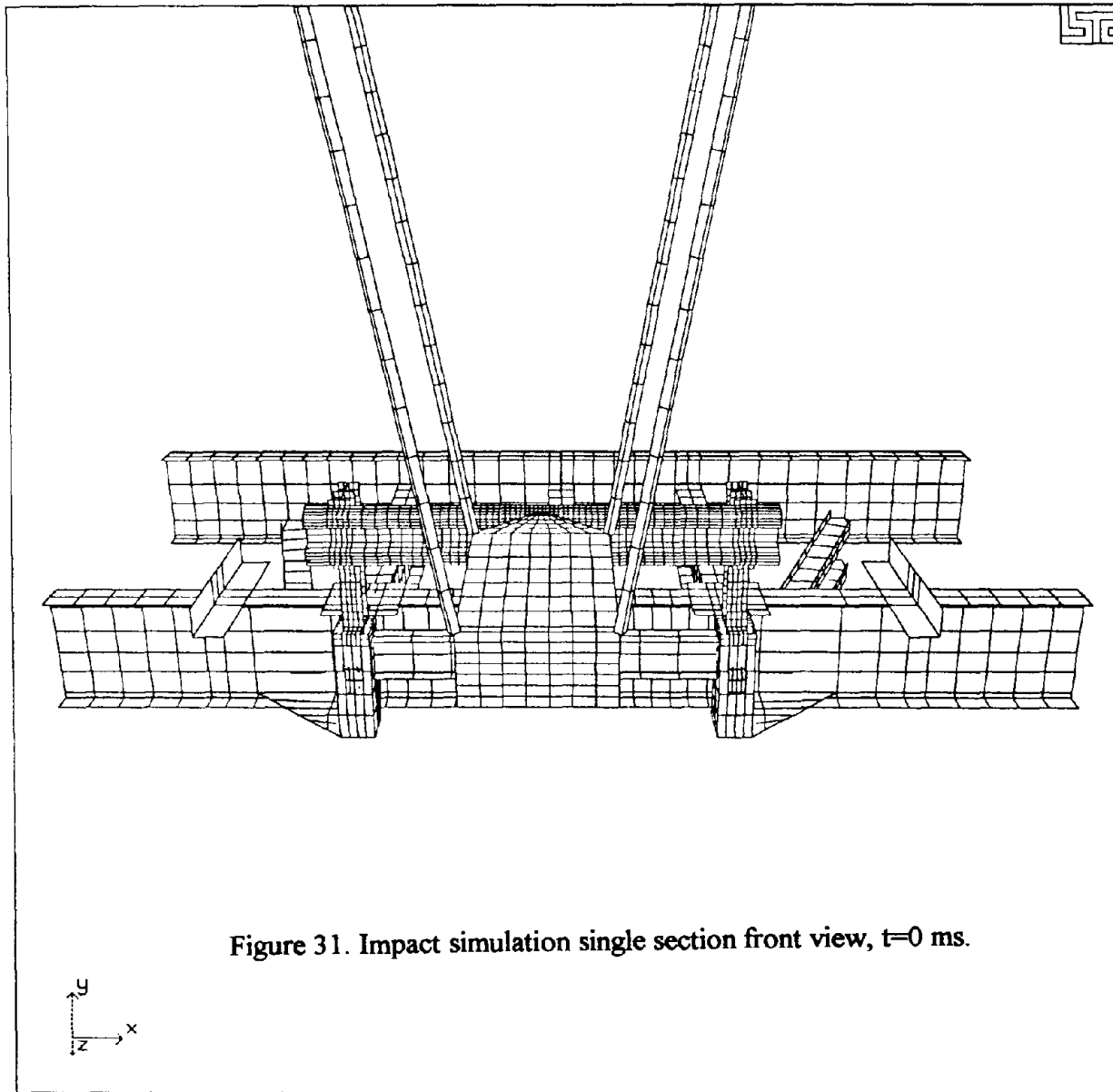
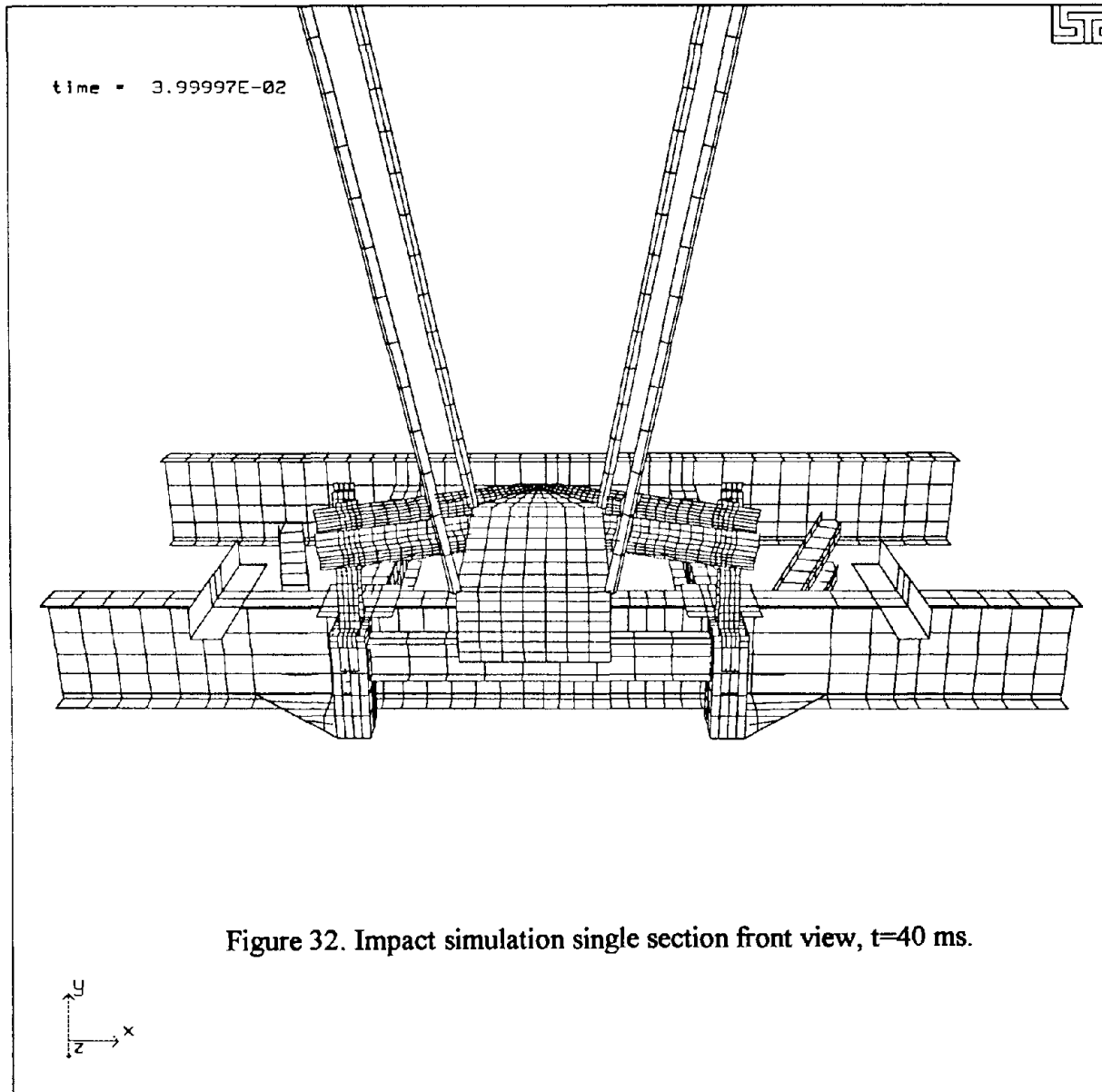
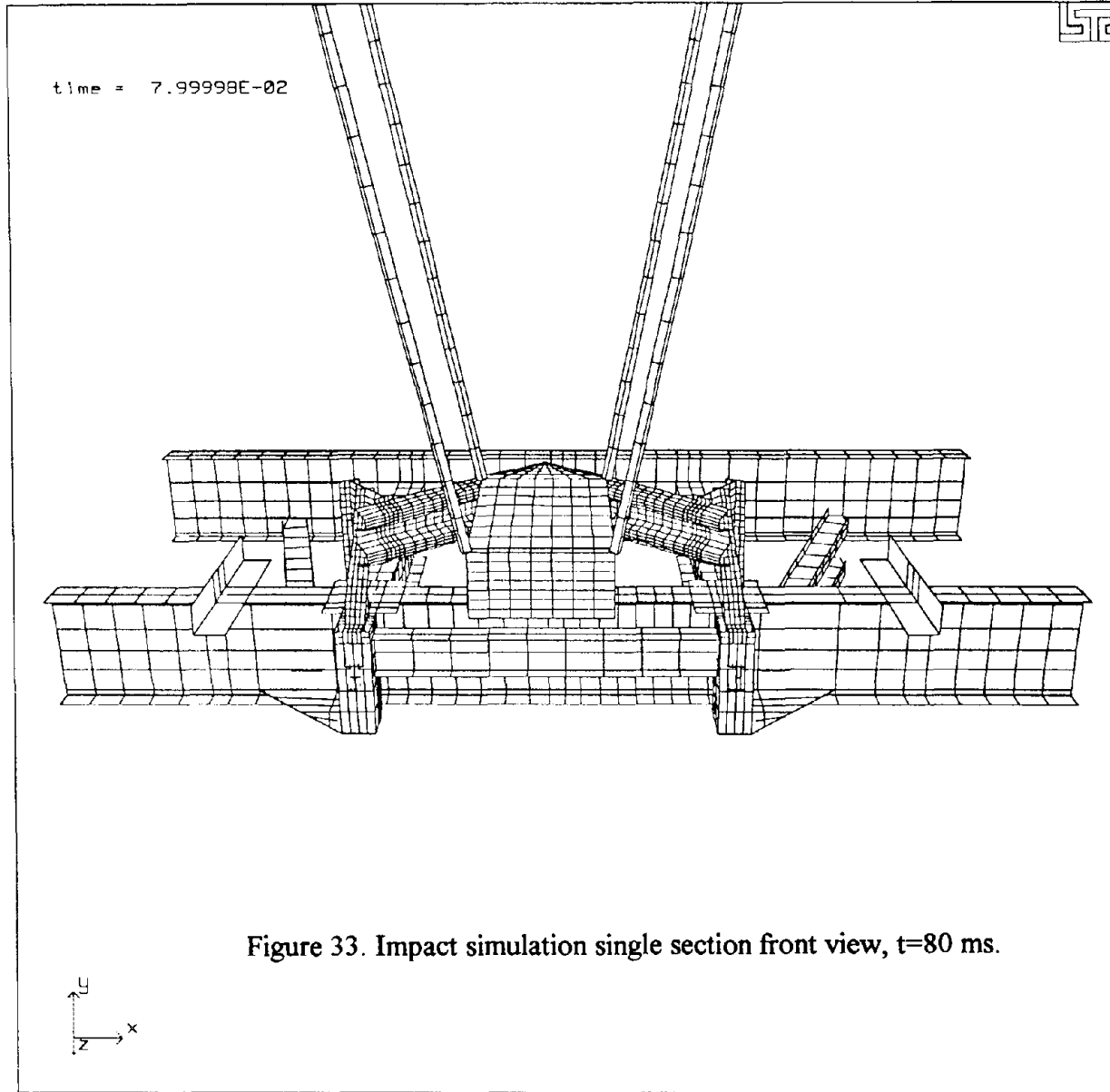


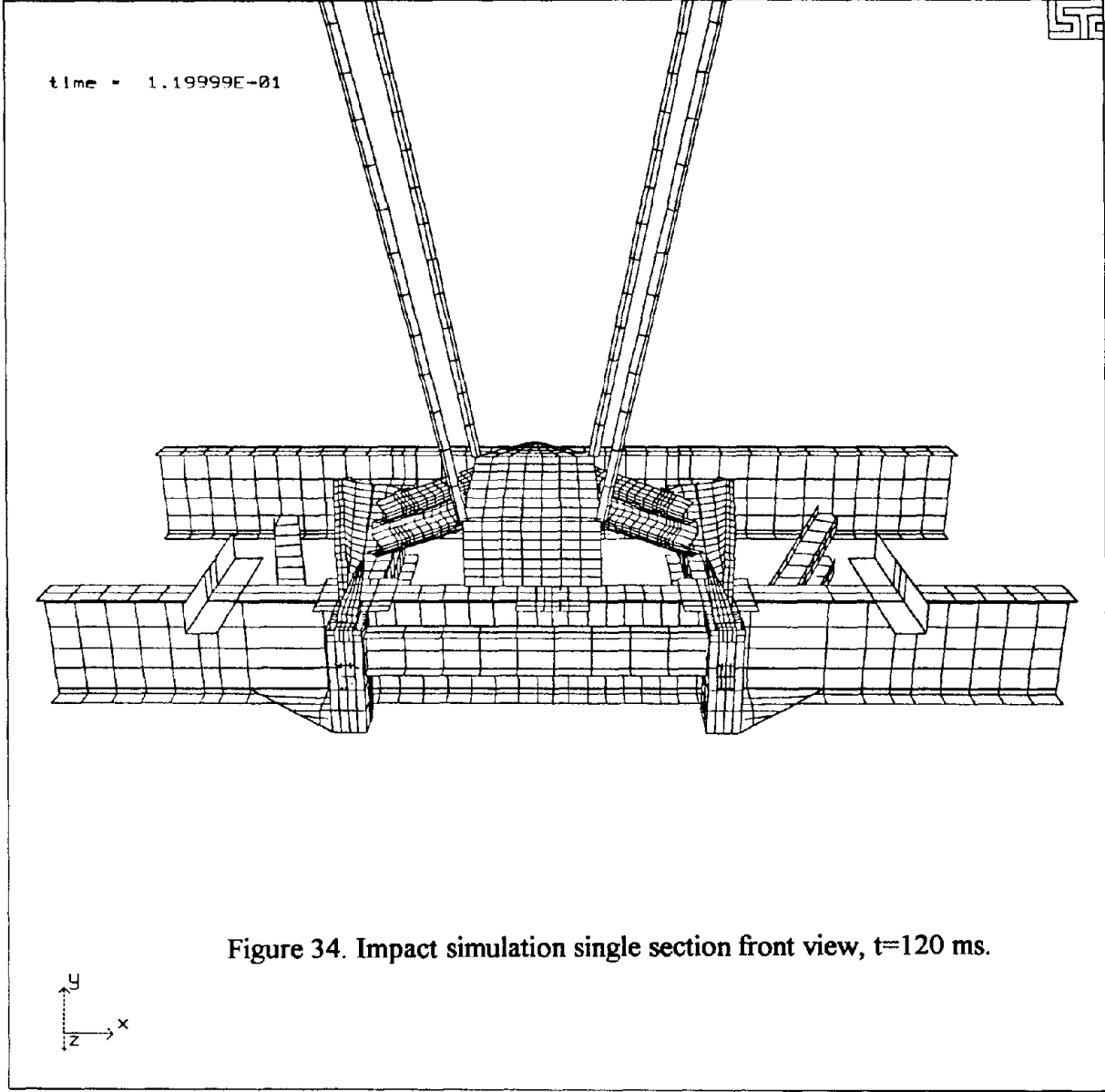
Figure 30. Pendulum acceleration versus time for multiple rail section FE model.

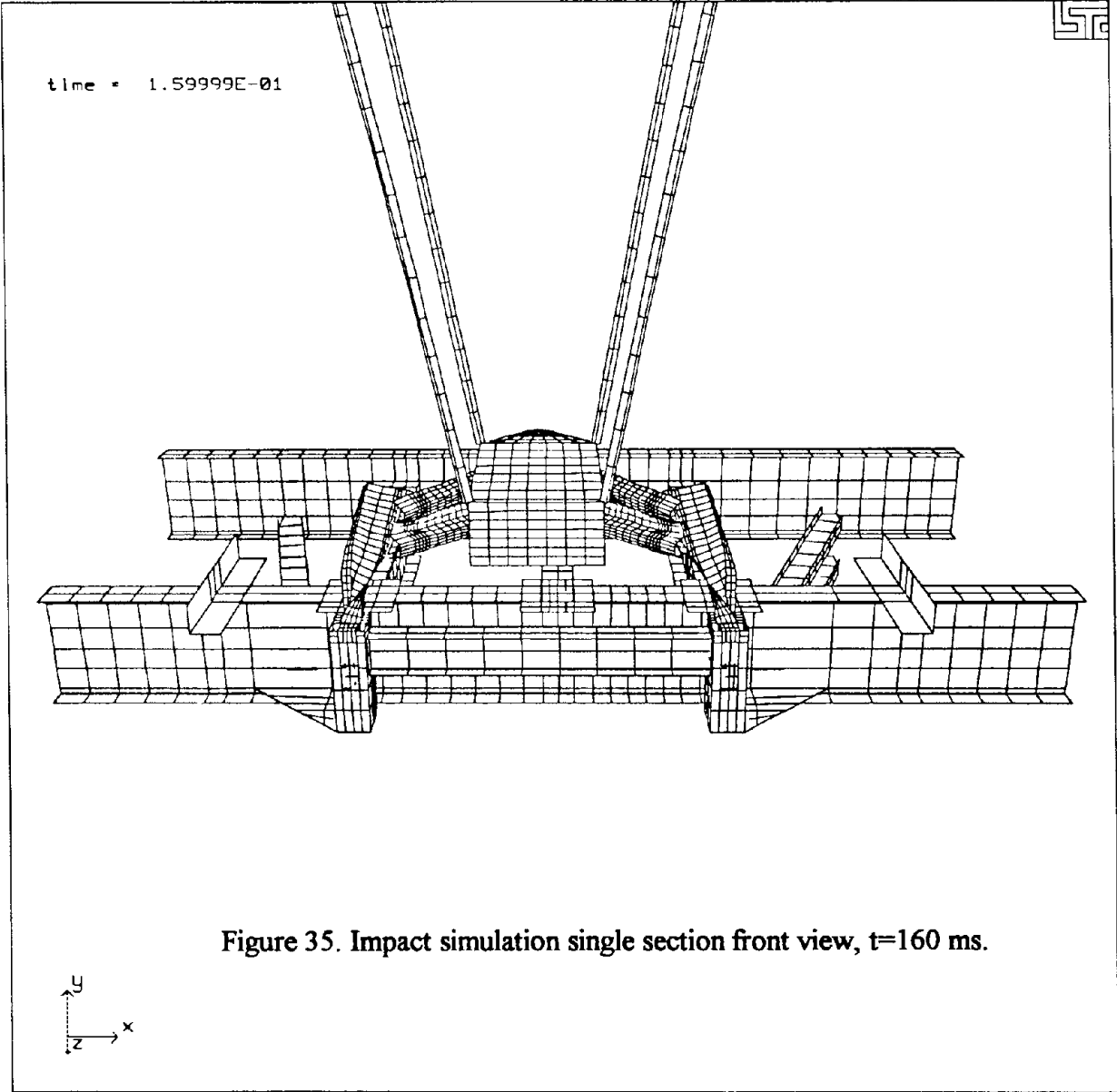
SS

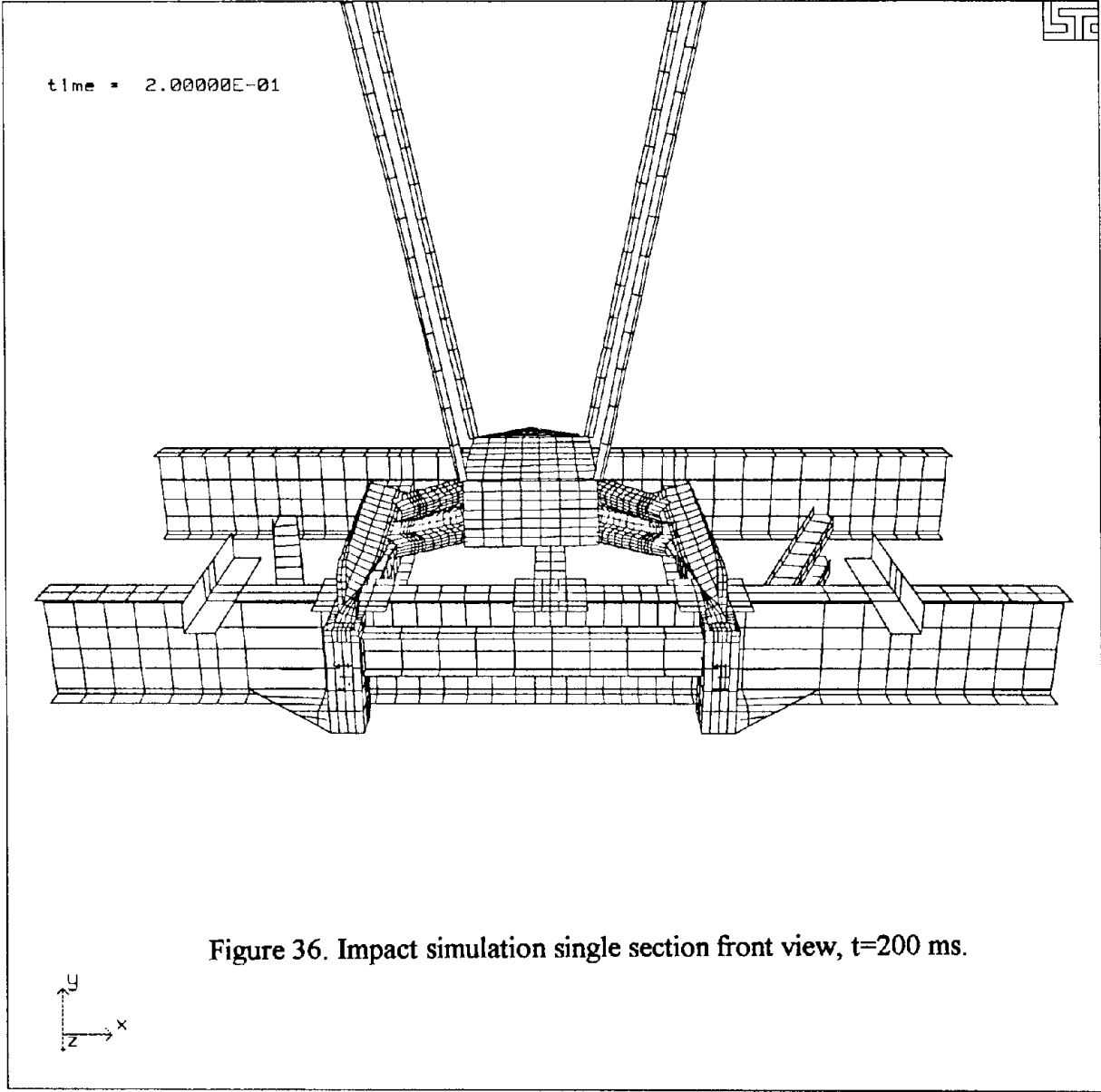


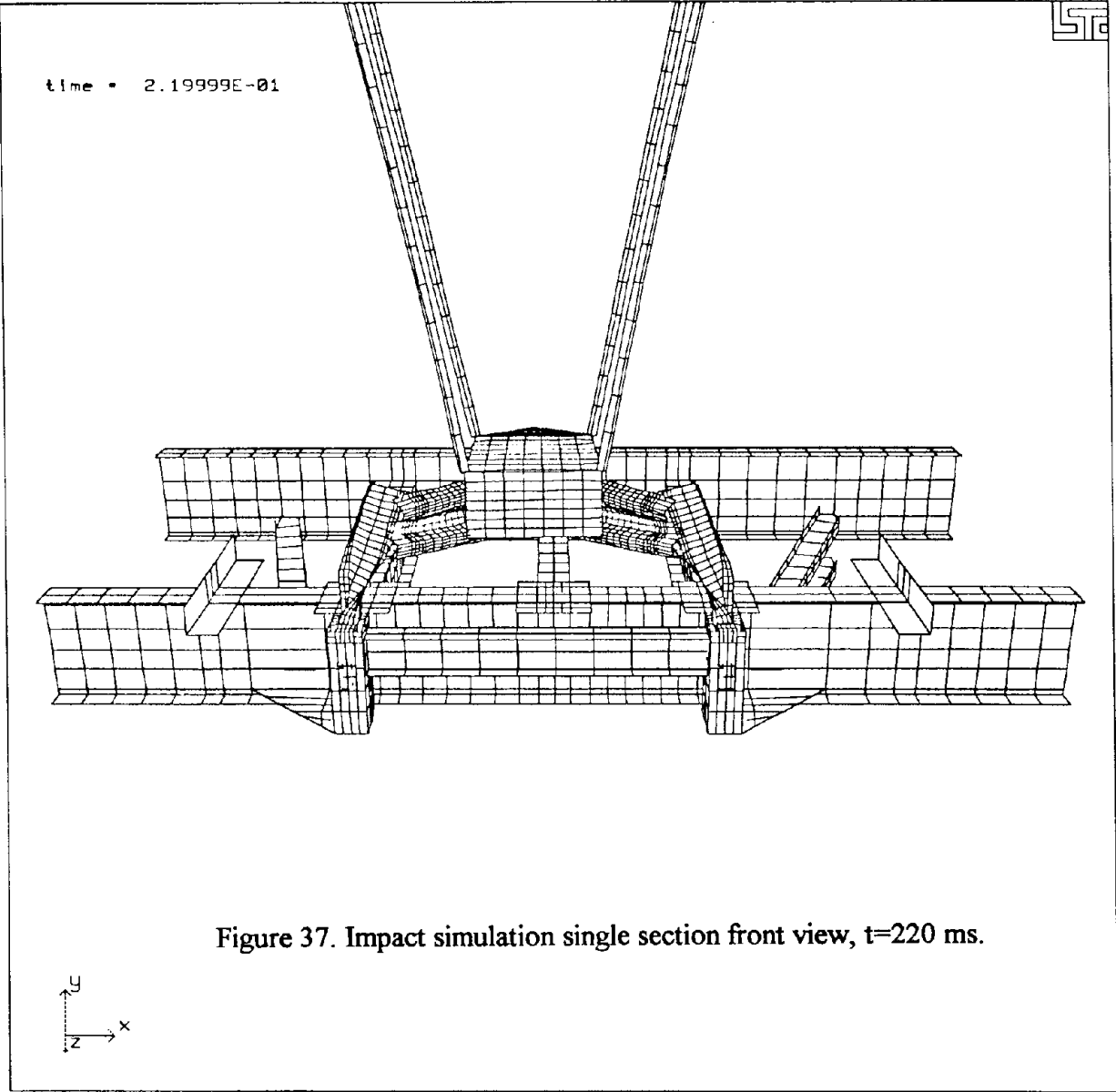












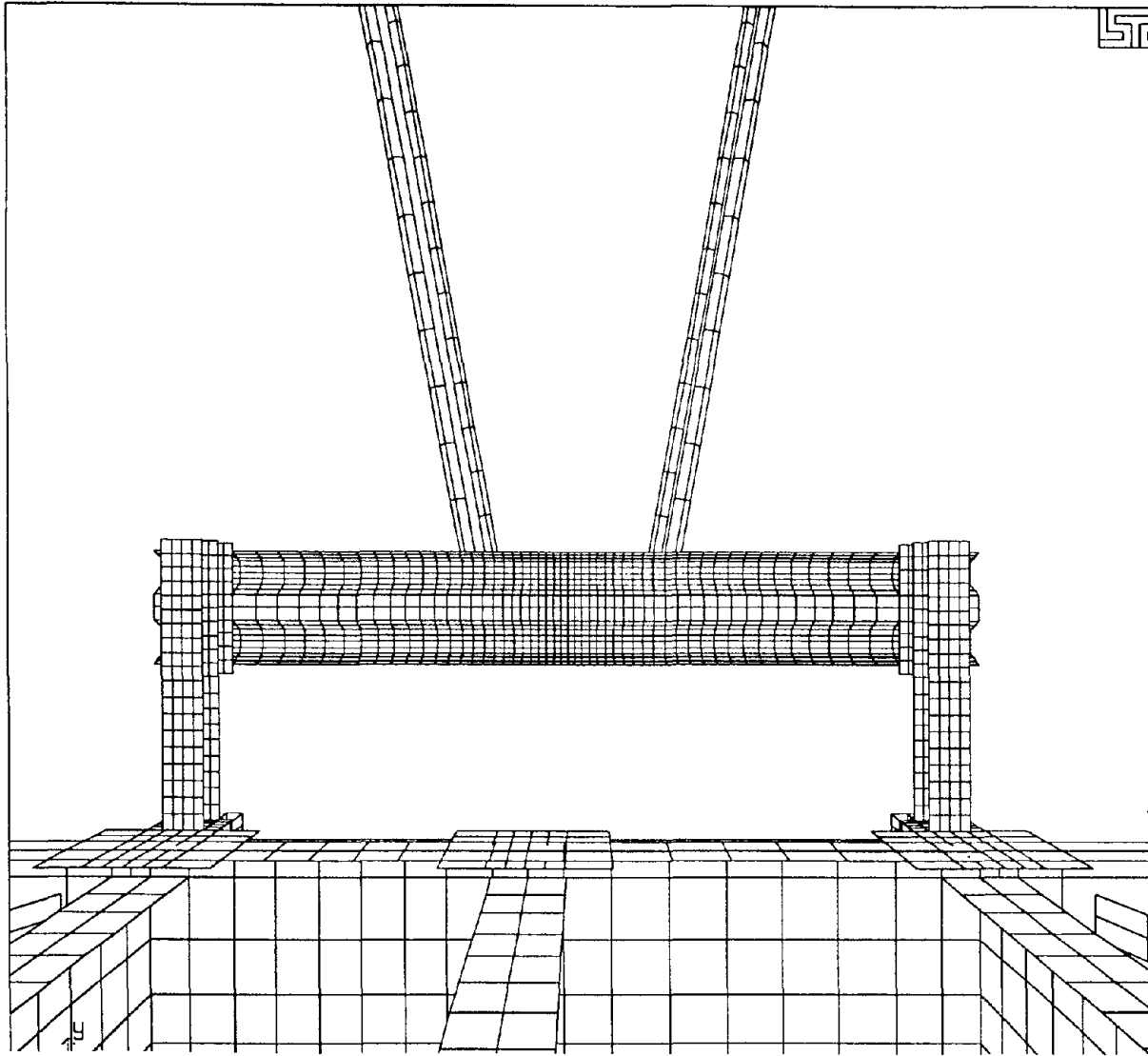


Figure 38. Impact simulation single section rear view, t=0 ms.

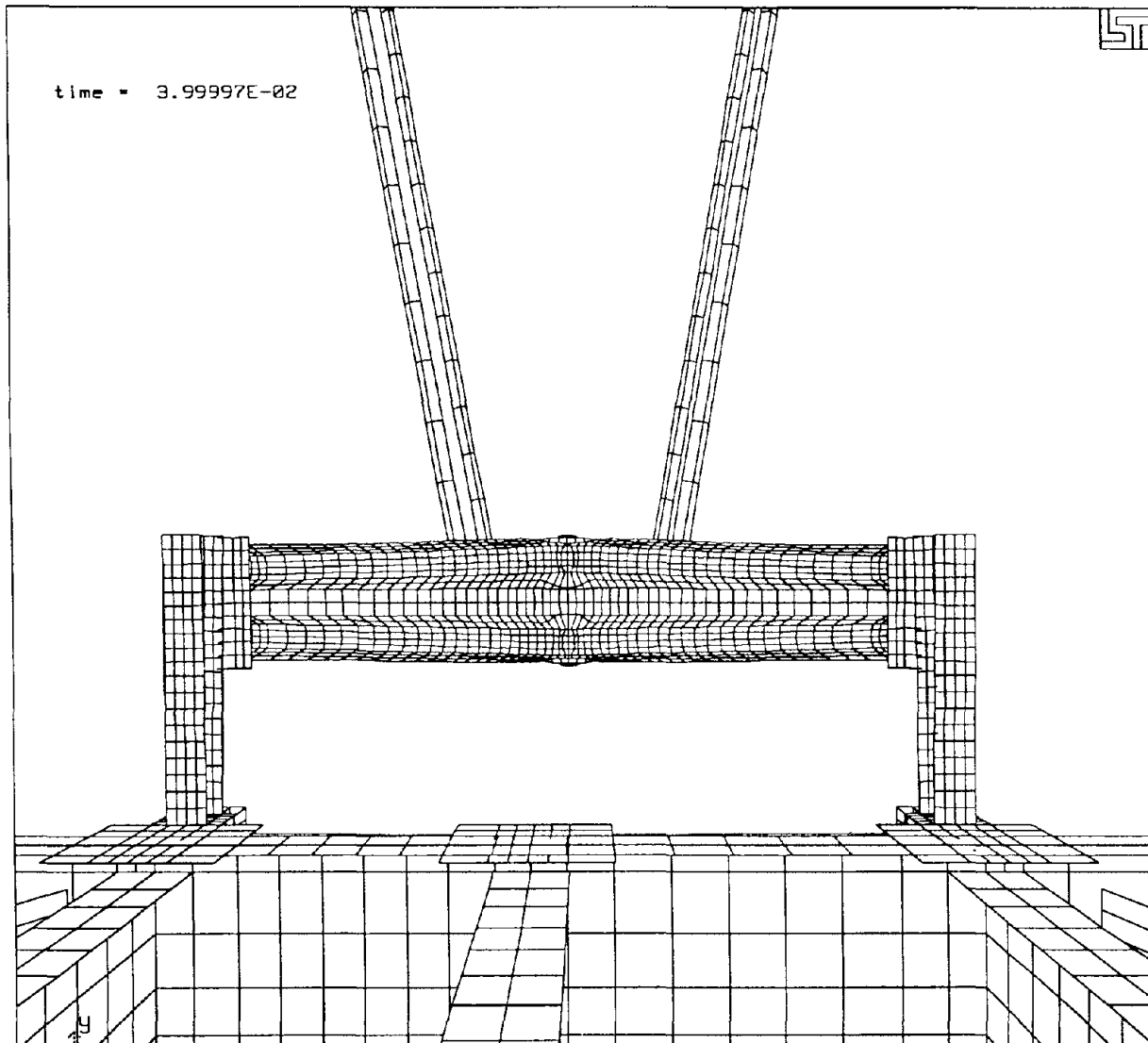


Figure 39. Impact simulation single section rear view, t=40 ms.

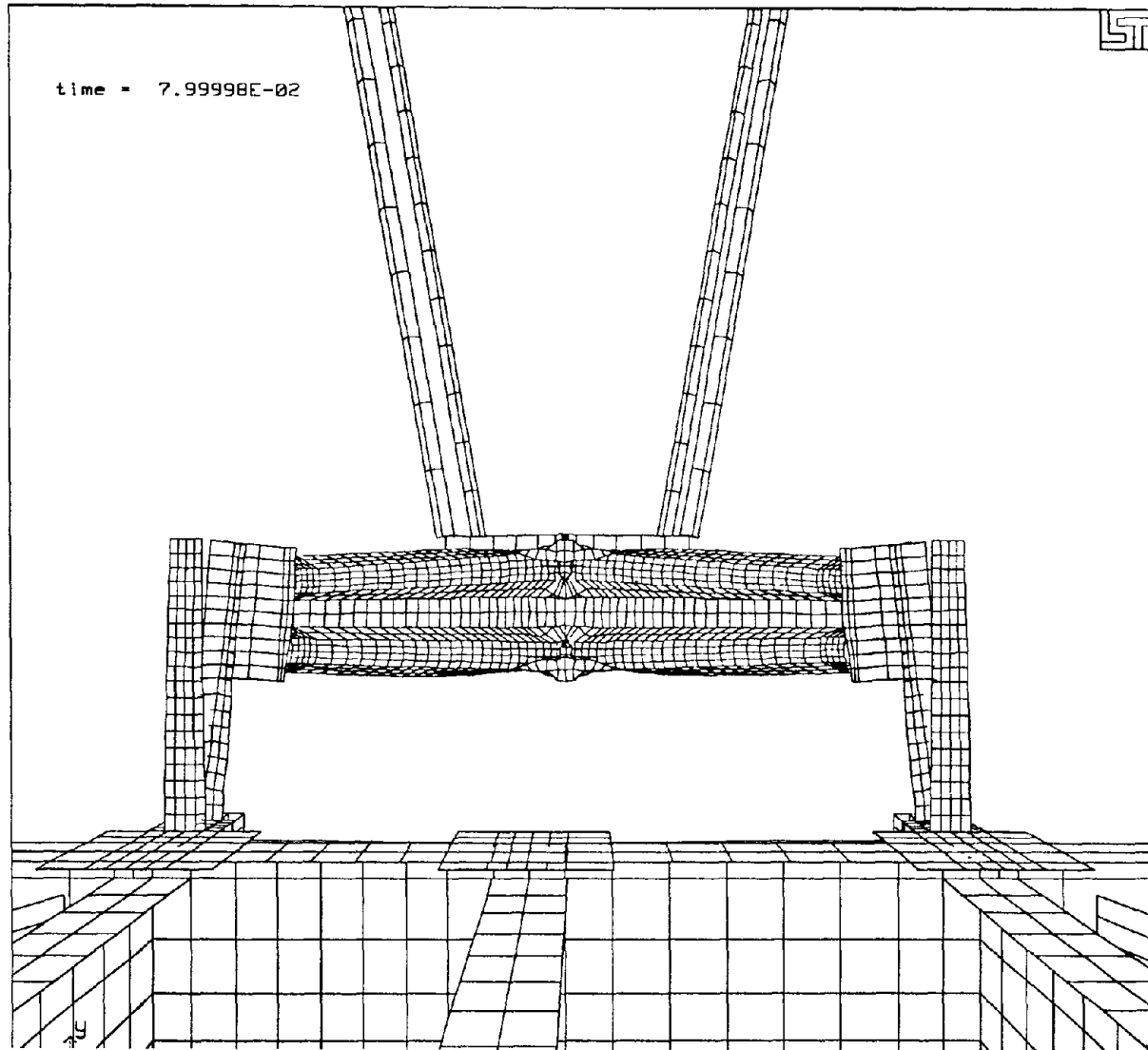


Figure 40. Impact simulation single section rear view, t=80 ms.

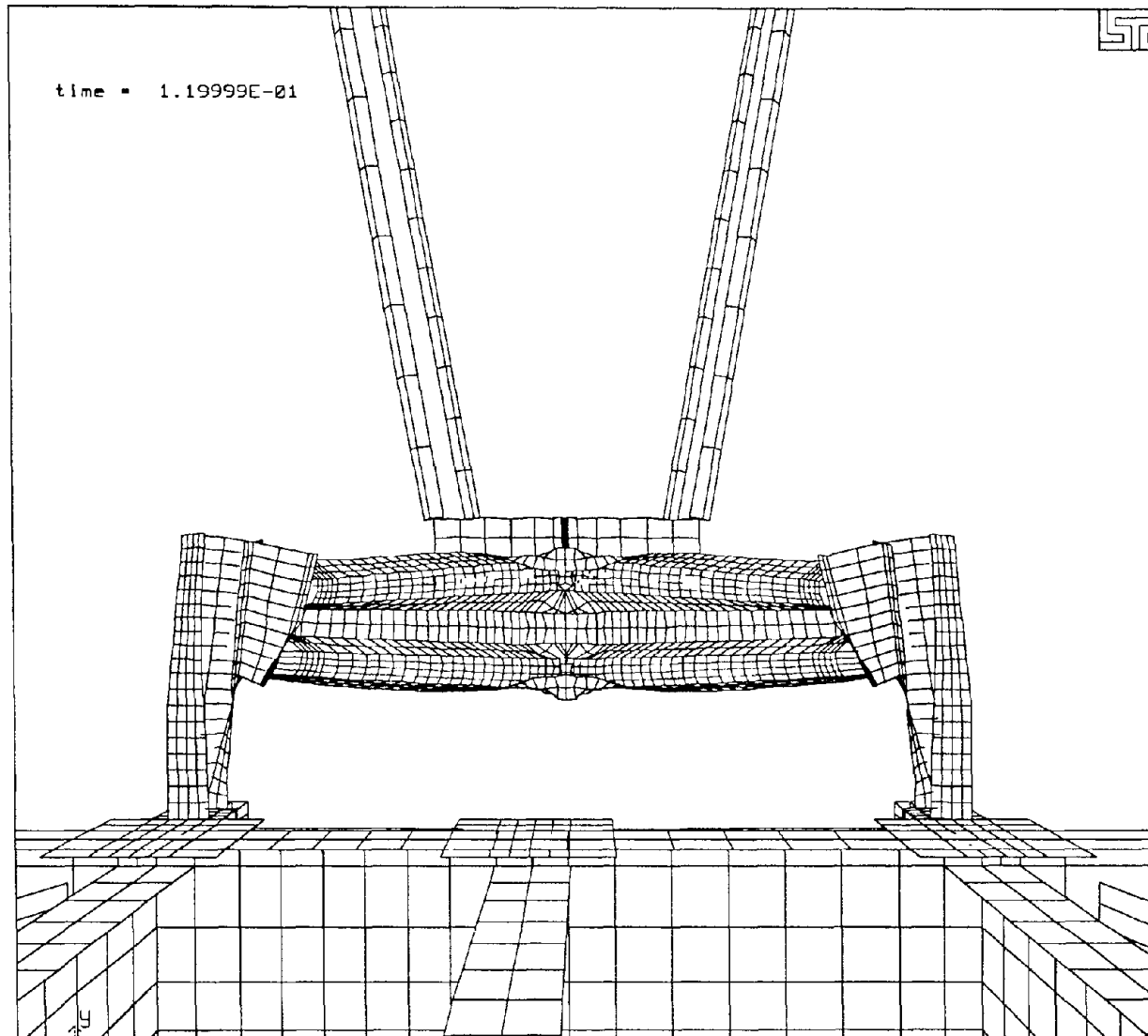


Figure 41. Impact simulation single section rear view, t=120 ms.

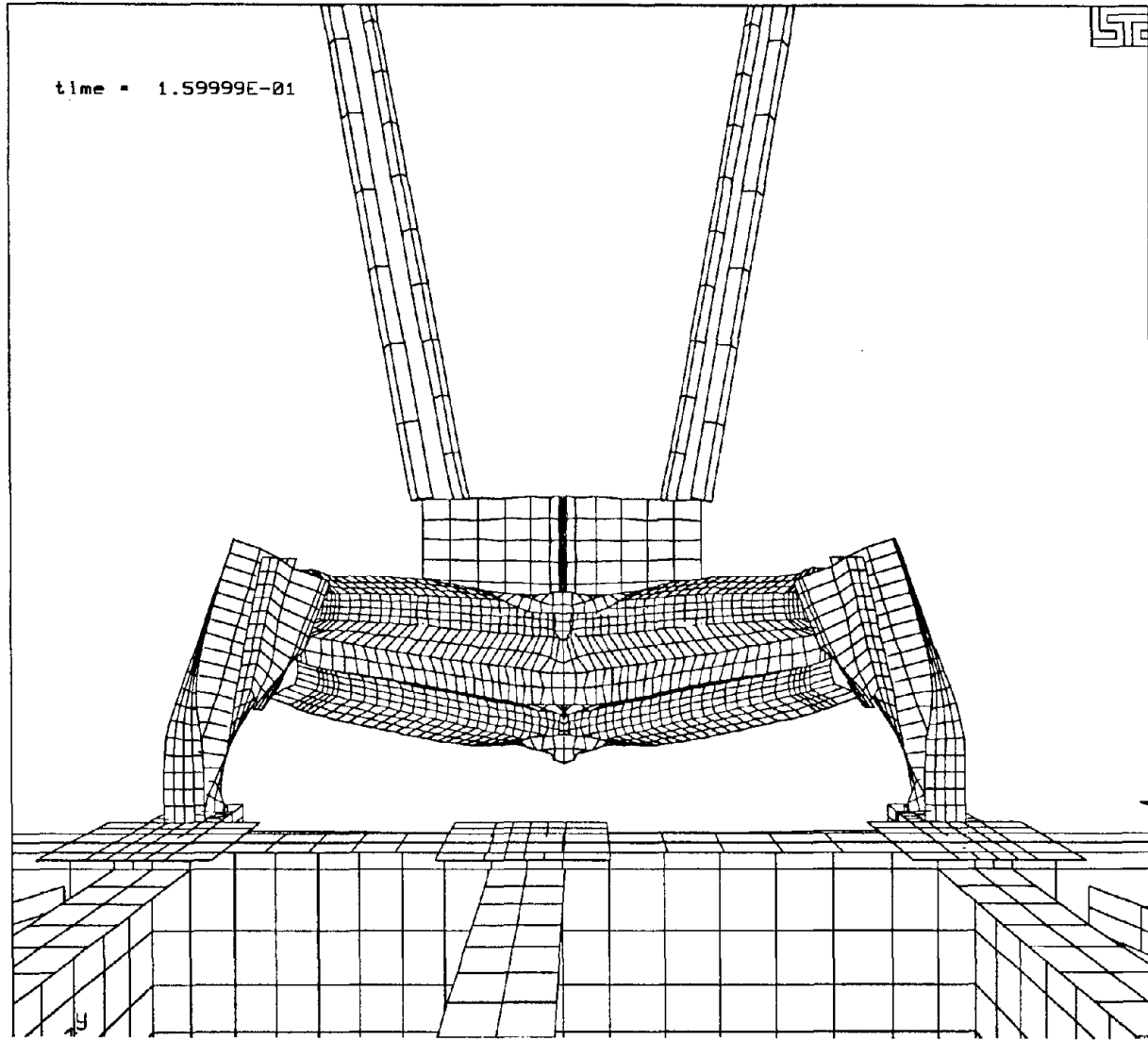


Figure 42. Impact simulation single section rear view, t=160 ms.

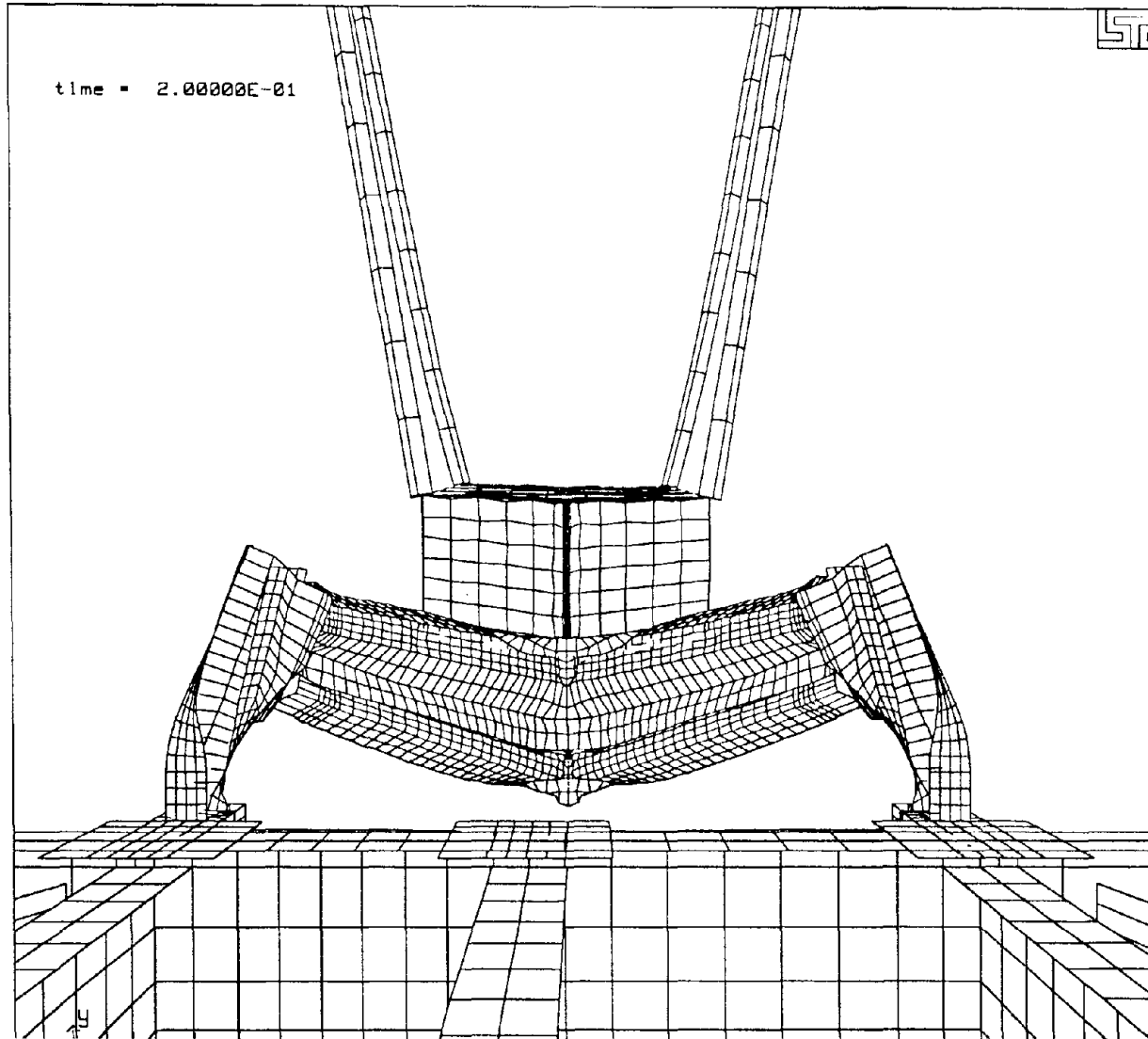


Figure 43. Impact simulation single section rear view, $t=200$ ms.

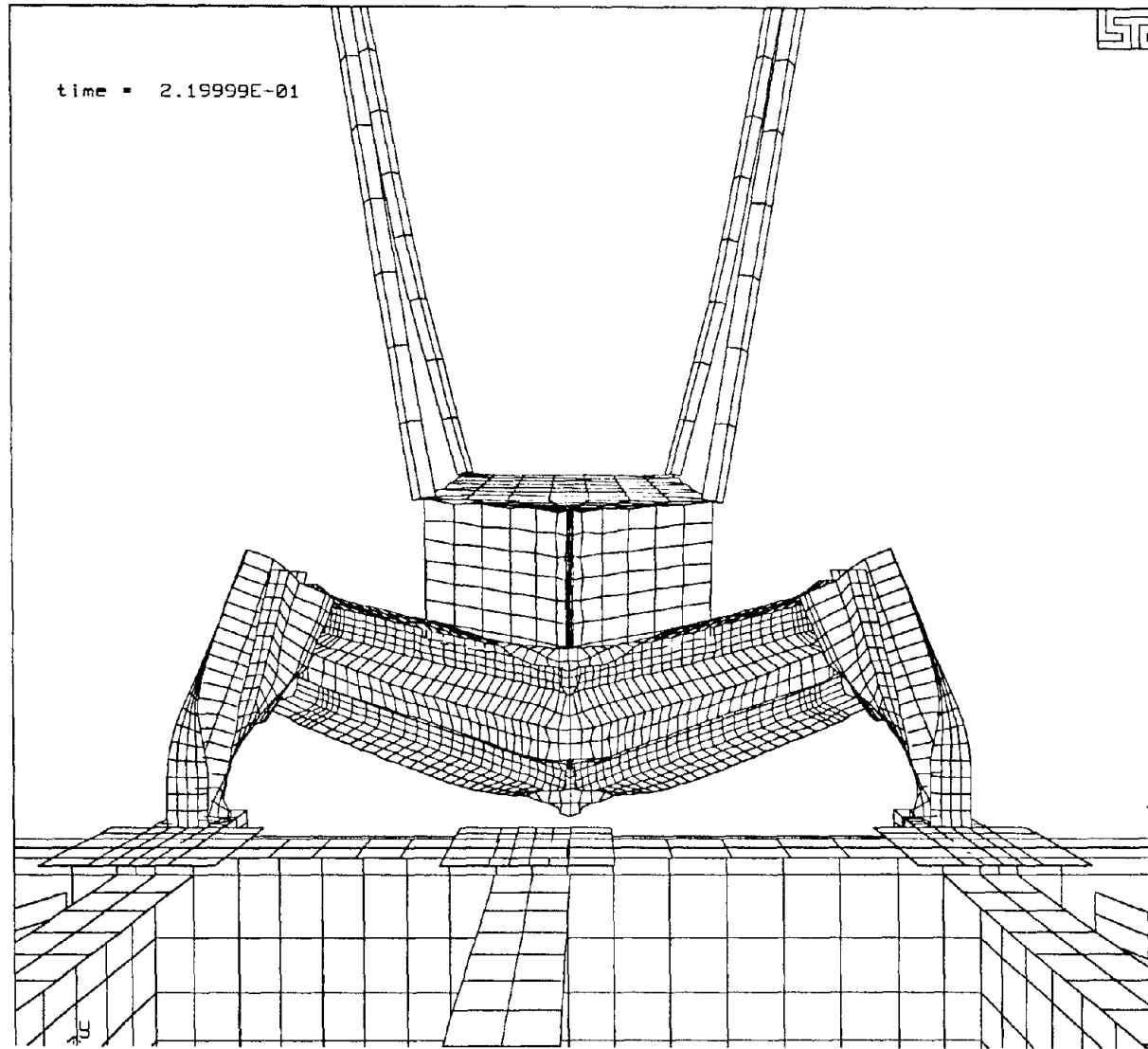


Figure 44. Impact simulation single section rear view, t=220 ms.

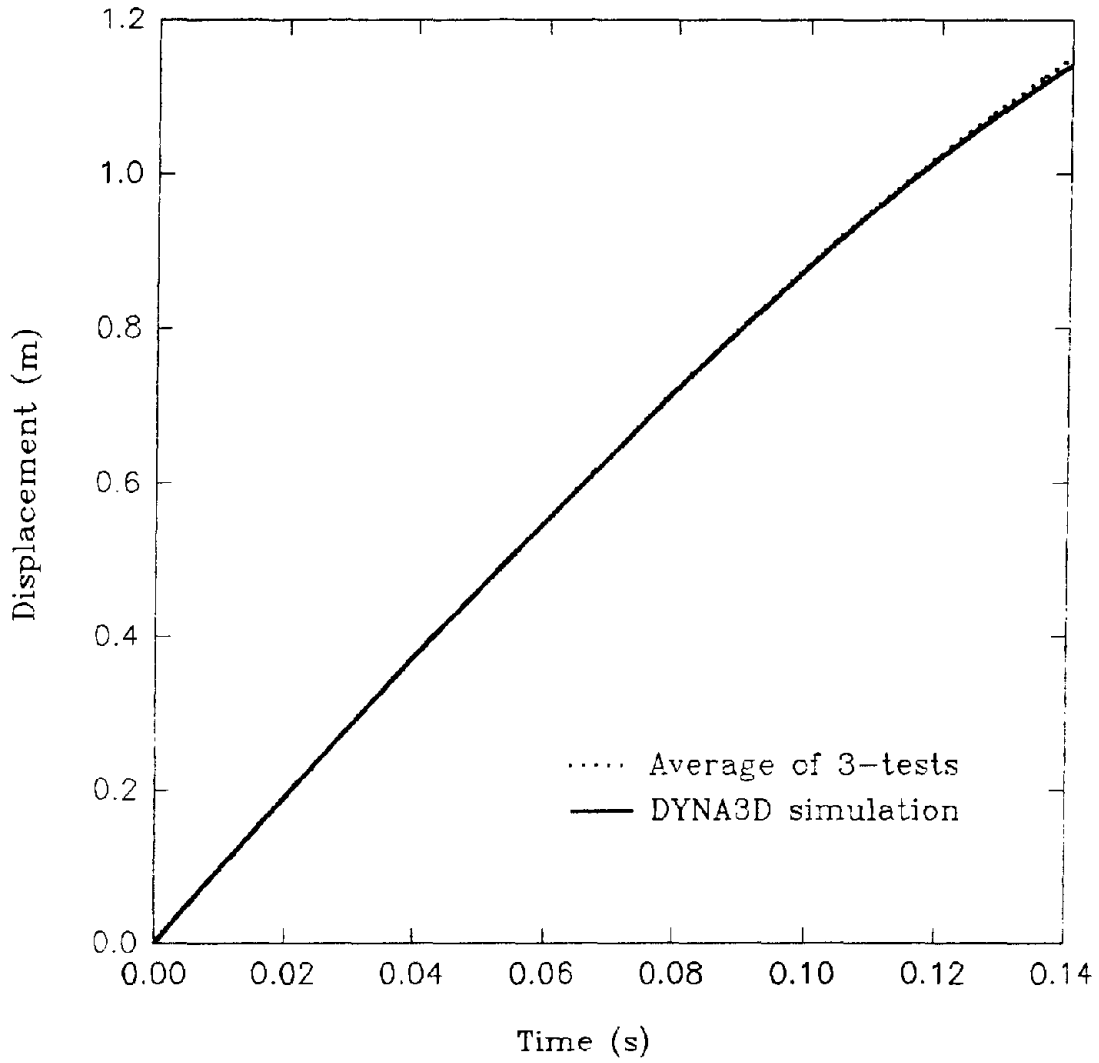


Figure 45. Average displacement of three tests and simulation prediction.

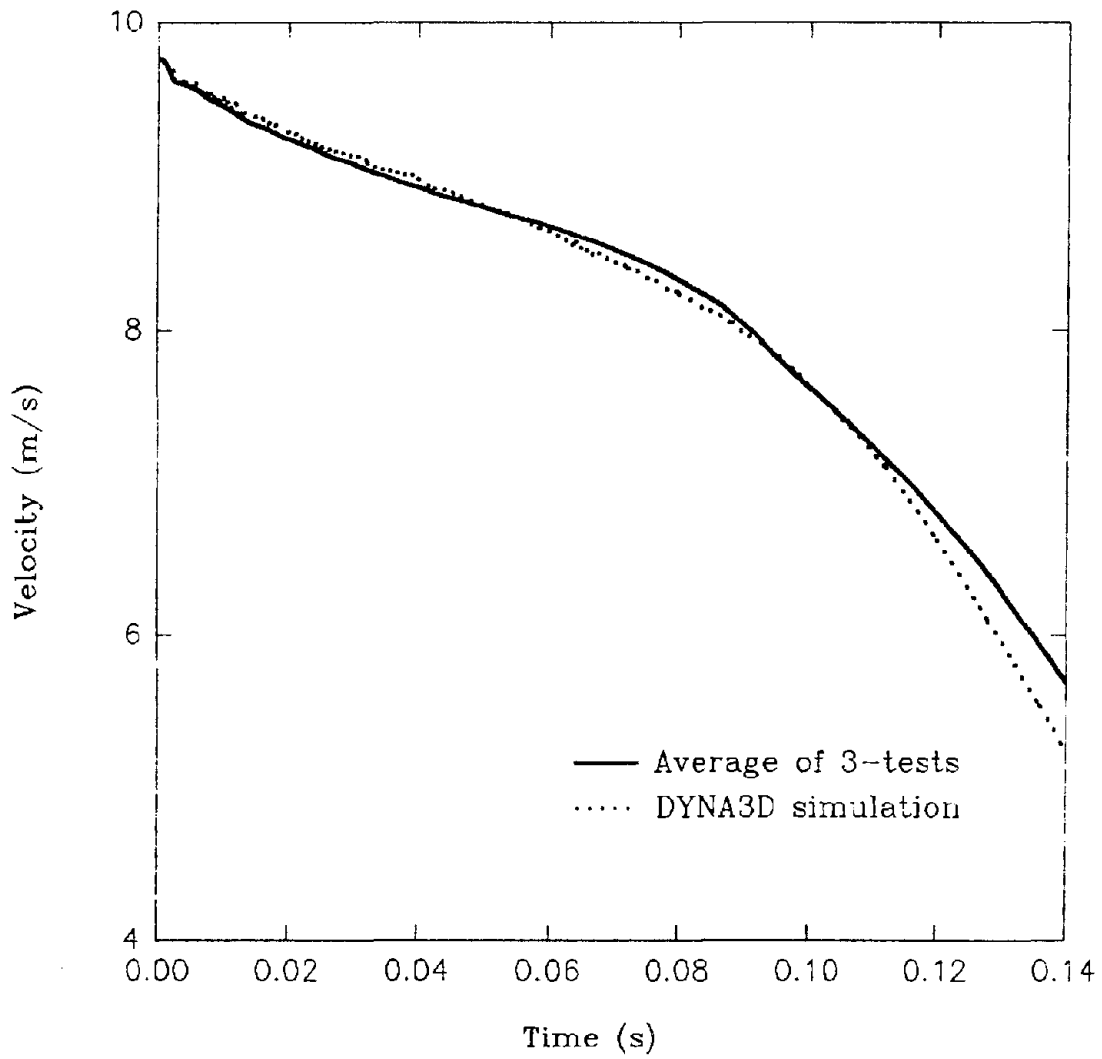


Figure 46. Average velocity of three tests and simulation prediction.

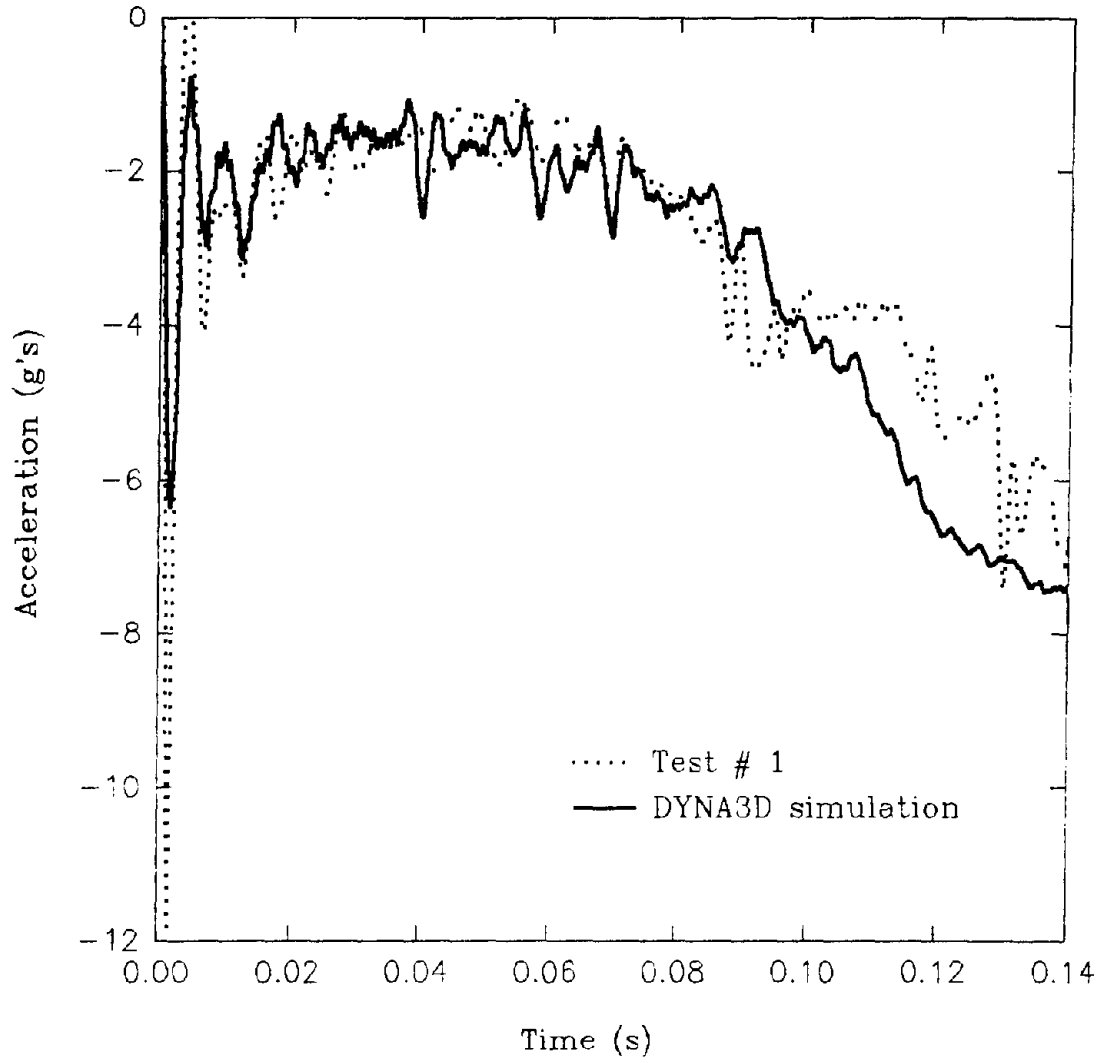


Figure 47. Pendulum acceleration of test #1 and simulation prediction.

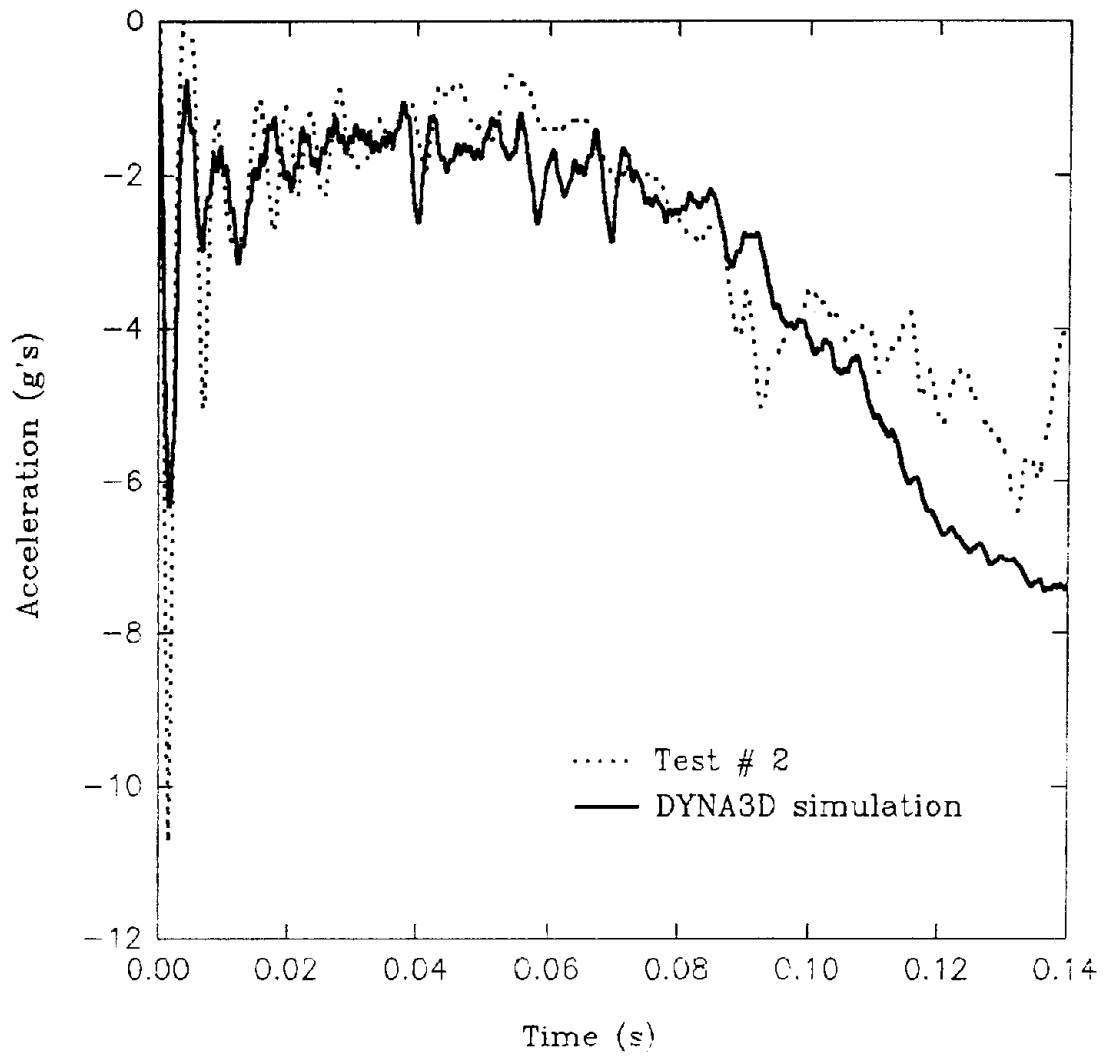


Figure 48. Pendulum acceleration of test #2 and simulation prediction.

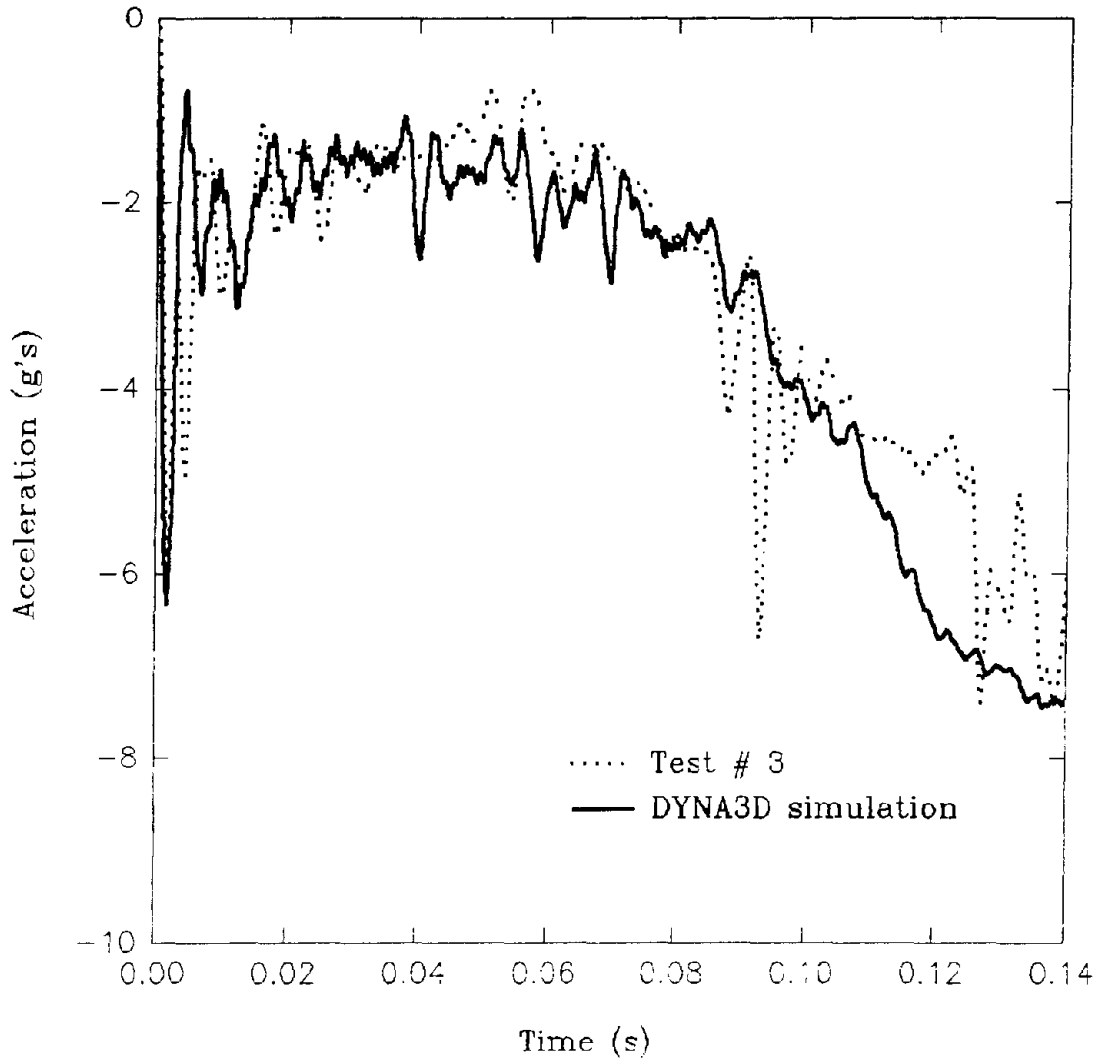
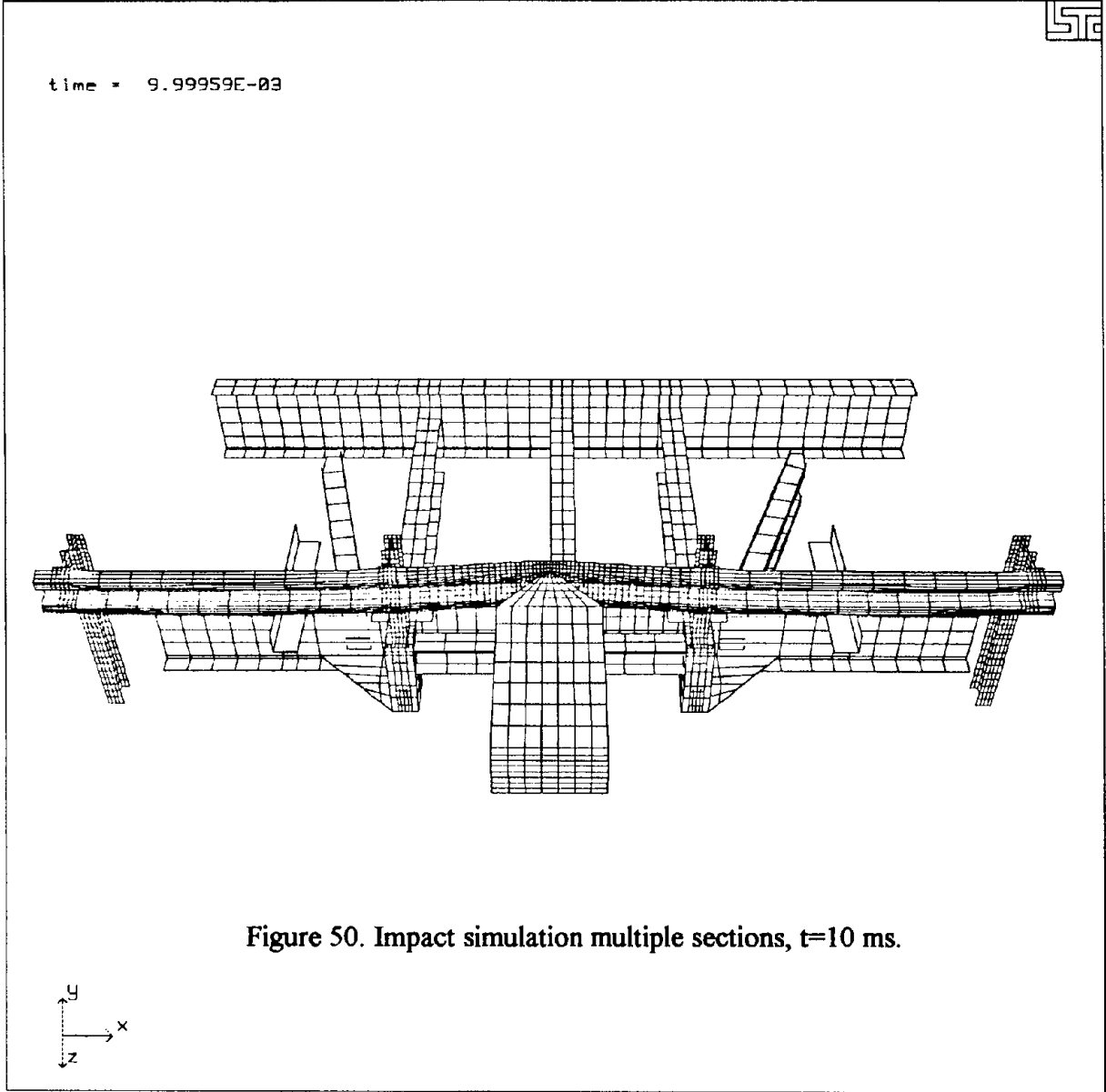


Figure 49. Pendulum acceleration of test #3 and simulation prediction.



time = 4.99990E-02

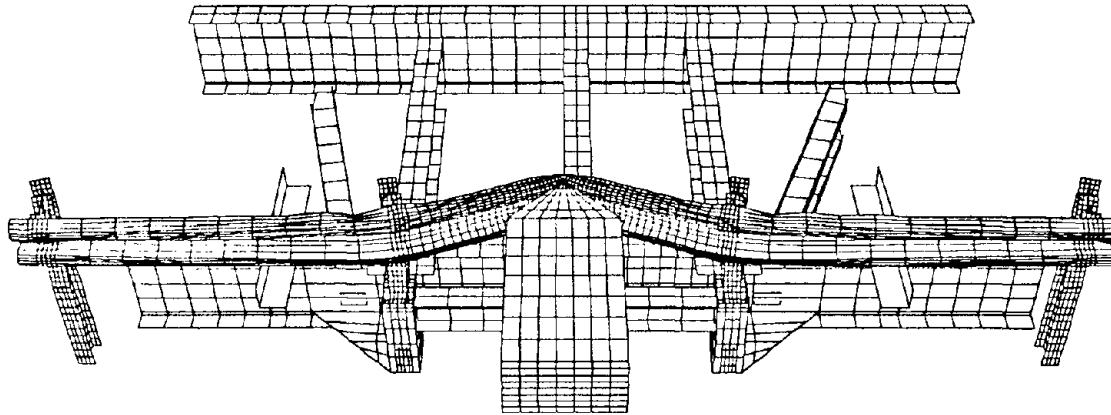
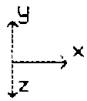
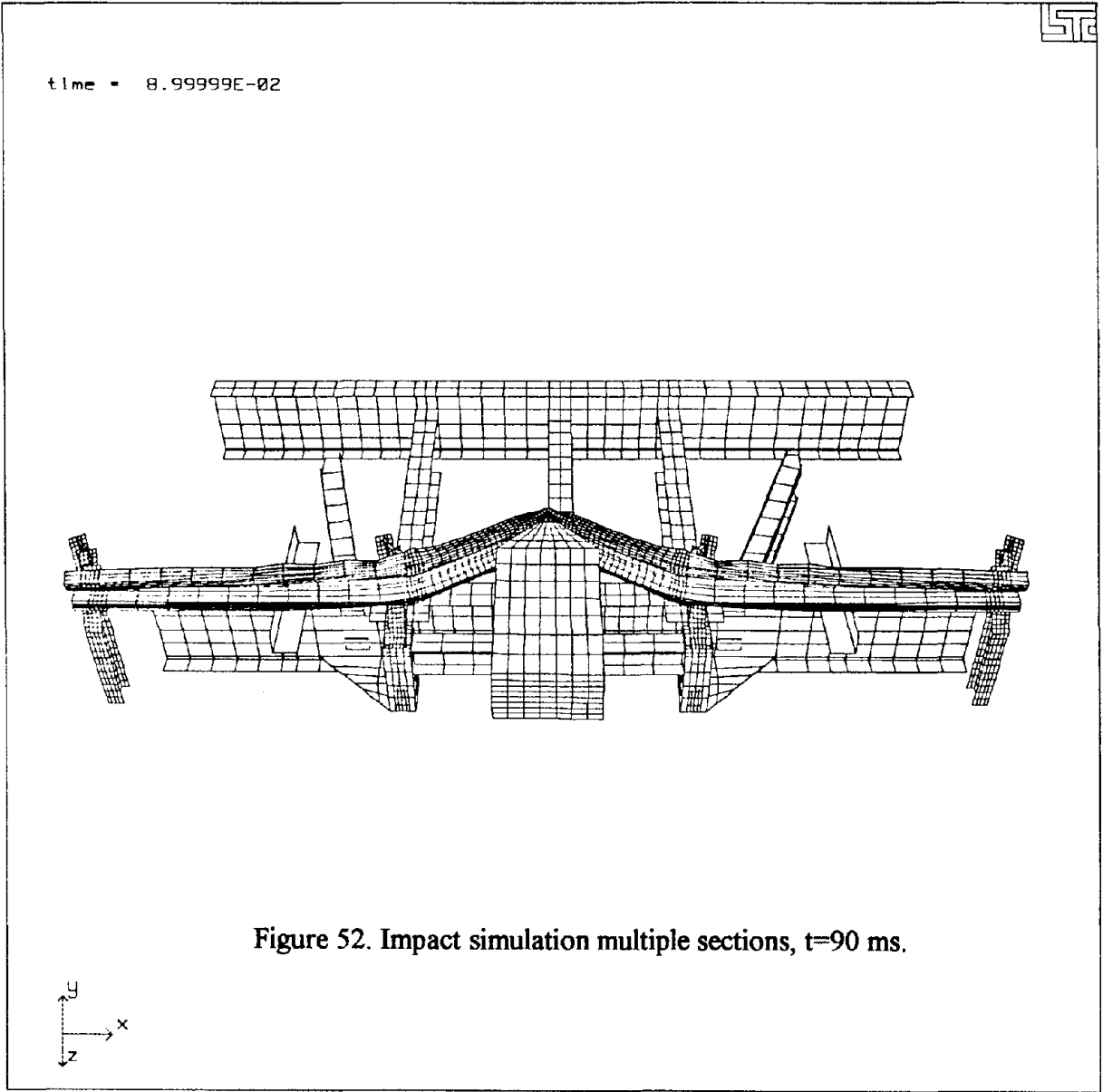
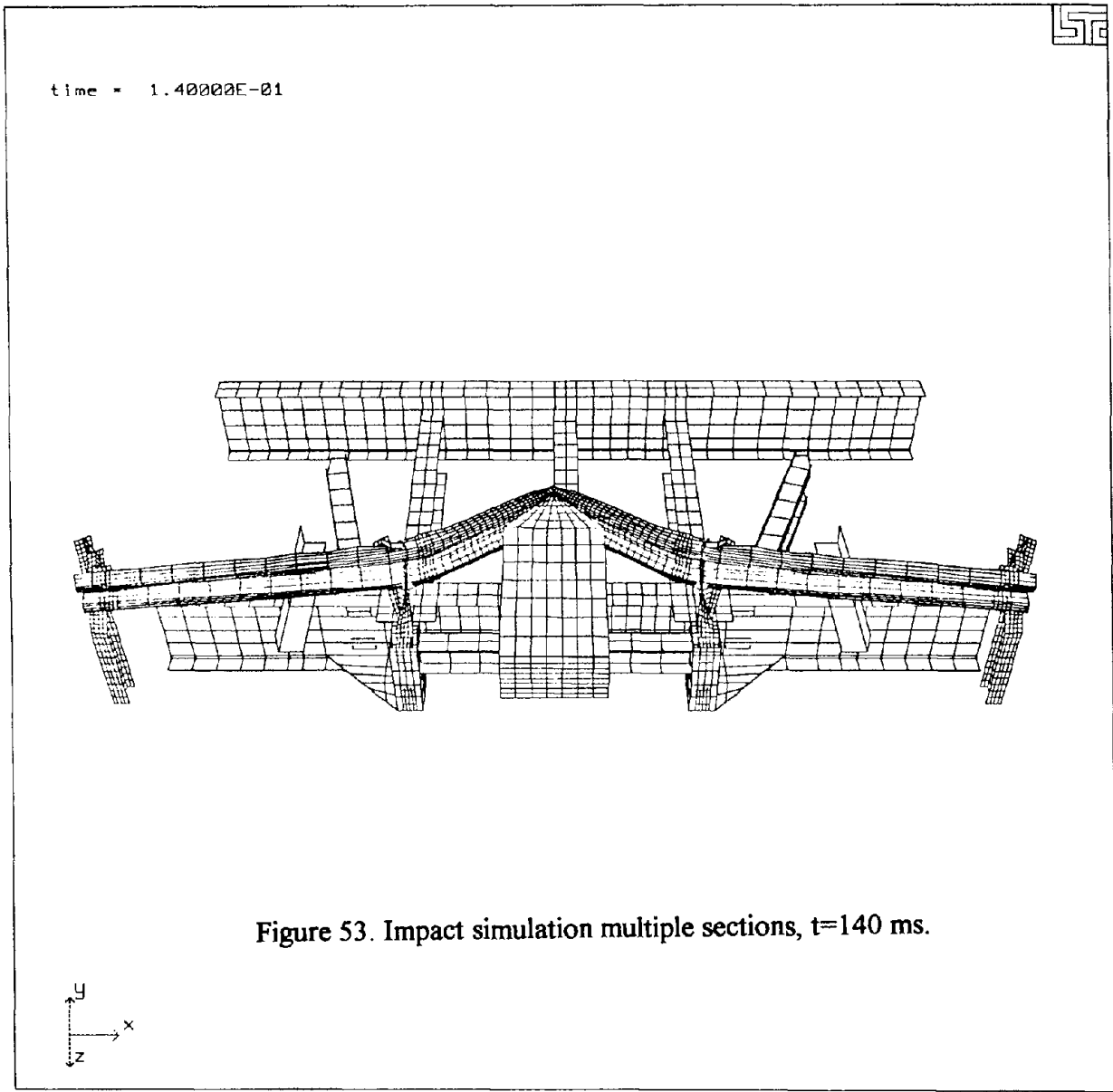
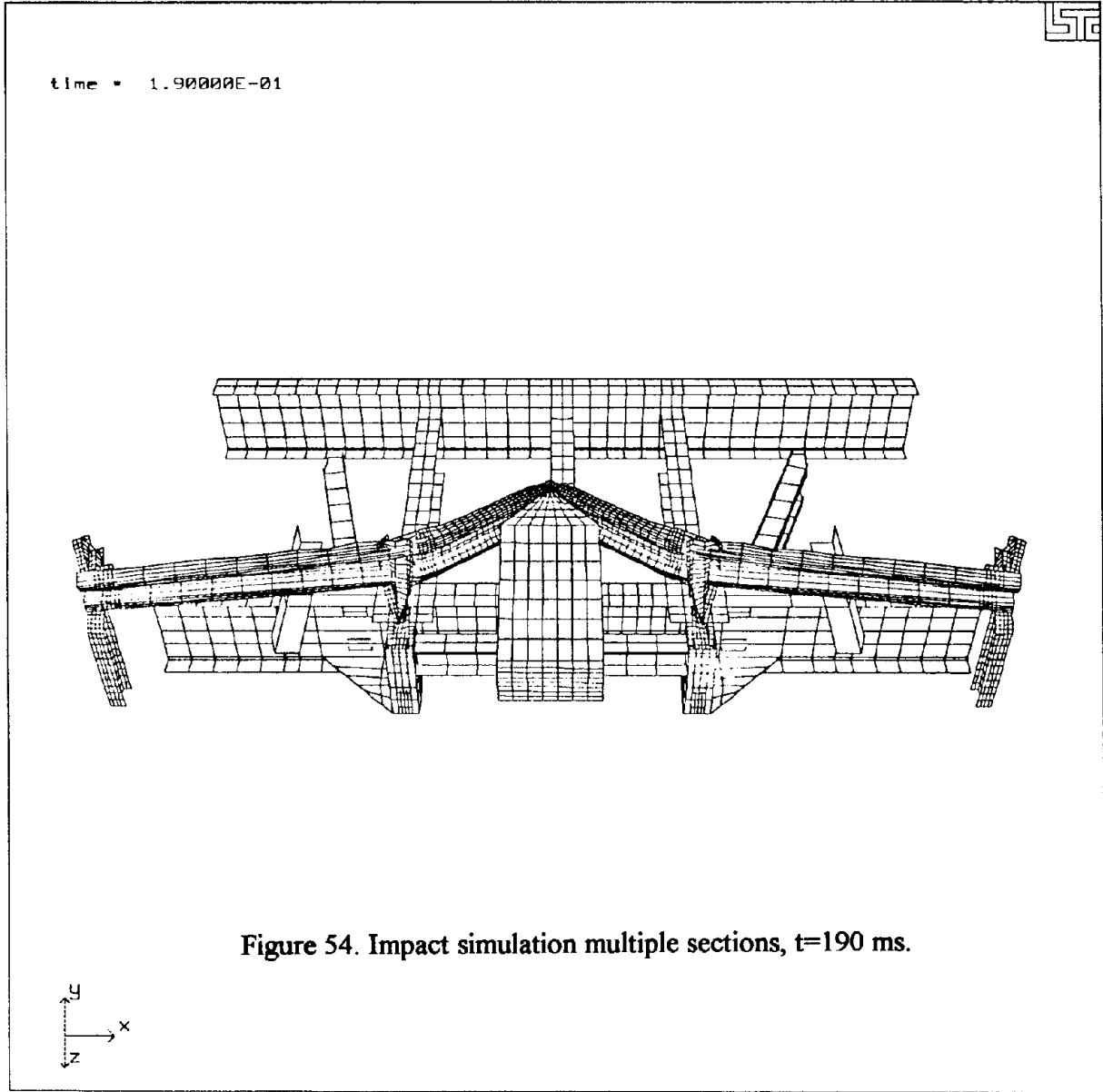


Figure 51. Impact simulation multiple sections, t=50 ms.









Chapter 8. DISCUSSION AND CONCLUSION

The finite element numerical simulation is successfully performed. The model captured most of the impact characteristics of the guard rails considered. The deformed shapes of the rails in the simulation and the tests were identical. The elastic plastic rate dependent material model is appropriate for predicting the impact behavior of such structural systems. Moreover, the simplified finite element model yield results almost identical to the full finite element model. This conclusion is based on the identical acceleration curves obtained by the two models. The simplified model has less elements which saved in computational time significantly.

The product of acceleration and the total mass of the pendulum yield the reactionary force. This force represent the total load carrying capacity of the guard rail. The first peak in the acceleration curves is an indication of the stiffness of the guard rail. Once a guard rail bends, significant reduction in the stiffness of the rail occurs. As the pendulum penetrated the rail further, the posts and the blockouts started to deform. The deformation was a combination of inward bending and twisting. In a complete guard rail system, the stiffness is mainly governed by the tension in the rail section. Deformation of posts and blockouts have less contribution compared to the current impact scenario.

A parametric study can be conducted numerically to optimize the design parameters. This numerical simulation serves as part of the initial effort of developing roadside barriers made of composite materials.

Chapter 9. FINAL REMARKS AND RECOMMENDATION

The objective of this study is to design a roadside barrier made of composite materials. Two concurrent studies are performed. The experimental investigation led to a better understanding of the failure modes of composite box beams, if they were to be used as a barrier. This study also, identified the necessity of addressing the end connections. It is important to investigate the barrier cross-section and end connections simultaneously for a better and more optimized design.

An experimental study of the above magnitude is costly and time consuming. To overcome this, a numerical simulation is used, as in this study, to minimize the cost of the final design. DYNA3D simulation is performed on a series of impact tests of steel guard rails. It is established that a numerical simulation is feasible and produce a good representation of the actual behavior. At this point, it is recommended that end conditions be addressed and only numerical simulation is performed for roadside barriers made of composite materials. Four composite material models with damages are available in the code LS-DYNA3D for performing the design iterations. In addition, a user defined material subroutine can be incorporated in the code for an additional composite material model if necessary.

REFERENCES

1. Broutman, L. J., and Rotem, A. 1975, *Impact Strength and Toughness of Fiber Composite Materials*, Foreign Object Impact Damage to Composite, ASTM STP 568, pp. 114-133.
2. Ross, Jr., H.E., D.L. Sicking, R.A. Zimmer, and J.D. Michie. 1993. NCHRP Report 350, Recommended Procedures For The Safety Performance Evaluation of Highway Features, Transportation Research Board, Washington, DC.
3. Dorey, G. 1993. *Impact and Crashworthiness of Composite Structures*, Structural Impact and Crashworthiness, G. A. O. Davies, Ed., Elsevier Applied Science Publishers, London and New York, pp. 155-191.
4. Ye, B.S. 1994. *Characteristics of Glass Fiber-Reinforced Composite Materials for Use in Roadside Safety Barriers*, Federal Highway Administration Report No. FHWA-RD-94-048.
5. Svenson, A.L. 1994. *Impact Characteristics of Glass Fiber-Reinforced Composite Materials for Use in Roadside Safety Barriers*, Federal Highway Administration Report No. FHWA-RD-93-090.
6. Creative Pultrusions, Inc., Design Guide, 1991, Vol. 2, Rev. 1, Creative Pultrusions, Inc., Alum Bank, PA.
7. Tabiei, A., Svenson, A., and Hargrave, M., 1995, *Impact Behavior of Pultruded Box-Beams for Road Side Safety Structures*, Proceedings of the Composite Institute's 50th Annual conference, Session 10-D, pp. 1-7, Cincinnati, OH.
8. Svenson, A., Hargrave, M., Tabiei, A., and Bank, L., 1995, *Design of Pultruded Beams for Optimization of Impact Performance*, Proceedings of the Composite Institute's 50th Annual Conference, Session 10-E, pp. 1-7, Cincinnati, OH.
9. Tabiei, A., 1995, *Impact Simulation of 850-kg Pendulum Into A Guard Rail Test Fixture*, Symposium on Numerical Implementation and Application of Constitutive Models in the Finite Element Method, ASME Winter Annual Meeting, S.F., CA.

NTIS does not permit return of items for credit or refund. A replacement will be provided if an error is made in filling your order, if the item was received in damaged condition, or if the item is defective.

Reproduced by NTIS

National Technical Information Service
Springfield, VA 22161

*This report was printed specifically for your order
from nearly 3 million titles available in our collection.*

For economy and efficiency, NTIS does not maintain stock of its vast collection of technical reports. Rather, most documents are printed for each order. Documents that are not in electronic format are reproduced from master archival copies and are the best possible reproductions available. If you have any questions concerning this document or any order you have placed with NTIS, please call our Customer Service Department at (703) 487-4660.

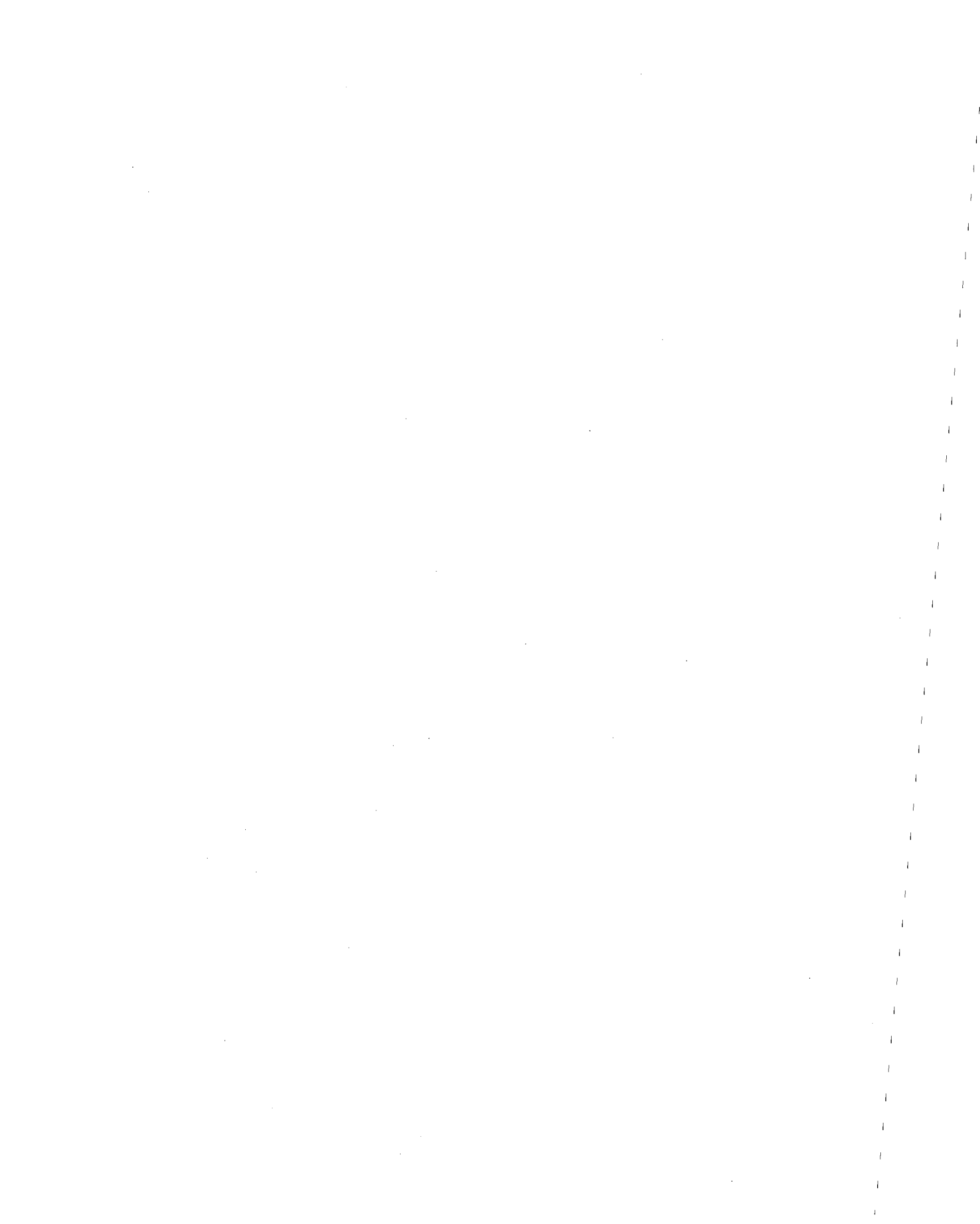
About NTIS

NTIS collects scientific, technical, engineering, and business related information — then organizes, maintains, and disseminates that information in a variety of formats — from microfiche to online services. The NTIS collection of nearly 3 million titles includes reports describing research conducted or sponsored by federal agencies and their contractors; statistical and business information; U.S. military publications; audiovisual products; computer software and electronic databases developed by federal agencies; training tools; and technical reports prepared by research organizations worldwide. Approximately 100,000 *new* titles are added and indexed into the NTIS collection annually.

For more information about NTIS products and services, call NTIS at (703) 487-4650 and request the free *NTIS Catalog of Products and Services*, PR-827LPG, or visit the NTIS Web site
<http://www.ntis.gov>.

NTIS

*Your indispensable resource for government-sponsored
information—U.S. and worldwide*







U.S. DEPARTMENT OF COMMERCE
Technology Administration
National Technical Information Service
Springfield, VA 22161 (703) 487-4650
